A NEW AGE OF FUEL PERFORMANCE CODE CRITERIA STUDIED THROUGH ADVANCED ATOMISTIC SIMULATION TECHNIQUES

BY

BENJAMIN ASHER HOLTZMAN

THESIS

Submitted in partial fulfillment of the requirements
for the degree of Master of Science in Nuclear, Plasma, and Radiological Engineering
in the Graduate College of the
University of Illinois at Urbana-Champaign, 2010

Urbana, Illinois

Master's Committee:

Professor James F. Stubbins, Advisor
Professor Rizwan Uddin
Eric Loewen

A NEW AGE OF FUEL PERFORMANCE CODE CRITERIA STUDIED THROUGH ADVANCED ATOMISTIC SIMULATION TECHNIQUES

Benjamin Asher Holtzman, M.S.

Department of Nuclear, Plasma, and Radiological Engineering
University of Illinois at Urbana-Champaign, 2010
James F. Stubbins, Advisor

A fundamental step in understanding the effects of irradiation on metallic uranium and uranium dioxide ceramic fuels, or any material, must start with the nature of radiation damage on the atomic level. The atomic damage displacement results in a multitude of defects that influence the fuel performance. Nuclear reactions are coupled, in that changing one variable will alter others through feedback. In the field of fuel performance modeling, these difficulties are addressed through the use of empirical models rather than models based on first principles. Empirical models can be used as a predictive code through the careful manipulation of input variables for the limited circumstances that are closely tied to the data used to create the model. While empirical models are efficient and give acceptable results, these results are only applicable within the range of the existing data. This narrow window prevents modeling changes in operating conditions that would invalidate the model as the new operating conditions would not be within the calibration data set.

This work is part of a larger effort to correct for this modeling deficiency. Uranium dioxide and metallic uranium fuels are analyzed through a kinetic Monte Carlo code (kMC) as part of an overall effort to generate a stochastic and predictive fuel code. The kMC investigations include sensitivity analysis of point defect concentrations, thermal gradients implemented through a temperature variation mesh-grid, and migration

energy values. In this work, fission damage is primarily represented through defects on the oxygen anion sublattice. Results were also compared between the various models.

Past studies of kMC point defect migration have not adequately addressed non-standard migration events such as clustering and dissociation of vacancies. As such, the General Utility Lattice Program (GULP) code was utilized to generate new migration energies so that additional non-migration events could be included into kMC code in the future for more comprehensive studies. Defect energies were calculated to generate barrier heights for single vacancy migration, clustering and dissociation of two vacancies, and vacancy migration while under the influence of both an additional oxygen and uranium vacancy.

ACKNOWLEDGEMENTS

This thesis would never have been written without the encouragement and support of many people. Science is not in a vacuum; rather scientists start with the work of their predecessors and further develop their ideas and incorporating their own work into the field. It is through this collaboration of ideas and theories that knowledge is accumulated over the course of many years. As such, it is prudent to acknowledge all those who have come before me in this field, though listing everyone individually would be an undertaking in the excess. Instead, I would like to recognize the other graduate students and professionals who worked with me on the nuclear energy advanced modeling and simulation project. Both the multi-university and national laboratory effort, as well as those graduate students at Illinois working on similar modeling efforts. Specifically Aaron Oaks, who took care of the computer cluster, owned the kMC code that became his thesis, and reviewed part of my thesis. Without his assistance, this thesis would have been more challenging and less meaningful.

This work was supported by DOE NERI DE-FC07-07ID14838 and by a Nuclear Regulatory Commission graduate fellowship, which paid my bills while in graduate school and allowed me to take the time to work on this project. I am indebted to my primary advisor Professor Stubbins for not only his assistance and guidance with the work, but for also being a pillar of support throughout the entire process. Additionally, I would like to thank Professor Uddin for his guidance and discussions regarding this work and for reviewing my thesis. Furthermore, I would like to thank Dr. Eric Loewen for his mentoring and reviewing my thesis.

Moreover, I would like to acknowledge my friends and family for being there to support me, and garner words of encouragement and sympathy as I trudged through the quagmire of the thesis process. I would especially like to acknowledge my parents, who I dedicate this thesis to, for not merely their encouragement and patience as I slowly made progress but for their support throughout my academic career. It would not have been possible without you.

TABLE OF CONTENTS

CHAPTER 1

THEORETICAL BACKGROUND

NUCLEAR FISSION

Nuclear power is the use of nuclear energy for civilian purposes, most notably, for the generation of clean, safe, and economic electricity. Nuclear fuel is the defining component of nuclear power because it differentiates nuclear energy generation from all other power production sources. The many forms of nuclear fuel vary in accordance with their intended application. The most common of these forms is uranium dioxide, or UO_2, which is used primarily in water cooled reactors. Water cooled reactors are the most common type of reactor and the uranium dioxide fuel used in it is the most important fuel form for designers to be able to accurately model. The ability to understand how the fuel will respond under known conditions allows reactors to operate safely and is the cornerstone of not only power production but also nearly all defense-in-depth analyses.

Irradiation damage affects microstructure in many ways. Most directly, it causes atomic defects, defect clusters, and introduces new elements through nuclear transmutation. When an atom undergoes a fission event, the nucleus splits into two smaller nuclei and releases energy. These lighter elements are called fission products and fall into two categories: solid fission products and fission gases. Furthermore, gaseous fission products can be grouped into two categories: noble gases and volatile fission products. Noble gas fission gases do not readily form complex chemical products within the fuel. Instead, the gas atoms nucleate under encountering other migrating gas atoms, or

on fission-fragment tracks or dislocation lines [1]. All fission gases in this work are treated as noble gases.

The Boltzmann distribution explains why more atoms will have low energies and fewer atoms will have higher energies since there are more arrangements of the system with the majority of the atoms at low energy, rather than one atom taking the lion's share of the available system energy that would leave the remaining atoms at significantly lower energies. This is precisely what happens during irradiation when an extremely high-energy atom comes into the system.

When nuclear fuel undergoes irradiation, the fuel lattice atoms are subjected to highly energetic fission fragments as well as high-energy neutrons. One fission fragment creates around 28 primary uranium knock-on atoms and over 20,000 higher order knock-on atoms. The primary or higher order knock-on atoms that escape from the surface are renamed, knocked-off atoms. While the mass and charge of the fission-product atoms are less than the fissile element, their range is significantly larger and it is an atom's range, or mean free path, which will determine whether the atom will escape the fuel. In addition to knocking atoms out of the fuel, fission fragments can knock gas atoms out of bubbles back into the matrix. The gas atoms will quickly precipitate out as bubbles unless trapped due to their insolubility in the fuel matrix [1, 12].

Radiation damage is the effect of energetic displacement cascades on a material's atoms, which can only be observed in solid materials since liquids and gases are amorphous in nature and therefore able to self-heal after displacement events – it is obvious that metallic and oxide nuclear fuels are both solids. The struck atom will be displaced if the incident atom has energy greater than the displacement energy – the

displacement energy barrier is between 20 eV to 50 eV. As such, thermal neutrons at ~1eV are not able to initiate displacement cascades. Instead, displacement cascades are linked to fast neutrons at energies greater than 1 keV. Nevertheless, all collisions induce forced vibrations into the atoms [48]. Fast neutron fluence has a direct correlation with displacements per atom (dpa) and therefore swelling.

A fission fragment damages the solid fuel lattice through direct hard sphere collisions as well as by electron excitation. Fission fragments are stripped of approximately twenty electrons along their path, but at the end, the fission fragments can still retain a significant charge [21, 48]. The effect will be greater in oxide fuel than in metallic because these ionization effects are more pronounced in materials of poor electrical and thermal conductivity [12]. Insulators lose energy through slow and weak electron-photon and photon-photon interactions [48]. Oxide fuels create a net positive charge that damages the connections between atoms causing disorder and atomic displacement since the oxide fuel is unable to quickly dissipate the spike effects [21, 39]. The dissipated energy causes a thermal spike in the surrounding material as well as an electron spike due to the intense ionization along the track [1, 8, and 21]. Metallic fuels achieve electrical neutrality by quickly dissipating the spike effects through the abundant free electrons [48]. Once the fission products have dissipated their energy, they stop in the material.

In this manner, the fission gases Kr and Xe become neutral, allowing themselves to behave according to the rules of classical diffusion – obeying Fick's second law of diffusion and temperature dependence governed by the empirical Arrhenius equation [21]. Until the fission gases attract electrons to become neutral gas atoms, they retain

their electrical charge and interact with the cations and anions of the fuel. During this interaction, the charged gas atoms have different migration energies compared to their neutral state [32].

FUEL PERFORMANCE

Good fuel cycle economics require that fuel elements achieve respectable burnups without failure; however, in order for fuel elements to attain these burnups, engineers and scientists must ensure that the fuel will not suffer a failure event. In the event of a fuel failure there is a release of fission products into the primary coolant, and the reactor's operators forcibly suppress the localized flux to minimize side effects. This suppression also lowers the power output as well as hampering the economic vitality of the reactor.

Fuel performance codes exist to provide the users a predictive indicator of how fuel will act under specific operating conditions. Most fuel performance codes are at least semi-empirical in nature, meaning the expressions for their parameters are fitted against existing data to obtain good predictions for a known set of physical and chemical properties of the fuel. From a technical perspective, the semi-empirical nature of the fuel codes is not a limiting factor, as there is more than 40 years of experimental data in use for these correlation curves.

Nevertheless, such models are by definition not predictive of results beyond the existing performance data since extrapolation outside of the range of existing data can very easily lead to misleading results. The consequence of this deficiency is that expensive fuel testing must be done experimentally to ensure safety. These results provide new data points for the code. Furthermore, the code must be manipulated to

ensure accurate correlation between the semi-empirical model and the existing data. This work seeks to fundamentally change this practice through the development of a fuel code from first principles. Analytical models that run based off the first-principles approach focus on fuel behavior and are designed to be able to predict potential issues in fuel performance that have not yet occurred in operating regimes unexplored experimentally or commercially. The validity of these calculations will always be directly linked to the strength of inter-atomic potentials and migration energies implemented in the models.

ATOMIC STRUCTURE

In a perfect or ideal crystalline solid, the crystal lattice of a substance is a three-dimensional array of atoms characterizing the symmetry of the structure. The atoms are grouped into unit cells, which are arrangements of atoms that displays the crystallographic features of the lattice type and through repeated translation alone can reproduce the entire crystal. The constitution of these unit cells determines the crystal's stoichiometric ratio. The cubic crystal system is the most relevant for oxide and metallic nuclear fuel.

The simplest of such cubic crystal systems is the simple cubic (sc) lattice. The crystal axes of this unit cell are orthogonal. Despite there being eight atoms, each atom is shared equally between eight adjacent unit cells not shown. Hence, only $1/8$ of any single atom belongs to a particular unit cell – in other words, the unit cell consists of one atom.

The next simplest of the cubic unit cells is the body-centered cubic (bcc) lattice. The crystal axes are rhombohedral in shape. This structure is created by inserting a single

atom into the center of the sc unit cell. As such, the bcc unit cell contains two atoms and is not considered primitive.

The last simple cubic unit cell is the face-centered cubic (fcc) lattice. The three edges of the unit cell are equal and the shape is rhombohedral, similar to the bcc lattice. There are six face-centered atoms that are shared between two adjoining unit cells, which contribute a net three new atoms to each fcc unit cell. As such, the fcc unit cell contains four atoms and is not considered to be primitive either.

The fluorite structure as shown in Figure 1 is the stable configuration of UO_2 for all temperatures below its melting point. Crystalline uranium dioxide is ionic and consists of U^{4+} and O^{2-} ions. The oxygen ions are arrayed on a sc sublattice while the uranium ions are arrayed onto a fcc sublattice surrounding the oxygen sublattice. The unit cell with fluorite structure contains four uranium dioxide molecules.

The magnitudes of all the crystal axes are equal and denoted by the common symbol a_0 that is called the lattice constant. The lattice constant is the distance between nearest neighbor locations on a particular lattice. This distance is a_0, $a_0\sqrt{2}/2$, and $a_0\sqrt{3}/2$ for the sc, fcc and bcc lattices respectfully [1]. There are six nearest neighbors for any given atom in a sc lattice, eight in a bcc lattice, and twelve in a fcc lattice.

Figure 1

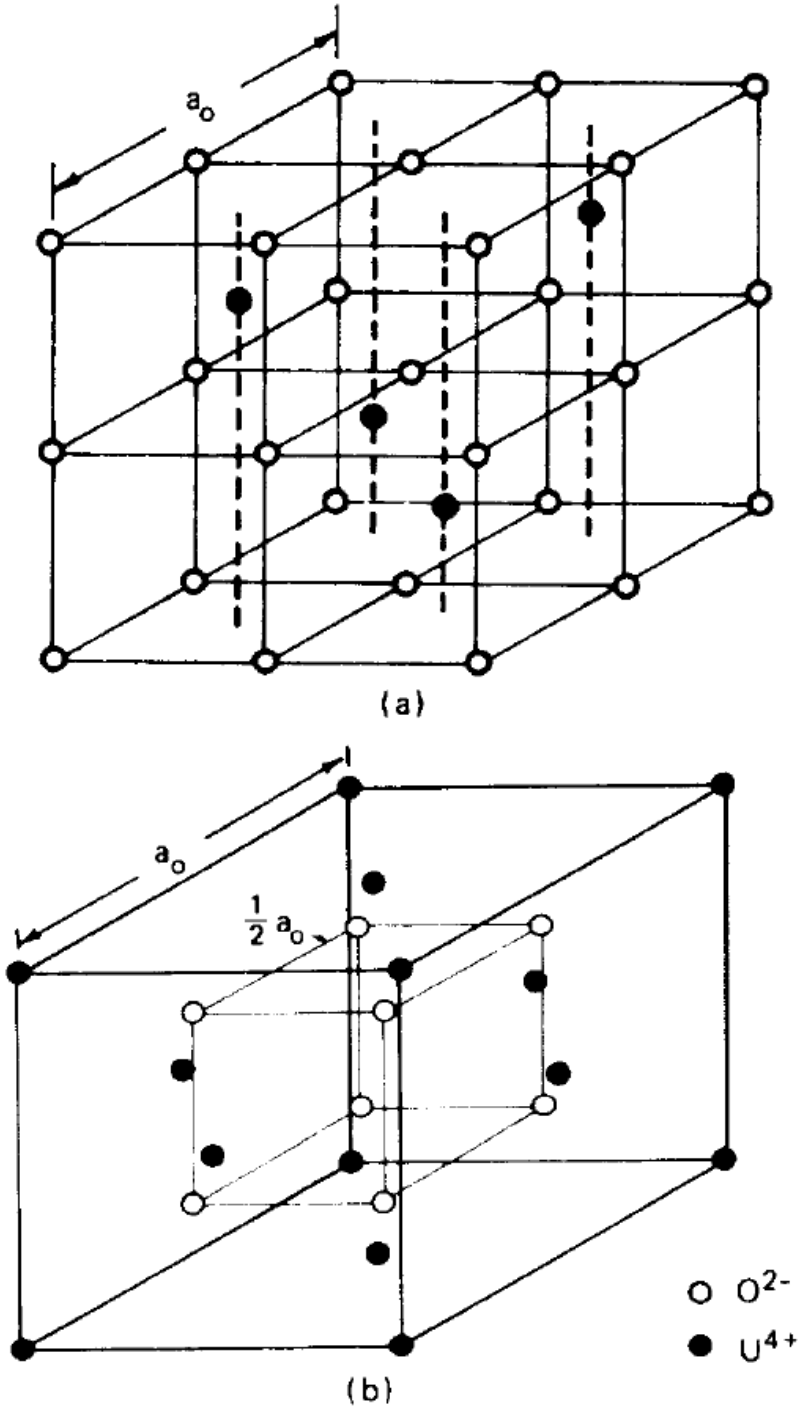

This figure shows the fluorite structure unit cell. (a) displays the simple cubic unit cell structure of the anion sublattice. (b) displays the face-centered cubic unit cell structure of the cation sublattice. This figure is Fig. 3.12 of [1].

These nearest neighbors create a cage that act as a barrier to the free migration of an atom through the crystal. The potential energy for an atom is at a minimum in the center of this cage, which is the atom's equilibrium position. Movement in any direction causes an increase in the potential energy due to the neighboring atoms. Therefore, each atom can be visualized as sitting in a roughly harmonic potential well created through the interactions between the atom in the well and the other atoms of the crystal lattice.

POINT DEFECTS

Unfortunately, there are numerous flaws in the structure of materials representing a loss of crystalline perfection and a perfect lattice is a non-physical abstraction. All materials, not at absolute zero, must have defects. While natural crystals rarely have less than one percent impurities present, nuclear fuel is artificially engineered and contains defects. Additionally, more defects are produced during irradiation through the interactions of high-energy particles with the atoms of the fuel material. These defects are uniformly generated across the grain bulk, grain boundaries, defect sites, and phase boundaries. The remaining impurities present in the fuel are retained cover gas and an off-stoichiometric ratio of oxygen to uranium in oxide fuel.

A point defect is a defect associated with one or two individual and independent lattice sites. There are two forms of point defects: vacancies and interstitials. The interstitials can be of the same species as the rest of the lattice or different, while a vacancy by definition is the same species as the parent lattice. In a physical system, dissimilar point defects can recombine and cancel each other out, or similar point defects can agglomerate into defects of higher dimensions.

An interstitial is the term given to describe an extra atom that is located in a position that is not located in a standard lattice site. The preferred sites for interstitials in a lattice are those that are relatively open and do not cause much distortion on neighboring atoms of the lattice – thereby minimizing the system's energy. There are two broad classifications of these sites: octahedral and tetrahedral. As their names suggest, octahedral sites are interstitial positions where an interstitial atom would be surrounded by an octahedron of atoms in standard lattice sites, whereas tetrahedral sites would have the interstitial surrounded by a tetrahedron. There are four octahedral sites in the fcc lattice, one at the center of the unit cell and along the edges, and eight tetrahedral sites, one at each corner. While the center of the unit cell is obviously entirely within the unit cell, the edge locations are shared between neighboring unit cells. Figure 2 shows the tetrahedral and octahedral interstitial site locations for face-centered cubic systems. There are six octahedral sites in the bcc lattice, along the faces and edges of the unit cell, and twelve tetrahedral sites, along the faces and corners of the unit cell. Figure 3 shows the tetrahedral and octahedral interstitial site locations for body-centered cubic systems. The interstitial sites form a sublattice inside the crystal's normal lattice structure [1, 19]. The sublattice may contain more or less positions than the parent lattice and the species that occupy those lattice positions may or may not be the same species as those on the parent lattice.

Impurity atoms that are smaller than those on the parent lattice are small enough to fit into these interstitial positions without significant distortion of the host lattice, however, larger impurity atoms must generally replace a parent atom on the lattice. Regardless of whether the interstitial atom is the same species as the parent lattice, or that

Figure 2

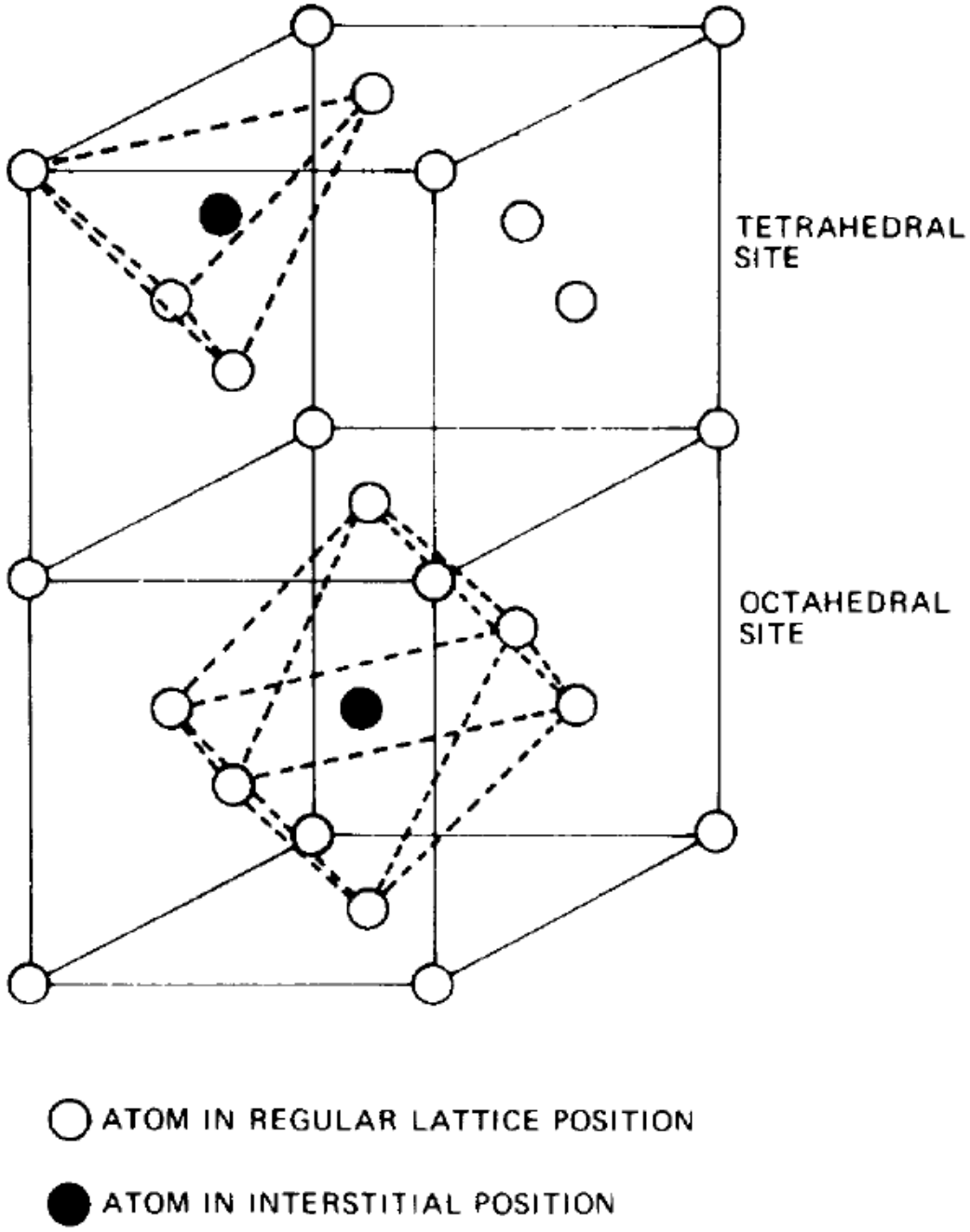

This figure shows the interstitial positions in the fcc structure.
This figure is Fig. 6.2 of [1].

Figure 3

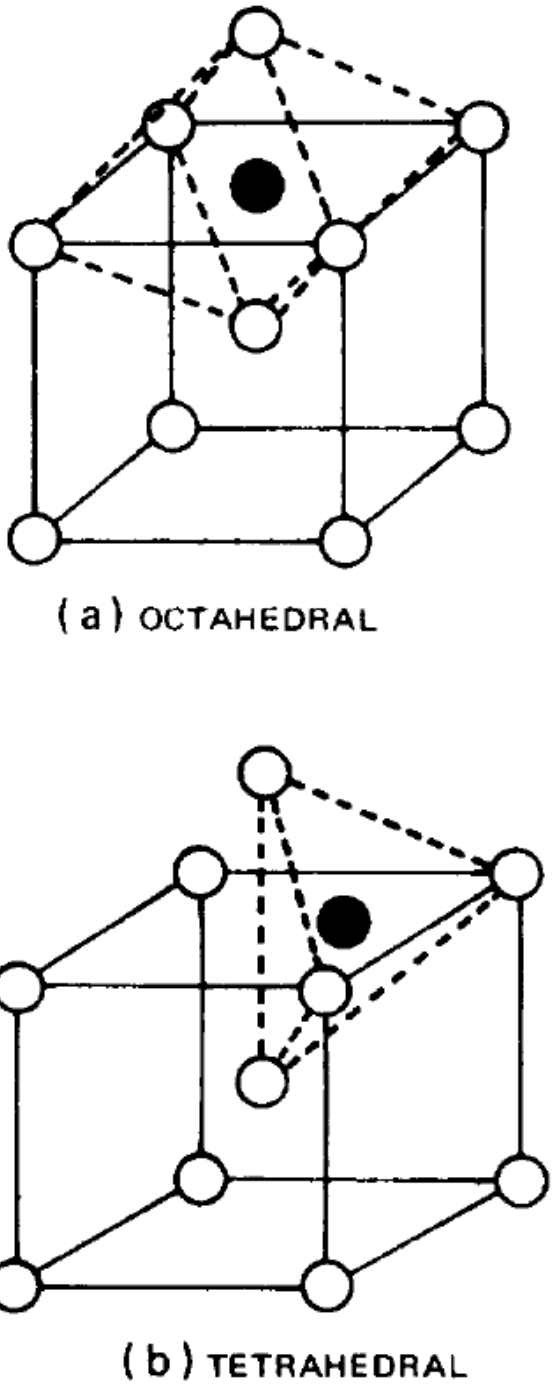

This figure shows the interstitial positions in the bcc structure.
This figure is Fig. 6.3 of [1].

of a different species, lone interstitials do not occupy an interstitial site amongst a perfect lattice in real crystal structures. Rather to attain a stable orientation, interstitials push the atoms on the lattice off their ideal lattice location via charge repulsion in order for the entire system to sit at the lowest possible energy. This is especially true when the interstitial is of the same species as the rest of the lattice with self-interstitial atoms (SIA). The SIA stable configuration is one where the two atoms share a single lattice position, the two atoms are symmetrically aligned on the empty lattice site in a dumbbell configuration – this is also known as a Willis Cluster [45]. In the case of the fcc lattice, the dumbbell orientation is along the <100> direction while in the case of a bcc lattice, the dumbbell orientation is along the <110> direction. These orientations are shown in Figure 4.

In order to accommodate these two atoms in a single lattice location, a stress is placed on the lattice that perturbs neighboring atoms in the form of an elastic displacement field that cause a compressive strain on the matrix [1, 19]. While in the case of a vacancy, the nearest neighboring lattice locations relax inward toward the vacancy causing a tensile strain. In either scenario, the vibrations of the atoms nearest the defect are altered by its presence, modifying the local system energy. Atoms further removed from the defect retain their original vibrational characteristics [1].

The radioactive decay process can also create point defects and gas atoms impurities. For instance, alpha decay emits a helium nucleus and a recoil nucleus that can have a kinetic energy on the order of 70 keV, as in the case of Th^{234} that is generated from the decay of U^{238}.

Figure 4

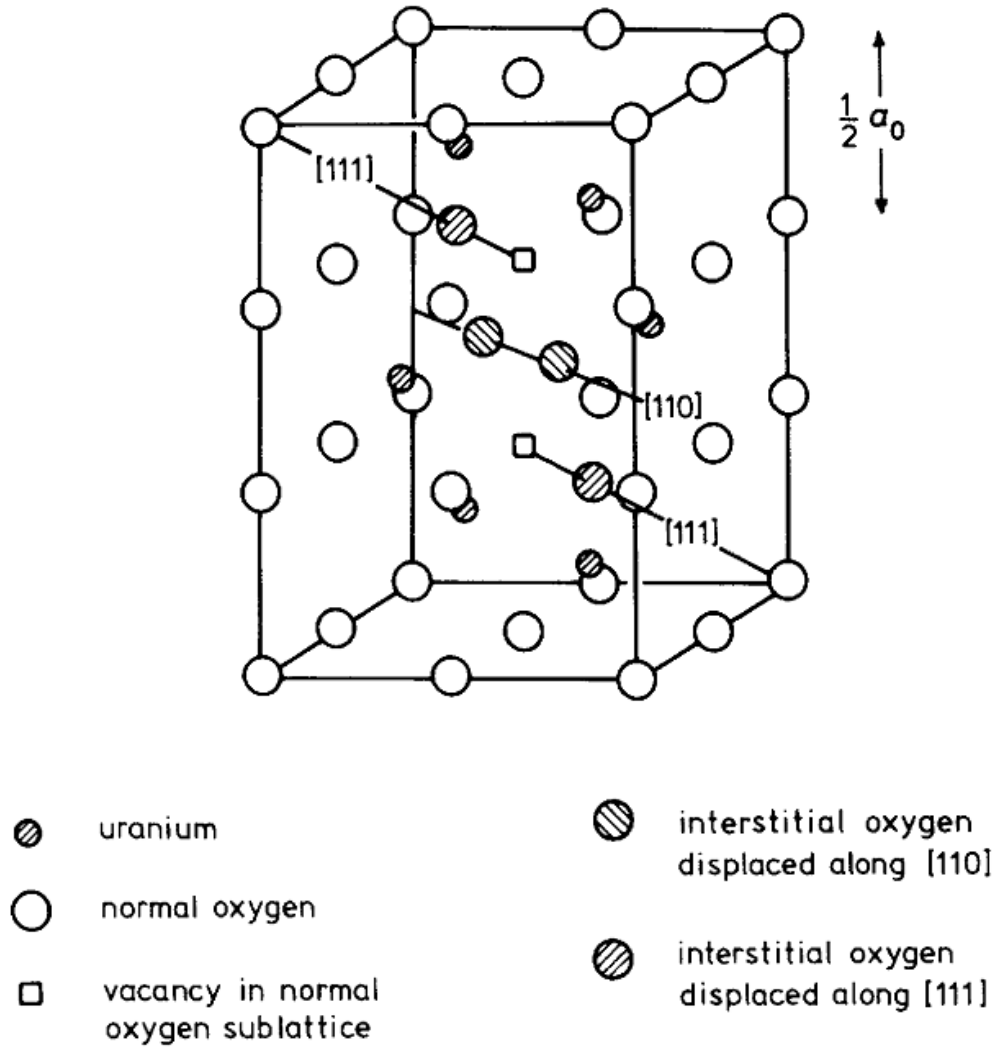

This figure shows the 2:2:2 Willis Cluster formation for $UO_{2.12}$.
This figure is Fig. 3 of [45].

The interior of an ionic crystal, such as UO_2, prefers to maintain electrical neutrality even on a very small scale [1]. As such, when a vacancy is created on the cation sublattice, two vacancies are needed on the anion sublattice within close proximity of the cation vacancy to neutralize charge. In fact, a pair of anion and cation vacancies occupying sites on opposing sublattices is quite common and is known as a Schottky defect. Another type of defect that maintains local electrical neutrality in ionic compounds is the Frenkel defect. In this case, an anion or cation – but not both – move from its normal lattice position to an interstitial position in the lattice leaving behind a vacancy defect. It is rare for a single ionic compound to have both forms of electrically neutral defects simultaneously as usually one dominates. The predominant mode of disorder in UO_2 consists of Frenkel defects on the oxygen sublattice, a very small amount of Schottky disorder occurs simultaneously [1]. Schottky and Frenkel defects are described as atomic disorder. The vacancies and interstitials forming these two complex defects are assumed to be dissociated and far enough apart to prevent immediate recombination [28].

TRAPS

All of these flaws serve as trapping locations for migrating species. A sizable reduction in system energy occurs when a free atom attaches to a defect. The strength of the attachment is called the binding energy of the specie to the defect. Traps can further be categorized by their trapping strength and the difficulty of the traps to be destroyed through either thermal annealing or fission fragments. For example, grain boundaries are deep traps where gas escaping by thermal processes is not likely. *Resolution* is the

process of cluster atoms returning to the fuel matrix due to irradiation caused knock-out. Resolution is only effective in shallow, temporary traps and at low temperatures. At higher temperatures, the atoms removed from the cluster are immediately returned. Resolution has a linear dependence on fission rate since it can be caused by irradiation [3].

In binary or multi-component systems, the formation of a defect is accompanied by a more or less pronounced redistribution of the component atoms or molecules around the defect. If the solute atoms segregate at the defect, then the total free energy of the system will be reduced. This decrease in energy can be assigned to either a decrease in the energy of the trapped solute atom or a decrease in the formation energy of the defect [13].

LINE DISLOCATIONS

Additionally, all real crystals contain one-dimensional defects known as dislocations. Dislocation lines are efficient sinks for atomic defects because the interaction energy is due to the unique nature of the stress fields in the neighborhood of the line, specifically the reduction in the stress field. For example, edge dislocations place the solid beneath the extra sheet of atoms in tension and create a region of compression above the glide plane.

In a material containing several types of point-defect sinks, different sinks have distinct capture efficiencies for vacancies and interstitials. While under irradiation, there will be unequal partitioning of point defects to sinks. The difference of these capture efficiencies is termed the bias. A larger flux of vacancies goes to voids and interstitials to

dislocations. This result grows both the voids and dislocations. In metallic fuels, the dislocation line has a slightly greater affinity for interstitials than vacancies. It is through this imbalance in capture rates that allows voids to grow in metals [1, 6, and 7].

Vacancies are attracted by the compressive stress field and interstitials by the tensile stress field. This enables a vacancy or interstitial to be captured by the line. Upon capture, the dislocation climbs in the opposite direction of capture. The movement of the dislocation lines ensures that more capture will occur than if the line was stationary. Nevertheless, dislocations are not perfect sinks for vacancies and interstitials since if they were ideal, the equilibrium concentration of vacancies and interstitials would be near zero, which is not the case. Rather through emission from the dislocation network, the concentration of these point defects is conserved in the crystal. In real crystals, the dislocations are not lined up in neat parallel arrays, instead the crystals are full of defects consisting of a tangle of dislocations [1].

The concentration of vacancies is high at low temperatures where diffusion coefficients are small and hence the removal processes is slow. As temperature increases, recombination and capture by dislocations become more rapid and the concentration of vacancies decreases. Although at very high temperatures, the concentration begins to rise again due to vacancy super saturation caused by the higher defect production rates and low dislocation line density [1].

ATOMIC VIBRATIONS

All particles have discrete amounts of energy that have three degrees of freedom for each form of energy. These forms of energy are translational, rotational, vibrational,

and electronic excitations [41]. The interatomic forces responsible for the thermodynamic behavior of the crystal are the vibrational frequencies [1].

All atoms are constantly in motion whether the atoms are on the lattice or some sort of defect. The random nature of thermal vibration gives rise to the random walk of atomic diffusion. The direction of any particular jump is random and independent of any previous jumps that may or may not have been undertaken. These jumps are the result of thermal vibrations of a very high frequency, however, the vibrational frequency of a lattice atom is several orders of magnitude lower than the jump frequency – the Debye frequency. As such, only few atoms in the Boltzmann distribution will have enough energy to overcome the energy barrier separating a particular atom from its next stable position – thus, successive jumps are also uncorrelated [1].

BARRIER POTENTIALS

The theory of absolute reaction rates states that in any rate process a barrier must be overcome by the migrating species for the migration to occur. This is the original concept of a jump frequency. An atom at the top of its barrier is referred to as an activated transition state. While in an equilibrium position, the atom behaves as a three-dimensional harmonic oscillator but once the atom reaches its activated state position, the potential energy is at a maximum rather than a minimum. In such a metastable position, the potential energy can still increase in directions perpendicular to the jump direction. Therefore, the potential energy resembles a horse's saddle, hence the descriptive term saddle point. Atoms on a saddle point have one degree of translational freedom, along the

jump direction, and two degrees of vibrational freedom, perpendicular to the jump direction [1].

A minimum displacement energy must be transferred in order for the atom to successfully jump from its ground-state equilibrium position to a neighboring ground-state equilibrium location through the activated state. Should the energy given to the atom be less than this minimum energy, the atom will vibrate in oscillation about its equilibrium position, its potential well, but will not be displaced. This barrier energy separates the well from neighboring wells, which are also local minimum energy positions [39]. These barriers cover the potential energy surface as peaks, which just as mountains have mountain passes cutting between the peaks, there are lower energy passages. Such passages connect neighboring atomic configurations that can be reached through the migration of displaced mobile defects.

Atomic vibrations are not contained to a single atom on the lattice; rather this surge of vibrational energy will be distributed to neighboring atoms through the interaction of their potential fields with the field of the struck atom. This energy is noticeable on a macroscopic scale as heat. As such, the potential fields of the atoms in the lattice construct an energy barrier that the struck atom must overcome in order to be displaced. This barrier potential is not uniform in all directions. Some directions will have a much higher potential barrier while other directions of high symmetry will have a much lower potential energy barrier analogous to the mountain passes [19].

The interaction potential between lattice atoms is required to accurately find the displacement energy. This can be accomplished through moving the atom in a direction and calculating the new potential energy of the system. By repeating this process many

times covering all possible directions and comparing results, a potential energy curve can be constructed. The potential energy barrier height is the difference between the minimum and maximum energy values along the direction of motion. Minimum values that occur at a physical location beyond the location of the maximum value are not included in the calculation, for that direction of motion. Only the minimum value that is located at a physical location before the location of the maximum value, along the path of motion, is used to calculate the barrier height. Atoms will fill locations after the maximum value without the need for an activation energy push, as the atoms will move down the potential energy curve into these locations on their own. This is the premise behind the molecular statics calculations that were undertaken using the GULP code in Chapter 4.

Diffusion is directly linked to the activation energy for migration of the species. This energy corresponds to the strength of the interatomic bonds [37]. The migration energy values or barrier heights for migration events to occur should vary significantly between uranium dioxide and metallic uranium due to the differences between the two lattice structures. Results that demonstrate this are discussed in Chapter 3.

METAL URANIUM FUEL

High burnup in oxide fuels is encumbered with problems with fission gas retention. This is why in old fast reactors, which utilized oxide fuel, the cores were designed with gas expansion modules to accommodate the fission gases without releasing the gases into the coolant [2]. Fortunately, current fast reactors do not need such fission gas collection methods, because metallic fuel is the current fuel planned for the high

burnups required in fast reactors – metallic fuels have already achieved over twenty percent burnup. Interestingly, there is a lot of operating and experimental data for metallic uranium as a nuclear fuel as it was used as one of the original fuel materials due to its ease of fabrication, lack of diluent atoms, and high thermal conductivity [8].

Metallic fuel has excellent steady-state irradiation performance characteristics and if enough space exists for expansion, inter-connected porosity will allow fission gas release directly to the plenum. Metallic fuel has other advantages over oxide fuel for use in fast reactors such as the Doppler coefficient, due to a low fuel operating temperature, and higher thermal conductivity that allow for a quicker cooling response in the event of a transient accident. Moreover, the higher thermal conductivity yields a smaller temperature gradient across the fuel [2]. Metallic fuel is not pure uranium, although, the uranium remains the major contributor so the alloy's behavior will be reflected by conduct of its uranium component.

Metallic uranium has three allotropic - different crystal structures - forms: alpha, beta and gamma phases. Many other metals also transform from one lattice type to another at specific characteristic temperatures, the transformation accompanied by small energy changes. The alpha phase has a distorted close-packed structure, face-centered orthorhombic spaced lattice with a basis of two atoms per unit cell [1]. The gamma phase is body centered cubic while the beta phase is a tetragonal unit cell containing 30 atoms.

The porosity structure in the alpha-uranium zone is so dense that a gas atom produced in fission has a high probability of escaping from the fuel as the fuel regions are thinner than the average distance that a fission-produced gas atom must travel before coming to a rest [6]. The alpha uranium is dimensionally unstable under irradiation [46].

This instability can be seen through the anisotropic growth and swelling of the orthorhombic crystal structure that leads to tearing or cavitation. The alpha phase of uranium only exists at lower temperatures compared to the beta and gamma phases. As the reactor is brought to temperature, the fuel will transform in accordance to its phase diagram. The phase diagram for U-Zr is shown as Figure 5 and the phase diagrams for U-Pu-Zr at 500°C, 670°C, and 700°C are shown as Figure 6. At the start of irradiation, most of the fuel structure is the alpha plus delta phase with the hottest sections already in the gamma phase [6, 47]. As irradiation continues and the fuel gets hotter, more of the fuel becomes the gamma phase.

There are two common approaches to stabilizing the uranium metal fuel. The first is to dissolve small amounts of another metal such as chromium, molybdenum, or zirconium into the uranium to stabilize the beta or gamma phases. The other approach is to add a more significant amount of metal to the uranium to permit retention of the gamma phase at temperatures below the normal transition temperature [8]. Upon irradiation, the slug's centerline operating temperature will ensure that the fuel is single-phase gamma [11]. Metallic fuel is also in pin form, but it is not composed of pellets rather it is fabricated as a single rod.

URANIUM DIOXIDE FUEL

Uranium dioxide has its own advantages over metallic fuel. It does not exhibit phase changes and has a very high melting point. Additionally it has coolant compatibility with the water coolant that is used worldwide in water cooled reactors and

Figure 5

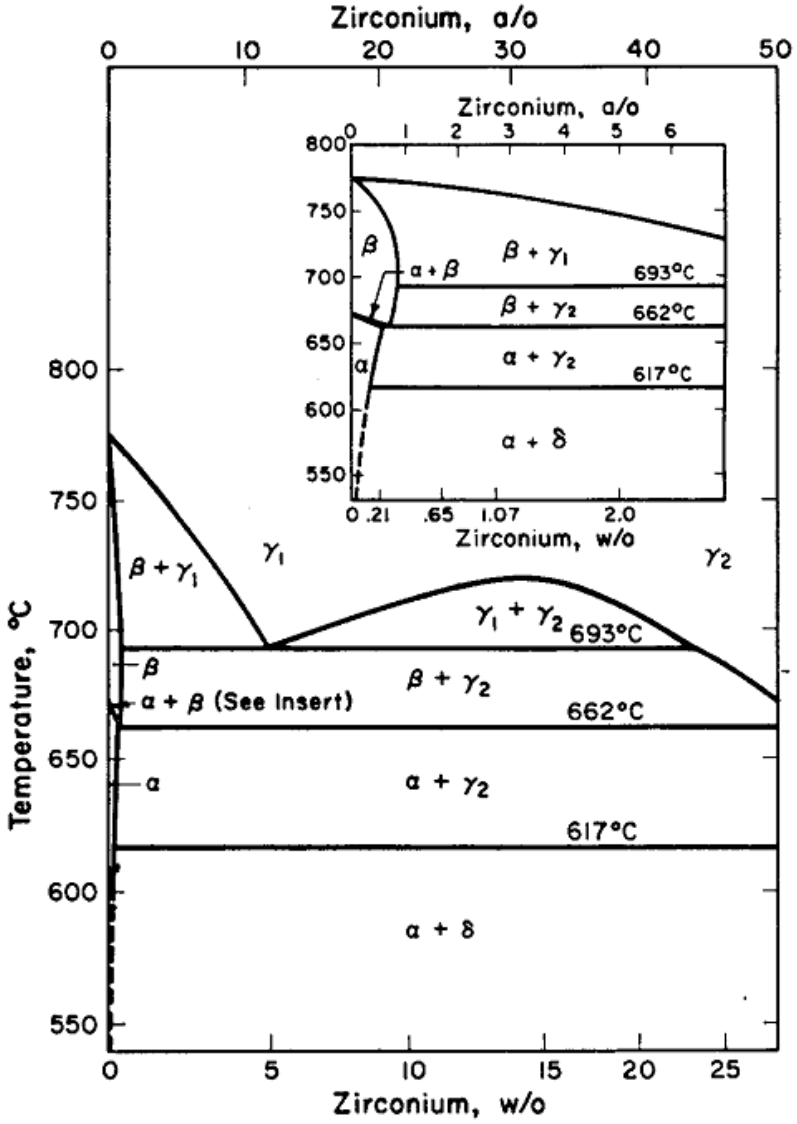

This figure shows the U-Zr phase diagram. This figure is Fig. 4 from [47].

Figure 6

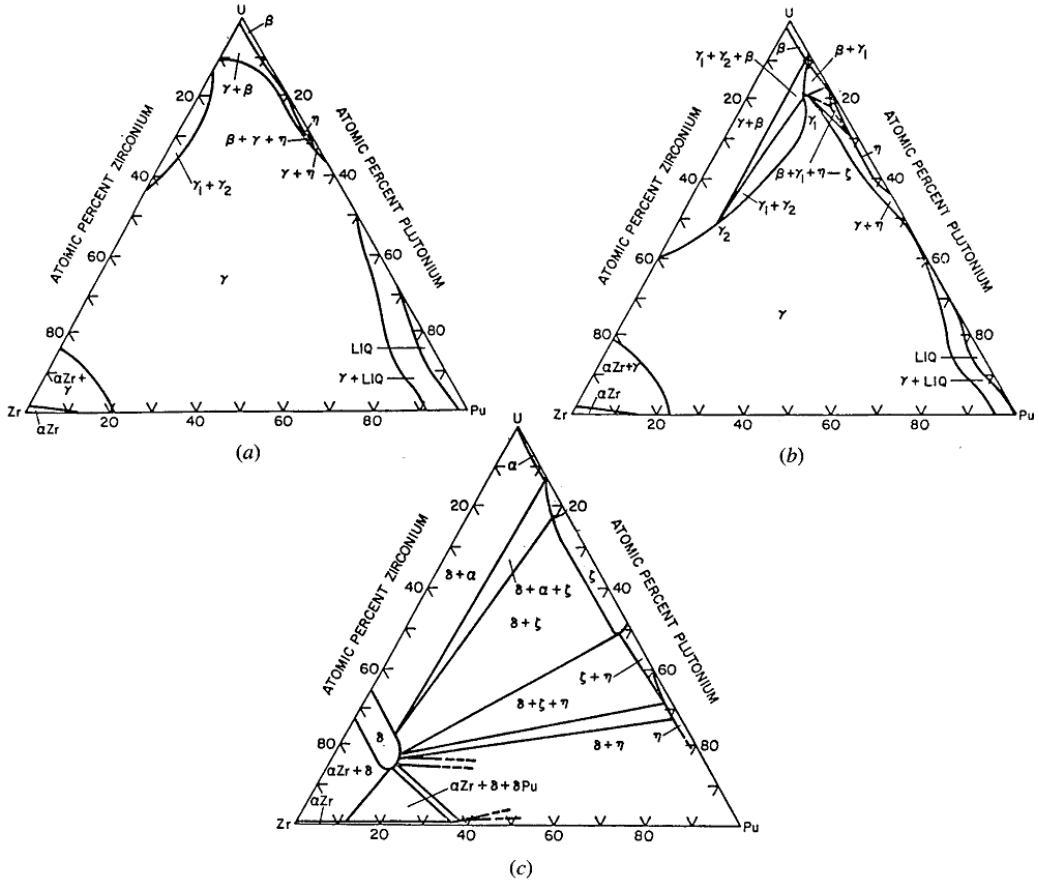

This figure shows the U-Pu-Zr phase diagrams at (a) 700°C, (b) 670°C, and (c) 500°C. This figure is Fig. 5 from [47].

has decades of operating experience. Uranium dioxide crystallizes in the fluorite structure where the cation valence is twice the anion valence. The U^{4+} ions form an fcc sublattice that meshes with a simple cubic O^{2-} sublattice. Materials with a fluorite structure such as UO_2 contain more than one type of point defect. In contrast to metals, where there is only a single lattice species, there are both anion and cation point defects in oxide fuels [1, 22].

In oxide fuel, the fuel is in the form of pellets that are staked into columns and enclosed in fuel pins. While core engineers and experiment designers work diligently to try to flatten the flux profile in a reactor, it is impossible to have a perfectly uniform burnup or temperature across the fuel pellets. The radial position of the fuel is quite relevant when looking at microstructure because there are unique characteristics of the different radial regions of the fuel. The variation in axial position along the fuel column height is much less significant for small changes, as these small position placement perturbations have minimal effects [11]. Overall, the mild dependence on axial position is near negligible and it will be treated as such in this work.

In addition to the low conductivity in oxide fuel, the accumulation of bubbles act as a thermal shield further retarding the conductivity of the fuel pellet. This low conductivity creates high temperature gradients that cause the pores created during the initial fabrication process to migrate through the fuel. This migration restructures the fuel and will occur anywhere that the fuel's burnup threshold is exceeded without dramatically raising fuel temperatures [5]. The effect is most commonly seen at the fuel pellet's rim.

At the pellet's surface, there is a general restructuring of the grains and a formation of dispersed micrometer-sized porosity of approximately 3 μm [15]. Furthermore, the rim becomes highly porous to the point it resembles a cauliflower in appearance once the fuel's average burnup reaches 40-45 MWd / kg M. The rim effects reflect a structural instability of the UO_2 under localized high burnup. In the porous band, the burnup increases due to the formation and additional fissioning of plutonium. The concentration of plutonium increases at the surface from the self-shielded capture of epithermal neutrons by the U^{238} present in the fuel [5] – most nuclear fuel used in light water reactors is at least 95% U^{238}. While it would seem that there is a direct correlation between the changes in the fuel microstructure at the pellet rim and the buildup of plutonium, the formation of plutonium does not play a direct role in the microstructure changes. Rather plutonium's importance is that it allows for more fission events to continue even as U^{235} is consumed, thereby enabling a higher local burnup to be reached. The increased irradiation produces extra fission gas and it is this high fission density that is responsible for the increased porosity [4].

It is important to note that the restructuring of the UO_2 grains involves recrystallization of the original UO_2. This recrystallization refers to the nucleation and growth of new grains and boundary lines rather than recrystallization of the form that occurs to cold-worked metals during annealing. This burnup-induced recrystallization usually occurs at temperatures too low for significant thermal diffusivities [5]. In fact, the low relative temperature and high burnup conditions on the outer rim of oxide fuels are excellent elements to create a highly refined microstructure through the production of

interstitial loops that generate an internal stress in the fuel leading to lattice displacement [3].

Small grain sizes allow more migrating species to reach boundaries since the species' mean free diffusion path is now larger relative to the distance needed for species to traverse to reach a boundary [15]. Additionally, the mobile sinks have a shorter distance to sweep gas atoms along until reaching boundaries [5]. It is no surprise then that there is a noticeable decrease in the xenon gas concentration in the grains at the pellet rim. In fact, the xenon concentration falls sharply near the pellet surface. While a large fraction of this missing gas is contained in the porosity, nearly 40% in one account [15], another sizable fraction of the gas is released locally [4]. The thermal conductivity at the pellet surface further decreases with the transformed microstructure since the large quantity of gas present acts as a thermal barrier that decreases the thermal conductivity of less than 1 W/(m K) [4, 15].

Many fuel codes separate the fuel into distinct radial regions in an attempt to model the microstructure changes that occur in these zones of recrystallization. This work does not divide the fuel into areas since the fuel is analyzed on a more localized level where such effects are merely taken into account as part of the bulk properties of the fuel.

VACANCY CAVITIES

A significant percentage of defects are formed in clusters rather than as single point defects. Vacancy clusters can grow to form voids and if the cluster is stable, it can migrate across the fuel to be absorbed at sinks – this is true for both interstitial and vacancy clusters. Interstitial and vacancy clusters must be treated separately since

interstitial clusters are considered stable while vacancy clusters are generally not. Additionally, the mobility of the different clusters is not equal. Vacancy clusters are slower than their interstitial counterparts who reach sinks through migration of the cluster as one entity. Moreover, vacancy clusters tend to form near the fission cascade core while interstitial clusters form near the cascade's periphery [19].

Densification of a vacancy cluster occurs through shrinkage caused by the emission of vacancies to the bulk solid, where they are absorbed by vacancy sinks. This process is prevalent in the last stages of sintering for oxide fuel [1].

Vacancy clusters shrink through the thermal emission rate of vacancies from the cavity based on the exponential of the inverse of the cavity radius at a given temperature. Additionally, at any given temperature, there is a specific critical radius above which the bias-induced net vacancy influx is larger than the net thermal vacancy outflux – thereby allowing the cavity to grow as a void. If there are sufficient gas atoms in a cavity, there will no longer be a physically meaningful critical radius. The gas can stabilize the shrinking and allow the cavity to continue growing. This result is not unexpected since if the concentration of gas atoms is high, a forming void will also contain a few stray gas atoms in it [1, 6, and 7].

Bias-driven growth is the absorption of excess vacancies produced through the irradiation damage. Growth of cavities within the bulk material is not expected because the effect of irradiation induced gas atom re-solution is strong and precludes the growth of intragranular gas bubbles to the critical size required for bias-driven growth [6].

In a system with a mixture of atoms, voids tend to sit next to the larger atoms since the larger atoms require more space. Interstitials sit near the smaller atoms since

there is more room relative to the larger atoms. Very large interstitial impurities, however, require multiple vacant sites due to their very large size.

In uranium dioxide, there are several specific vacancy clusters that are important as preferred sites for large gas atoms, such as xenon. These are the divacancy, the neutral trivacancy and the tetravacancy. The divacancy is composed of one anion and one cation vacancy. The neutral trivacancy is comprised of two anion and one cation vacancy and is separate from the charged trivacancy that is one anion and two cation vacancies. The tetravacancy is made up of two anion and two cation vacancies [34]. Not even these vacancy clusters are equal. The preferred trap location for xenon is the neutral trivacancy. The formation energy of this defect may be expected to be between 2 and 3 eV less than that of a Schottky defect because of the defect interaction. The volume of a neutral trivacancy is ~40 angstroms and the volume of a Xe atom is ~26 angstroms so there would be no added strain in the lattice for one gas atom [16].

Melting occurs when there are sufficient vacancies to cause enough disorder in the lattice to change the material from solid to liquid. Therefore, materials with a high melting point have similarly high vacancy formation energies. A material with a low melting point will have few displacements present after the cascade due to local melting, while a material with a high melting point will have many more displacements remaining since local melting did not occur. A material that has a low melting point would be indicative of a material that will take relatively less damage from the radiation cascade.

PORES

There are two types of closed pores in ceramic nuclear fuels. The first are the pores formed through the precipitation of fission gases from the solution while the second are the pores formed from an incomplete densification of oxide fuel during manufacture. This manufactured porosity helps to accommodate fission gases. As such, pores are soon filled with gas atoms from fissions and helium gas from manufacture. The pores created from this process are usually larger than 1 μm, and are at 1 atm or zero excess pressure gauged against the fuel. In order for these pores to grow in size, their internal pressure must increase to maintain mechanical equilibrium. This pressurization is from the addition of fission products – gaseous atoms being the most effective. These gas atom additions are gathered through diffusion. Similarly, pores will shed vacancies to achieve mechanical equilibrium and will continue to do so until the pressure defect is neutralized between the pore and the surrounding material.

Bubbles caused by fission gas coalescence and pores remaining from manufacture are shaped differently. Bubbles are usually very spherical to minimize surface energy while pores tend to appear more like a disk with their major axis perpendicular to the temperature gradient. As pores migrate to the central void, they leave trails that are the distinctive radial streaks in the columnar-grain region of the fuel. These mobile pores also sweep up fission gases generated during irradiation and deposit the gas into the central void and in doing so act as an important release mechanism from the fuel. In fact, the poor thermal conductivity in oxide fuel causes the large temperature gradient across the pellet's center that entices pore migration to the center of the fuel pellet creating the central void [1].

INTRAGRANULAR BUBBLES

Intragranular bubbles are fission gas atoms that are generated in the grain and are assumed to be spherical in nature. Their size grows or shrinks based on the difference between bubble pressure and hydrostatic stress imposed on them, or upon interaction with other intragranular bubbles. Small bubbles coalesce as they move through the fuel volume until they reach the phase or grain boundaries. The size of these bubbles is determined by the equilibrium between resolution rate and growth rate and is in the order of 2 nm [10].

BUBBLE CLUSTERS

Bubbles are voids with gas atoms inside the cluster of vacancies. There can be clusters of vacancies without any gas atoms inside the cluster but this is only considered to be a cluster of vacancies, not a bubble.

In the case of bubbles, the bubbles are trapped until they have grown large enough so that the force due to the gradient – usually temperature – is large enough to tear the bubble away from the defect. The mechanism for bubble growth is through coalescence with additional bubbles captured by the defect. Once the bubble is detached from the defect it again travels freely through the fuel until it reaches a new defect for which the critical size for detachment is larger than its current size. This process continues until the bubble migrates out of the fuel [1].

Clusters of gas atoms, also known as bubble clusters, come together through coalescence. Coalescence is defined as the joining of gas atoms or clusters of gas atoms

together to form a larger collection of gas atoms. Gas bubbles can be formed through the precipitation of gas atoms at pre-existing pores or through gas-gas interactions in the fuel matrix. This is caused through one bubble or atom overtaking another of different size and velocity. Bubble nucleation is assumed to occur at identical rates for sites in the bulk fuel material and grain boundaries because fission occurs uniformly over the small microscopic areas under investigation. Therefore, the process of uniform bubble nucleation is not influenced by the strength of any sinks present [6].

In this kinetic Monte Carlo model there is no ability for the formation of giant gas bubbles via the mechanism of fuel liquefaction, where the fuel matrix is destroyed creating a weakened matrix that cannot restrict the growth of extremely large bubbles. Instead, the model assumes steady state operations with an unchanging and unyielding matrix.

Fission gas atoms have a lower thermal conductivity than the fuel material. Therefore, the incorporation of gas atoms in the fuel as defects lowers the overall thermal conductivity of the material. This results in higher temperatures in a manner similar to prefabricated porosity. Regardless of the method of formation, all bubbles interact with defects in the fuel and are influenced just like other defects in the fuel in terms of forced migration. The diffusion of bubbles relies on the movement of the bubble itself and resolution of atoms from the bubble back into the fuel. Bubbles are considered permanently out of the fuel once they reach open porosity, which includes the central void in addition to the plenum. Furthermore, regardless of formation method, gas atoms raise temperatures and assist in the buildup of rod internal pressure [20].

SWELLING MECHANICS

Fuel swelling is a multifaceted process that strongly depends on as-fabricated properties as well as in-pile conditions. Although, since swelling and fission gas release are complementary phenomenon, the mechanisms that are required to accurately model gas release are the same that are needed for swelling. In addition, regions that release large quantities of fission gas do not exhibit high quantities of swelling because there are not many gas atoms remaining in the fuel. The fission gases that are contained in the fuel cause fuel swelling because these gas atoms have a significantly lower density than the surrounding solid atoms. As such, these less dense gas atoms take up more volume than the solid atoms that were replaced. The lion's share of this swelling is caused by the relatively larger intergranular bubbles on the boundary and not the smaller intragranular bubbles. Swelling occurs as the cavities on the boundaries grow due to an influx of gas atoms.

All theories of swelling are predicated on the principle of biased loss of vacancies and interstitials. Some sinks, such as voids or dislocations, exist that prefer interstitials, where more vacancies are grabbed by neutral sinks [42]. As more gas atoms migrate to the boundaries from the increased diffusivity of the gas atoms at high temperature, swelling would increase; however, once all the gas is released, the additional swelling will be small. Therefore, near the center of oxide fuel pellets, nearly all the gas atoms have been released to the central void and there is minimal swelling. Conversely, near the cooler periphery of fuel, more gas atoms are trapped and there can be more swelling [1, 3].

The fission gas that has escaped to the free volume of the plenum inhibits swelling due to the increased pressurization of the fuel pin. This increase in external pressure promotes the collapse of internal porosity and bubbles as the gas pressure for the open porosity is equal to that of the free volume plenum. Therefore, as the fuel swells and increases the pressure of the fuel pin, a higher pressure acts on the fuel inhibiting additional swelling. Swelling is dependent on fuel temperatures and grain size, which are in turn dependent on radial positioning in the fuel.

The difference in swelling between the binary and ternary alloy fuels can be attributed to the existence of a lower dislocation density. Metallic fuel is restructured when high amounts of plutonium are present - 15 weight percent or higher. Fuels containing low amounts of plutonium, 8 weight percentage or less, do not show significant restructuring except for homogenous development of fission gas bubbles and grain boundary cavities [6, 11].

BULK RELEASE MECHANICS

At high temperatures, during irradiation and post irradiation annealing, atoms and vacancies move much quicker through the bulk due to the higher value of the diffusion coefficient and the effects of thermal annealing that causes the destruction of traps. The result of these actions is that the number of gas atoms available to migrate increases with an increase in mean free diffusion path [15]. The higher the temperature the lower the saturation level of retained fission gas [10]. Fission induced resolution from intragranular bubbles is postulated to be the mechanism that maintains gas of the atomic form in the

solid and thereby allowing for a macroscopic concentration gradient in the grain for gas-atoms to diffuse to the sink that is the grain boundary [1].

The diffusing species can be captured by sinks of all strengths. The stronger the sink, the greater the activation energy needed to propel the entity out of the sink. The capturing sink may not be stationary, thereby acting as an effective mechanism for sweeping the bubbles out to the boundary [14, 20].

GRAIN BOUNDARY RELEASE MECHANICS

Once gas atoms arrive at the grain or phase boundary – the strongest sinks – the existing face and edge bubbles collect them. The gas that accumulates at these boundaries will be released if the intergranular gas density is large enough to cause interlinkage. This interlinkage causes the formation of interconnected tunnels that provide pathways to the original free surfaces or porosity thereby allowing gas to escape through this tunnel and out of the fuel even from previously remote interior regions. These tunnels have a triangular cross section despite being formed from lenticular bubbles before interconnection [1, 9, 17, and 18]. When gas is released through this passage, the pressure of bubbles decreases and bubbles cease to grow, begin to shrink, and are annihilated [20]. This helps explain why fractional gas release becomes asymptotic in behavior once the fraction of release becomes very large. Once this happens, the release of gas atoms is governed by the rate of gas atoms arriving at the boundary from the bulk material since the atoms are immediately transported away down the tunnel's highway system.

In this sense, the grain boundaries are an important fission gas release path for both oxide and metallic fuel since the fission gas generated moves to sinks and can be released if there is a path for it to flow out. One subtle difference between the two fuel varieties is that there are prominent phase boundaries in metallic fuel, in addition to the grain boundaries, while phase boundaries are not prolific in the normally phase-stable uranium dioxide.

The grain boundary is assumed to consist of two zones, one zone for newly arriving intragranular gas atoms and another for intergranular bubbles. Internal grain boundaries that are not vented to open porosity act as intermediate storage locations for the gas-atoms, however, once the tunnels become interconnected – usually during some sort of transient event – the previous build up of gas will cause a considerate amount of gas to be released [1, 20]. Moreover, grain boundaries act as regions of rapid diffusion even without interconnected grain boundary porosity because an atom has a higher probability of jumping to an adjacent site inside the grain boundary than the probability of jumping back into the grain. It is for these reasons that as burnup increases and the number of gas atoms nucleating everywhere increases. Bubbles are favored to grow in dislocations and subgrain boundaries because there is lower resolution at these locations than in the general fuel bulk. These bubbles range in size from 10 nm to 40 nm [10].

Phase and grain boundaries are excellent locations for bubbles to grow to critical size because while resolution rates at the grain and phase boundary are not negligible, the boundary's recapture distance is large. The majority of atoms that are knocked out of the bubble, on a boundary, do not escape the boundary's range of influence and are immediately recaptured as the average distance traveled by an ejected atom is not far

enough to avoid the boundary's pull and is quickly pulled back into the boundary due to the stress gradient. Stress gradient migration while not an important means of causing bubble motion, within the bulk fuel material, is influential in regions of locally high stress. Most prominently, this can be seen in the large stress gradients surrounding a dislocation that drive bubbles to the dislocation lines where they become stuck [1, 22]. Resolution of gas-atoms along the grain boundary occurs when fission fragments or knock-on atoms strike the grain boundaries but this is not an effective knock-out method. As such, the effects of resolution are neglected and not included in the kMC code [3, 6].

The bubbles are considered to be the immobile partner that is dragged by the moving grain boundary due to the forces of the grain boundary tension. This is not to say that the grain boundary is not also affected by this interaction, rather the shape of the grain boundary becomes distorted around the bubble. This interaction is analogous for pores and bubbles [1].

Bubbles do not escape the deep sink of the grain boundary through thermal mechanisms but they can escape. The gas instead will remain in place for the most part until one of two events occurs. As previously discussed, if extensive bubble interlinkage occurs, a pathway for the gas to travel to an even larger sink such as a crack or the plenum will be opened and then the gas will flow down the pathway out of the fuel. The other mechanism results from stresses in the fuel that initiate cracking along the grain boundary and are caused by power cycling, thermal expansion, or cladding restrain. Grain boundaries are a likely location for these cracks to develop because they have reduced the contact area due to the presence of the gas bubbles on the internal surfaces [1].The interlinkage of gas atoms that provides pathways to open porosity also can

sufficiently weaken the grain boundaries to the point of cracking. The rate of accumulation of intergranular gas is a major determining factor as to whether is causes swelling or grain boundary separation. During rapid heating of more than 10 C/s, grain boundary separation occurs. The microcracking allows for significant inventories of fission gas to be released [22, 24, and 25].

DIRECT RELEASE

There are two direct release mechanisms during irradiation: the direct recoil of atoms across the free surface and the knock-out of gas atoms situated close to the free surface by energetic ions from the fission process. These release mechanisms operate independent of both the temperature and temperature gradient in the fuel; however, they only influence the outermost layer of the fuel surface, approximately the outer 10 μm of the fuel. Therefore, their contribution fraction to the total fission gas released is small [1, 12]. A gas atom is considered to have permanently escaped from the fuel once it reaches an external surface. These include central void, cracks in the fuel, and the plenum. Once a gas atom reaches one of these surfaces, its probability for reentry into the fuel matrix is essentially zero.

CHAPTER 2

DIFFUSION

DIFFUSIVITY

Diffusion is the result of continuous local atomic mixing because the movement of atoms on a microscopic scale causes the macroscopic phenomenon of diffusion to occur. There are multiple diffusion processes, all of which operate in series. The point defects are formed uniformly within the grains and then diffuse to the grain boundaries by bulk diffusion that is diffusion through the material's crystal structure. The other diffusion modes have different activation energies. Diffusion along grain boundaries is faster than bulk diffusion because the grain boundary is a more open structure. The crystal surface is even more open than the grain boundary region, as such, surface diffusion allows for the fastest atomic transport mechanism because fewer atoms hinder it [9, 35]. This result does not mean that surface diffusion is the most important process despite having the largest diffusion coefficient. Materials with a small grain size and therefore a large grain-boundary area will be dominated by grain boundary diffusion [35].

Various species move through the bulk material through a combination of Brownian Motion and biased migration from gradient sources. Brownian Motion, or the random walk model, is temperature dependent in that as temperature increases the velocity of the random motion of the species increases. The random walk model can be described as a diffusion process so that the Arrhenius equation can be utilized in lieu of the statistical analysis of the random walk model. Without a temperature gradient present, diffusion is caused by Brownian Motion, while where there is a larger temperature differential present in the fuel, diffusion is dominated by the migration induced by the

temperature gradient. At extremely low temperatures, there is not a significant temperature gradient and the diffusion caused through Brownian Motion is low as well. Without mobility, gas atom release is limited to direct knockout mechanisms until a temperature gradient or temperature increase allows for release through diffusivity and the interconnected grain network. Due to the poorer thermal conductivity in oxide fuel, there should be a larger temperature gradient; however, the diffusivity is not solely linked to this factor. The diffusion of fission gases during irradiation has more than one rate controlling mechanism. An expression for diffusion coefficient should ideally include dependent variables for temperature, fission rate, burnup, and the decay constant [9, 12, and 21].

DIFFUSION MECHANISMS IN LATTICE STRUCTURES

There are several mechanisms of lattice diffusion: the exchange and ring mechanism, the vacancy mechanism, the interstitial mechanism, the interstitalcy mechanism, the dumbbell interstitial mechanism, and the crowdion mechanism. These are discussed below.

The exchange mechanism consists of the swapping lattice positions between two atoms located in neighboring crystal sites. It does not require the presence of defects and it is highly unlikely in close packed crystals because it requires considerable deformation and therefore enormous activation energy. The ring mechanism is less energy intensive but requires the coordinated movement of several atoms. Since the probability of this is low and the energy required is still high, both the exchange and ring mechanisms are unimportant in crystals containing defects, which include all real crystals [19].

The vacancy mechanism is the simplest mechanism of diffusion. Diffusion occurs through the jumping of an atom from its lattice site to an adjacent vacant site. There must be a neighboring vacancy since movement of the vacancy is in the opposite direction of the lattice atom. Vacancy diffusion is regarded as either a movement of the atom or the equivalent movement of the vacancy [19].

The interstitial mechanism involves the movement of an atom from one interstitial position to another. This requires a lot of energy in order to push through the barrier atoms that separate the interstitial sites in the lattice. The intersitialcy mechanism allows for the displacement of neighboring lattice atoms into a new interstitial site. The dumbbell interstitial mechanism is the symmetrical placement of an interstitial and a lattice atom around a single lattice site so the two atoms share the lattice site [19].

The crowdion mechanism occurs when an atom is added to a lattice plane but does not reside in an interstitial position, rather numerous atoms shift slightly to accommodate the new atom. This configuration is unstable and usually only exists temporarily [19].

Although there are numerous mechanisms for diffusion, in the lattice kinetic Monte Carlo code, diffusion only occurs by either the vacancy or interstitial mechanisms for vacancies and interstitial atoms respectively. Self-diffusion of uranium and oxygen in UO_2 occurs by vacancy mechanisms on both the anion and cation sublattices. Uranium vacancies occur on the fcc uranium sublattice while oxygen vacancies occur on the sc oxygen sublattice. While in metallic uranium, self-diffusion of uranium occurs by the vacancy mechanism on the sole lattice. A Kirkendall effect has been observed during

previous interdiffusion studies that indicate that the uranium atoms move via a vacancy diffusion mechanism and not through interstitials [37].

HALF-LIFE DEPENDENCE

The release of two isotopes of the same element can have different temperature dependencies depending on their half-lives. Longer-lived species have lower activation energies and therefore have a lower energy barrier for migration. Hence, diffusion preferentially enhances the release of long-lived species over short-lived ones [9].

Accurately modeling the migration of short-lived fission products is further complicated since the transport equation contains additional loss and gain terms to account for the radioactive decay of the diffusing nuclides and their precursors. While this does not affect stable or long-lived gases, it would suppress the release of short-lived species because the grain-face bubbles act as a reservoir. The result of this is that the half-live dependence predicted from simple diffusion theory is not very accurate [17]. Fortunately, the coefficients in the transport equations are independent parameters that can be evaluated separately. This work will not specify specific isotopes of elements and as such will not include half-life dependence while calculating diffusion coefficients. Future work can be done to verify this independence.

RADIATION INDUCED SEGREGATION

Some species migrate by interstitials and others migrate via vacancies. Vacancies migrate due to the vacancy diffusion mechanism, which is in the opposite direction of the rest of the species in the system. As such, there will be different concentrations of species

at trapping sites based on which mechanism allows for the species movement. The inverse Kirkendall effect is the counter-flow of atoms during the migration of vacancy point defects. This effect appears to occur when the radius of one species is significantly larger than another.

The movement of atoms, or atomic intermixing, generates the diffusion fluxes that can cause the buildup or depletion of elements at local trapping sites depending on the flux direction. When including impurity species in computer models it is important that the proper migration mechanisms are identified and implemented correctly. An erroneous selection of migration mechanism creates a non-physical representation of the movement of these elements that can lead to disastrous consequences for the structural properties of the material. The resulting concentration discrepancy between the code and actual behavior leave the material susceptible to adverse processes, such as corrosion damage, because the variation in the concentration of specific species can have large macroscopic effects on a material.

CHAPTER 3

KINETIC MONTE CARLO

INTRODUCTION

Kinetic Monte Carlo simulations utilize algorithms based on random numbers to solve computational problems and are a powerful stochastic tool that is used to evaluate the dynamic propagation of species through a state system according to a known set of predetermined rate constants. Rate constants are dependent on the atomic configuration of the system.

Kinetic Monte Carlo simulations attempt to capture the effects of atomic processes that directly contribute to macroscopic changes through statistical averaging of the results. These results are statistically equivalent to running extremely long molecular dynamics simulations except for the fact that kinetic Monte Carlo cannot predict previously unidentified paths since the code only models those paths that already have a rate constant [36].

In the future, information will be seamlessly passed between models of various lengths and time scales; however, the current link between scales is imperfect and in this case, absent entirely. It is for this reason that accurate activation energies be given to the Monte Carlo code or the results can become non-physical. These sensitive data values are found through molecular dynamic and static calculations. These simulations are an atomistic representation of the classical equations of motion. The time steps involved in such a calculation must be extremely small, less than or equal to 10^{-15}s in order to resolve atomic vibrations accurately. For this reason, the real world time scale being modeled is

also very brief, frequently limited to less than one microsecond. Kinetic Monte Carlo works on longer time scales by implementing the fact that longer time system dynamics consist of jumps between states. Hence rather than following the trajectory through every vibrational period, the kinetic Monte Carlo code treats the transitions directly. In Chapter 4, molecular statics calculations are undertaken with the GULP code [43] to find migration values for future kinetic Monte Carlo calculations.

The kinetic Monte Carlo code used in this work was developed based off a kMC code originally developed at Georgia Institute of Technology. The code is a lattice based code as the atoms in the system are mapped onto a lattice. Atoms begin on a lattice site and terminate on a different lattice site. The atoms in a crystal are spatially distinguishable because each one has a unique location in the crystal lattice structure that serves as a marker, which differentiates it from other particles. This fact allows the kinetic Monte Carlo code to track each particle's movement and locations over the time of the simulation.

The kinetic Monte Carlo code does not implement a correlation effect. A correlation effect is used to account for imperfections in the lattice that remain in the wake of a successful migration jump to an adjacent site. This imperfection theoretically creates a bias that makes subsequent jumps more likely in the direction of the previous equilibrium position. The kinetic Monte Carlo code does not consider this because there is no jump history in the code. There is no aftermath of imperfections because the lattice positions are fixed and the migration events are infrequent relative to the vibrational period. As such, the species 'forgets' how it reached its new position.

RATE EQUATION

The event catalog is a list of all possible interactions between the allowable actions and entities in the system that is generated from the inclusion of all possible events in the system. An event is a specific migration action, for a specific entity in the system, and each event has its own rate that is proportional to the probability of that unique event occurring. The transition rate is dependent solely on the initial and final states. After the system is in its new state, the event catalog is updated before the procedure is repeated.

A random number is generated and used to select an event from the event catalog. After which, the time is updated and a new random number is generated. Since each random number generated is unique and independent of any previously generated random number and this number is responsible for selecting what event is picked from the event catalog, the kMC algorithm is stochastic in nature. It is worth noting that if the same initial seed number is used, the same series of random numbers will be generated by the random number generator and in such a scenario, identical results will be obtained.

The present work has an event catalog of only migration events. That is the code does not treat clusters or dissociation events differently from standard migration events. The migration rate parameters were obtained from literature [29] that employed first principle calculations. The rate of migration, $r^i_{migration}$, as shown in [40], is calculated in the following rate equation and is dependent on the activation energy or activation barrier - $E^i_{migration}$, the attempt frequency - $v^i_{migration}$, the temperature - T, and the Boltzmann constant - k_B.

$$r^{i}_{migration} = v^{i}_{migration} \exp(-\frac{E^{i}_{migration}}{k_B T}) \quad (3.1)$$

The jump attempt frequency specifies the number of times a second a jump would be attempted and is specified in the configuration input file. The exponential term specifies the probability that the jump will be successful. As the temperature increases the migration rate becomes closer to its maximum value.

DIFFUSION ALGORITHM

A time step in Monte Carlo does not correspond to any fixed about of time in the physical world. Although a time step in kinetic Monte Carlo has a direct correlation to the fastest process in real time. The determination of the time step begins with the selection of a random number, ζ, between 0 and 1, which is plugged into the following equation where R is the total sum of the rates.

$$\Delta t = -\frac{\ln(\zeta)}{R} \quad (3.2)$$

Time starts at zero and is incrementally increased in accordance to equation 3.2. When all time steps are completed, the displacement of the particle is calculated from its origin. The vector 'r' is the displacement of the displaced particle calculated by evaluating the initial position subtracted from the final position.

This displacement is unique to that particular run and due to the stochastic nature of the process, the displacement will not be identical for repeated runs under identical circumstances – such as using the same initial seed number in the random number

generator. Moreover, the statistical weight of the six dimensional space – three position coordinates and three momentums – is independent of its position.

If the random number used in the calculation were identical then the results would also be identical. The mean square displacement, r^2, is the quantity most suited to describe the extent of migration and is defined as the summation of all displacements squared averaged over the total displacement of the migrating particles in the system as mathematically explained in equation 3.3.

$$\left\langle r^2 \right\rangle = \sum_{i=1}^{N} \frac{r_i^2}{N} \tag{3.3}$$

As shown in detail in [39], and utilized in [27], the mean square displacement is related to diffusivity by the relation.

$$\left\langle r^2 \right\rangle = 6Dt \tag{3.4}$$

A simple rearrangement allows the code to calculate diffusivity.

$$D = \frac{\left\langle r^2 \right\rangle}{6t} \tag{3.5}$$

BLOCKING

Atomic diffusion works by having an atom jump from one lattice location into an adjacent lattice site that is vacant. If the terminal site was occupied, the two atoms would be violating the Pauli Exclusion Principle. To prevent this, a blocking model is utilized to prevent any two species from occupying the same lattice location. The kinetic Monte Carlo model does not allow one species to bump-out the other analogous to a bowling ball hitting the pins out of the way.

In the case of vacancies, the movement of atoms in one direction is equivalent to the movement of vacancies in the other direction. The kinetic Monte Carlo code, however, views vacancies as a separate species. As such, the blocking model prevents a vacancy from terminating a jump onto a lattice site that is already hosting a vacancy. Recombination is currently precluded from happening, as an interstitial and vacancy cannot share the same lattice location in kMC. In order for recombination to be implemented, it would need to be explicitly added into the code. The prospect for recombination and other additional events beyond simple migrations are discussed in Chapter 6 – Future Work.

COMPARISON TO CLASSICAL DIFFUSION

The standard diffusion equation is shown in equation 3.6 and can be rewritten in the case of cubic crystal structures due to the structures' isotropic nature into the form of equation 3.6, which is recognizable as Fick's second law, where D is an Arrhenius equation as shown in equation 3.7.

$$\nabla(D\nabla C) = \frac{\partial C}{\partial t} \tag{3.6}$$

$$\frac{\partial C}{\partial t} = D\nabla^2 C \tag{3.7}$$

$$D = D_0 \exp(\frac{-E}{k_B T}) \tag{3.8}$$

The diffusion coefficient in equation 3.5 and 3.8 are identical thereby allowing for direct comparison.

KMC SCENARIO MODELS

The kinetic Monte Carlo models were set up as a cube containing fifteen unit cells in all directions coupled with periodic boundary conditions to represent an infinite system. These cubes were utilized to simulate systems of CeO_2, UO_2, and metallic or U. Some sample input files are included in Appendix A.

Temperature is statistical in nature or to be more precise, temperature is a bookkeeping artifact used to keep track of the average energy of atoms in a specific object. In fact, the macroscopic property of temperature can be considered the manifestation of the microscopic vibrational energy of atoms. Hot objects have more energy per atom and cold objects have less. As such, the temperature is altered by manipulating the vibration energy as shown in equation 3.1 and allows the computer to maintain the position and energy of everything in the model. The jump frequency used is the Debye frequency.

IONIC FUEL MODELS

The first structure modeled was a CeO_2 system with four percent lanthanum impurities present on the Ce sublattice, in addition to the one percent vacancies present in the oxygen sublattice. This scenario was also modeled without the four percent lanthanum impurities present. The results from these computer simulations can be seen in Figures 7, 8, and 9. At low energy, La doped Ce traps migration of species because La affects migration energy and structure. This affect can be seen in the Figures 7 and 8, showing total squared displacement and RMS displacement respectively.

Figure 7

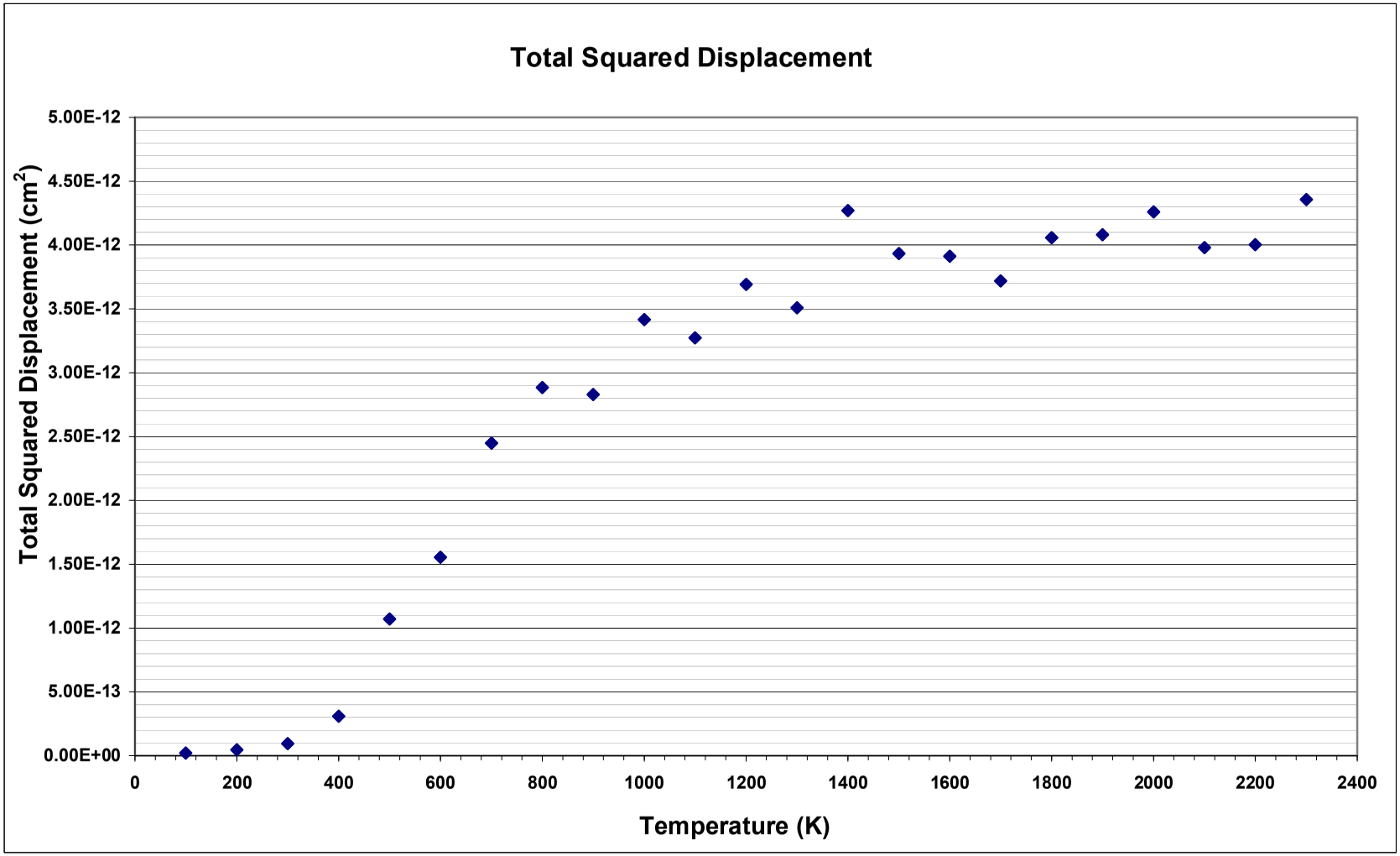

This figure shows the total squared displacement of the oxygen vacancies in CeO_2 with 1% La impurities present.

Figure 8

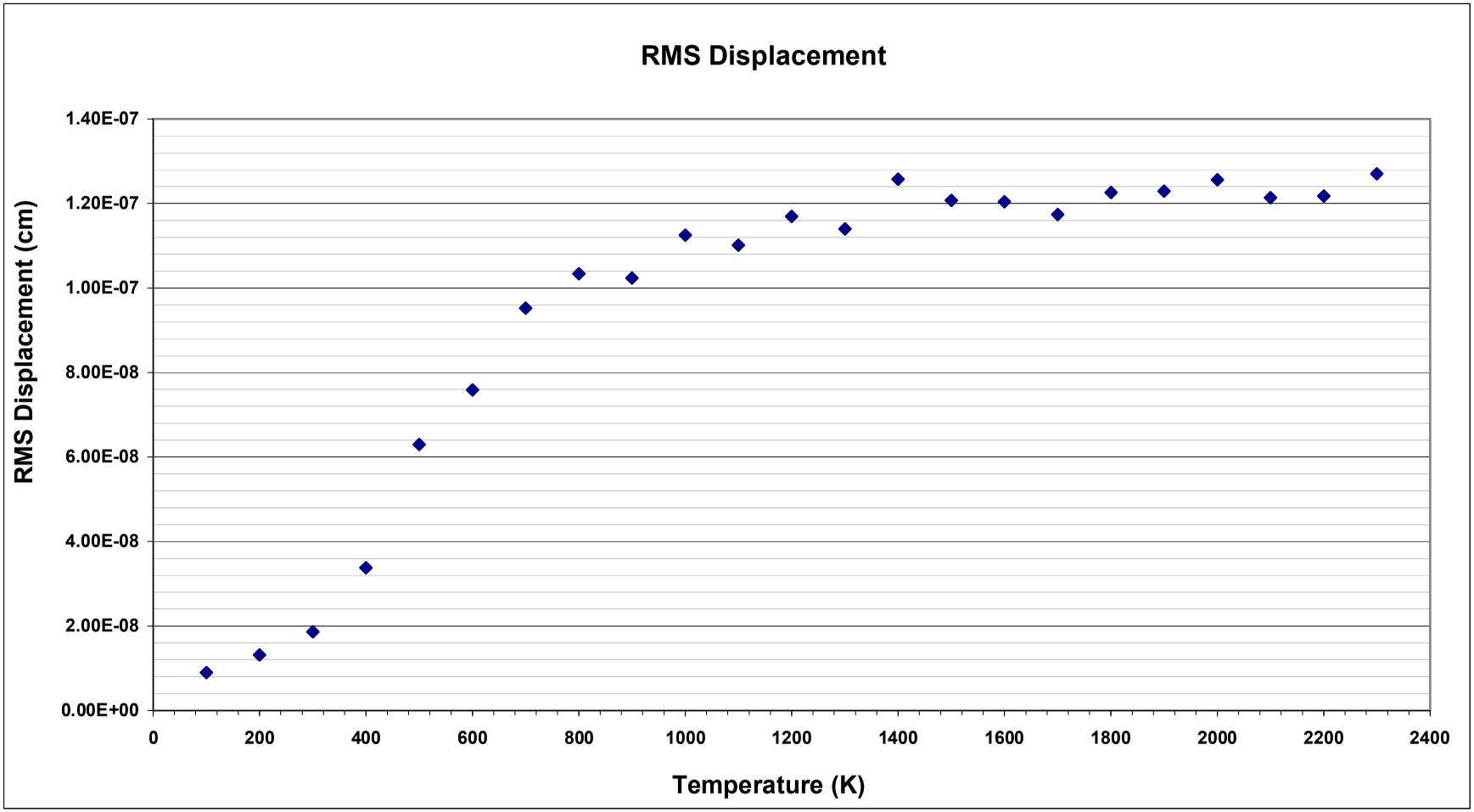

This figure shows the RMS displacement of the oxygen vacancies in CeO_2 with 1% La impurities present.

Figure 9

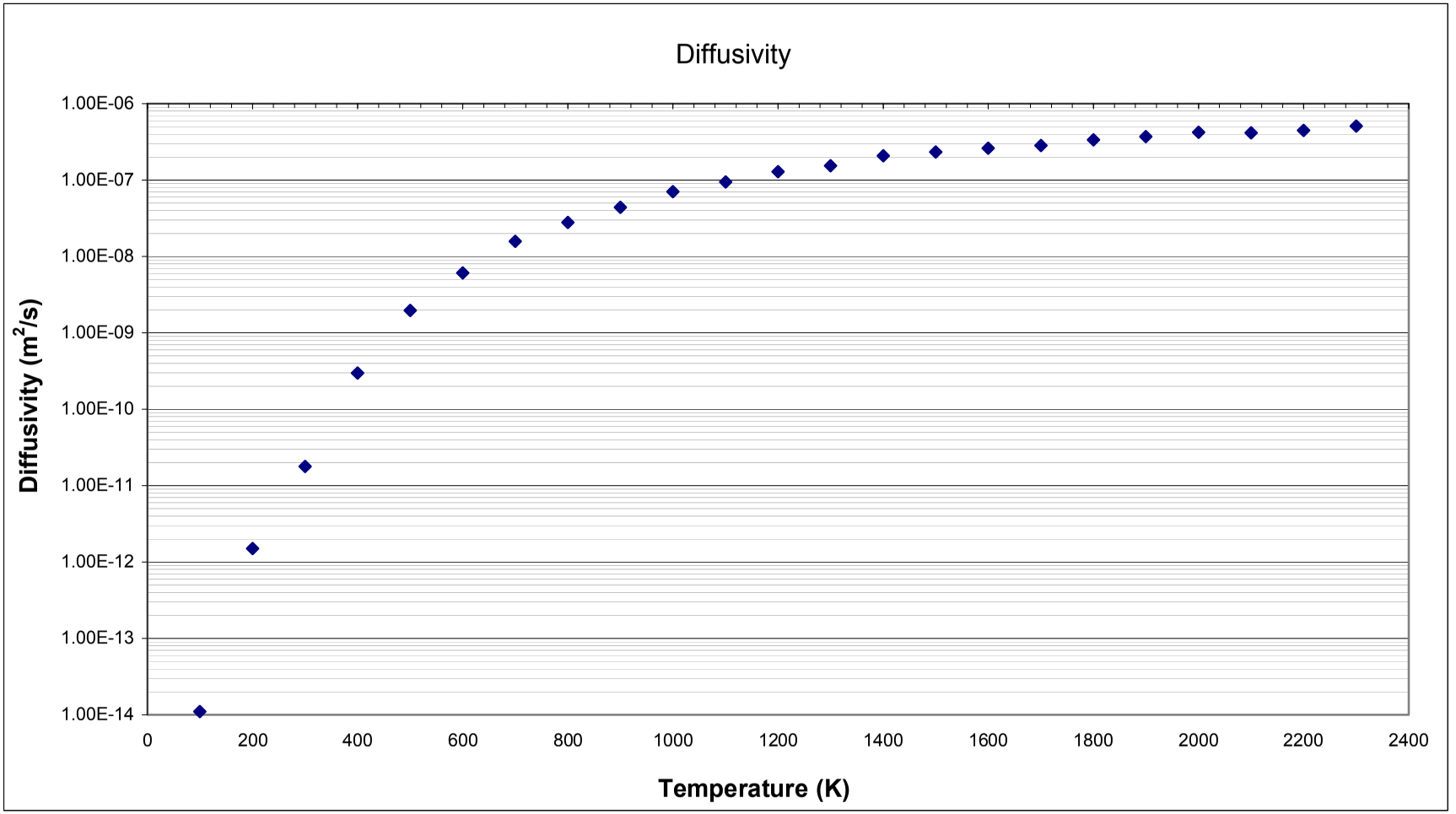

This figure shows the diffusivity of the oxygen vacancies in CeO_2 with 1% La impurities present.

While CeO_2 is not a typical nuclear fuel used in a nuclear reactor for commercial electricity production, it is a common surrogate material for UO_2 as it has an identical fluorite structure. At one point, the results from these simulations were going to be used to compare diffusivities against experimental values, however, due to delays in the experimental machine's construction this plan was abandoned, these runs are its vestige.

The UO_2 fuel was modeled with oxygen vacancies and interstitial atoms separately, while the cation sublattice is treated as ideal. The dominant production method for generating defects is Frenkel defects on the oxygen sublattice. As such, the concentration of cation vacancies and interstitials is considered to be negligible. It is worth mentioning that while, in reality, a very small quantity of Schottky defects does occur; the fraction of sites on this sublattice is many orders of magnitude lower than the fraction of sites on the anion sublattice. For instance, this fractional ratio is approximately seven orders of magnitude at 1400°C [1], hence the scenarios modeled are focused on defects on the oxygen sublattice rather than the uranium sublattice.

In these models, the UO_2 was hypo and hyper stoichiometric since the number of uranium atoms remained constant even as oxygen atoms were added and removed. In practice, these two forms are not as easy to create as modifying an input file to change the initial concentration. The stoichiometry of the model does not change over the course of the runtime since the release of additional oxygen nuclei through fission events are not taken into account as fission events are ignored.

Hypostoichiometric UO_2 can only be realistically achieved at very high temperatures, over 1800K and at low partial pressures of oxygen due to the large amount of energy required for reduction of U^{4+} to U^{3+}. Conversely, hyperstoichiometric UO_2 can

easily be achieved during fuel irradiation since an excess of interstitial oxygen atoms are present to accommodate U^{5+} cations [27]. At low stoichiometry, diffusivity is dominated by the interstitials while at higher stoichiometry, there is also diffusion of vacancy clusters – these clusters also influence the diffusivity of the interstitials [27]. In this way, not all the models make physical sense. Then again, since the model does not consider burnup or fission events, there is still a long way to go before this becomes a viable fuel code.

It is generally accepted that thermally driven release of fission gas from UO_2 starts at temperatures between 1100°C and 1200°C, although there is a strong dependence on burnup. Throughout most of the fuel's life, temperature of the LWR fuel is below 1100°C; however, during temperature transients it is not only possible but probable that higher temperatures will be attained. Obvious examples of this are during a control rod shuffle in the first or second reactor cycle when the linear heat rating is high, above 25 kW/m [4]. It is true that under transient heating, a significantly larger amount of fission gas release occurs than during steady state operation; however, because of the scale of the model, there is no difference in how the code will perform. Instead, the transient heating would be taken into account by altering the conditions acting on the fuel. The scenarios run in the kMC code had temperature variance from 100K to 2300K.

TEMPERATURE GRADIENT AND THERMOMIGRATION

In order to maximize the temperature gradient's effect, one direction of the unit cell cube was dramatically increased to allow for a greater temperature difference between the boundaries without significantly causing a significant increase in runtime for

the code or worse preventing the code from accurately constructing the system. Before the implementation of the temperature gradient itself, the newly enlarged system was compared to that of the 15x15x15 unit cell cube. The results of this comparison are shown in Figures 10 through 13. Figures 10 and 12 show the diffusivities for UO_{2-x} and metallic U_{-x} respectively while Figures 11 and 13 show the UO_{2-x} RMS displacement and the metallic U_{-x} total squared displacement respectively. As shown in the figures and explicitly compared in Tables 1 and 2 there is no affect on the output values by increasing the system from a perfect cube to a comically lopsided rectangle.

The value of the temperature gradient range was determined by first calculating the temperature gradient present existing in fuel rods that had undergone irradiation for both UO_2 and metallic uranium fuel. This temperature gradient was then transferred into the model by scaling the temperature gradient down to the length used in the model through comparison against the actual radius of the fuel. The maximum and minimum temperature values are implemented in the input file to initiate the temperature array as a gradient rather than a flat temperature profile. The other option would have been to add an additional term to the activation energy to account for the temperature gradient. The value for the temperature maximum and minimum values and thereby the temperature gradient was calculated from operating fuel data based off peak centerline temperature and wall temperature. The limitations of the computational resources prevented the entire distance from the centerline to fuel cladding wall from being modeled. The model would have to be scaled up to such a distance through improved computational capabilities.

In the implementation of the temperature gradient, a linear temperature gradient was designated across the entire mesh despite the inherent ‘saw-tooth’ effect that it

Figure 10

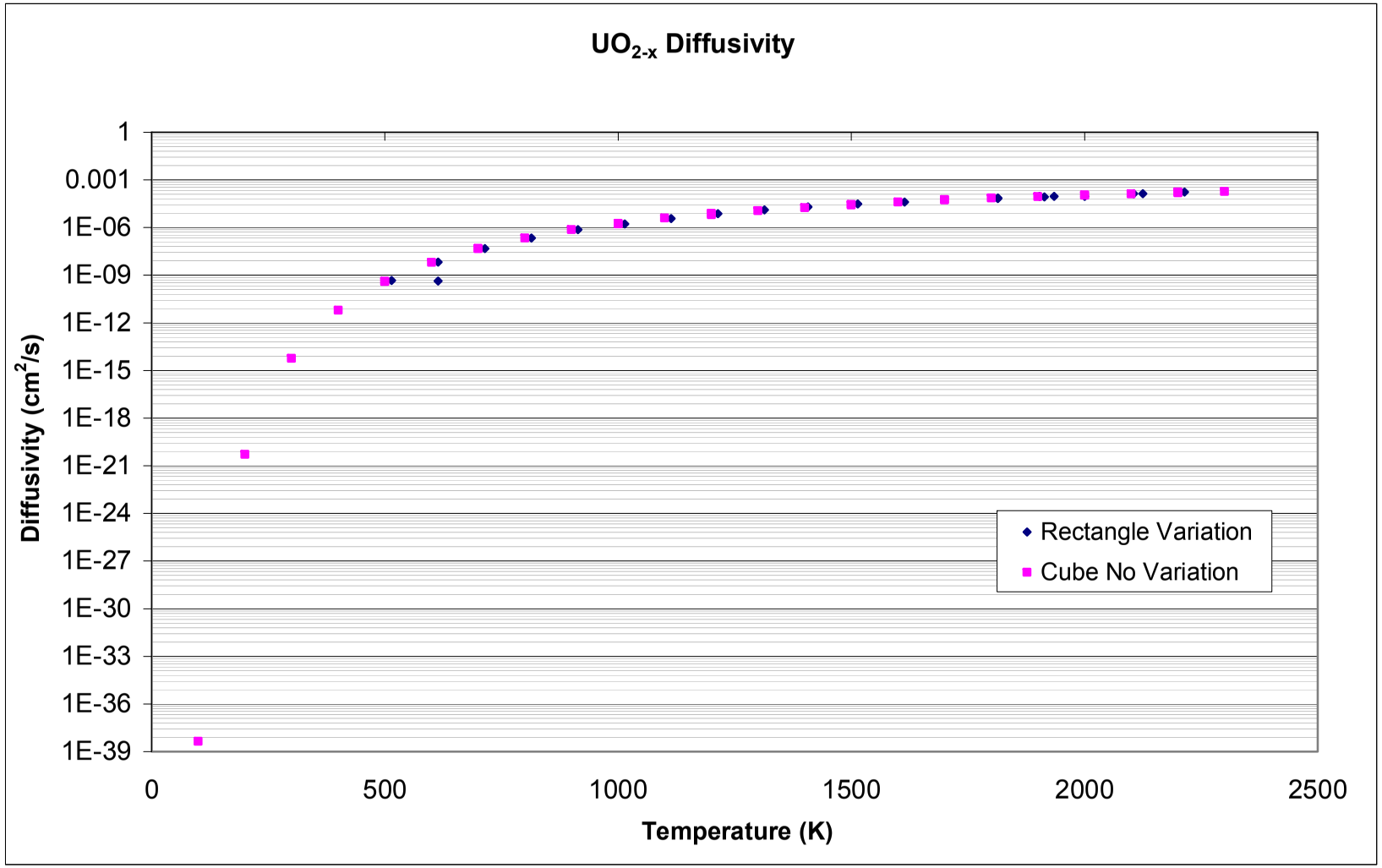

This figure compares the diffusivity for oxygen vacancies on the UO_2 anion sublattice between the 15x15x15 unit cell cube and the elongated rectangle model.

Figure 11

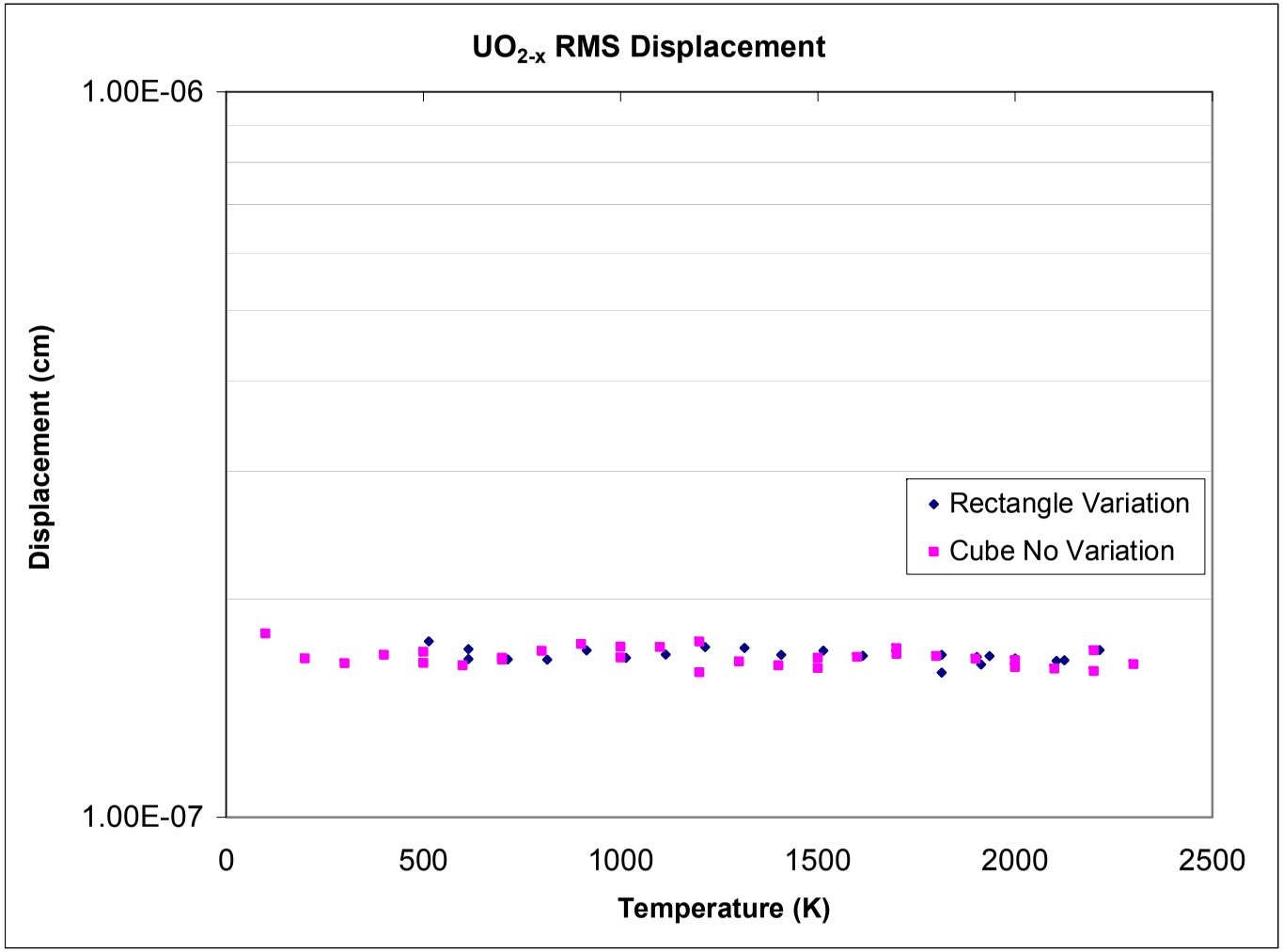

This figure compares the RMS displacement for oxygen vacancies on the UO_2 anion sublattice between the 15x15x15 unit cell cube and the elongated rectangle model.

Figure 12

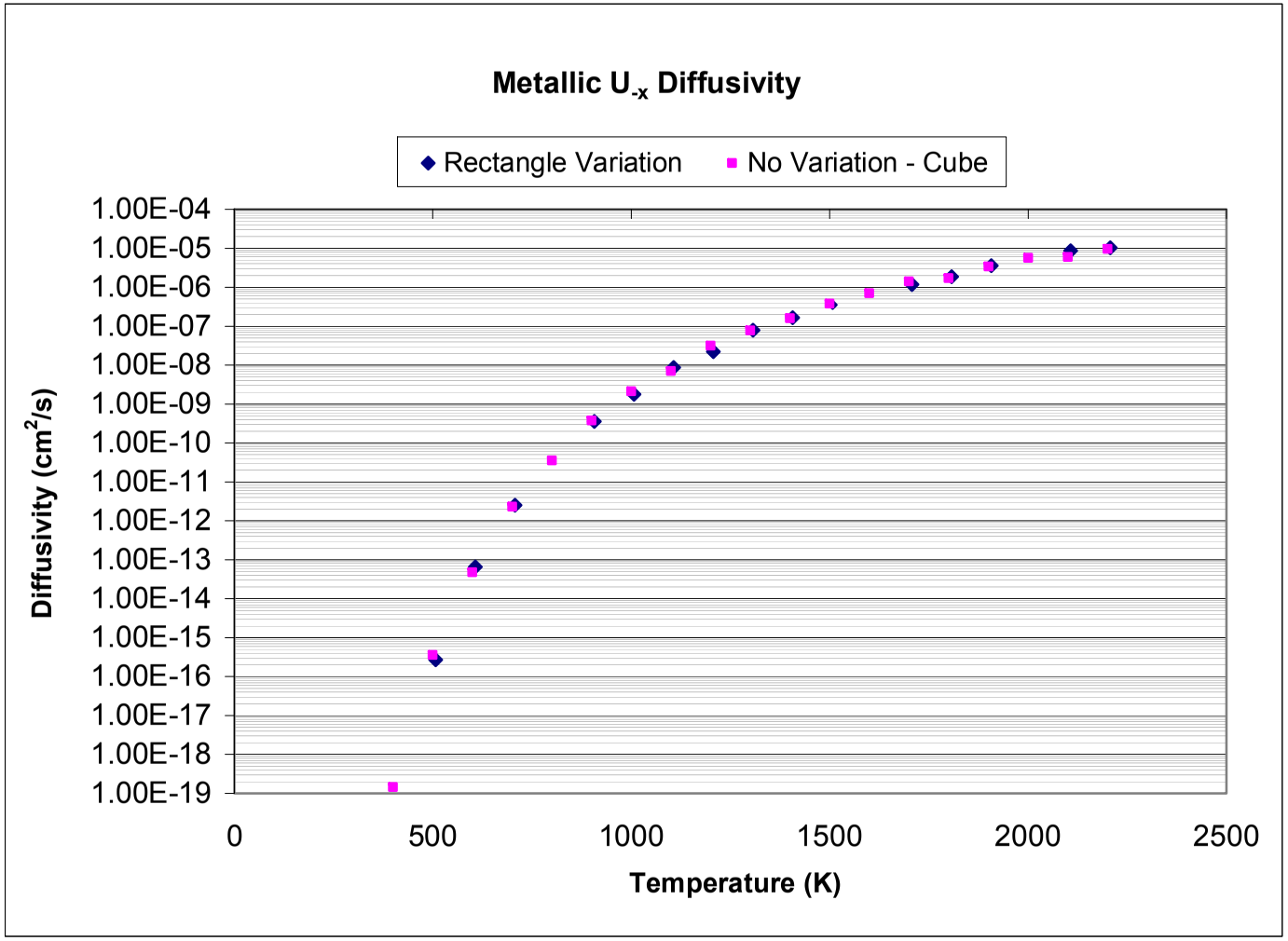

This figure compares the diffusivity for uranium vacancies in metallic uranium between the 15x15x15 unit cell cube and the elongated rectangle model.

Figure 13

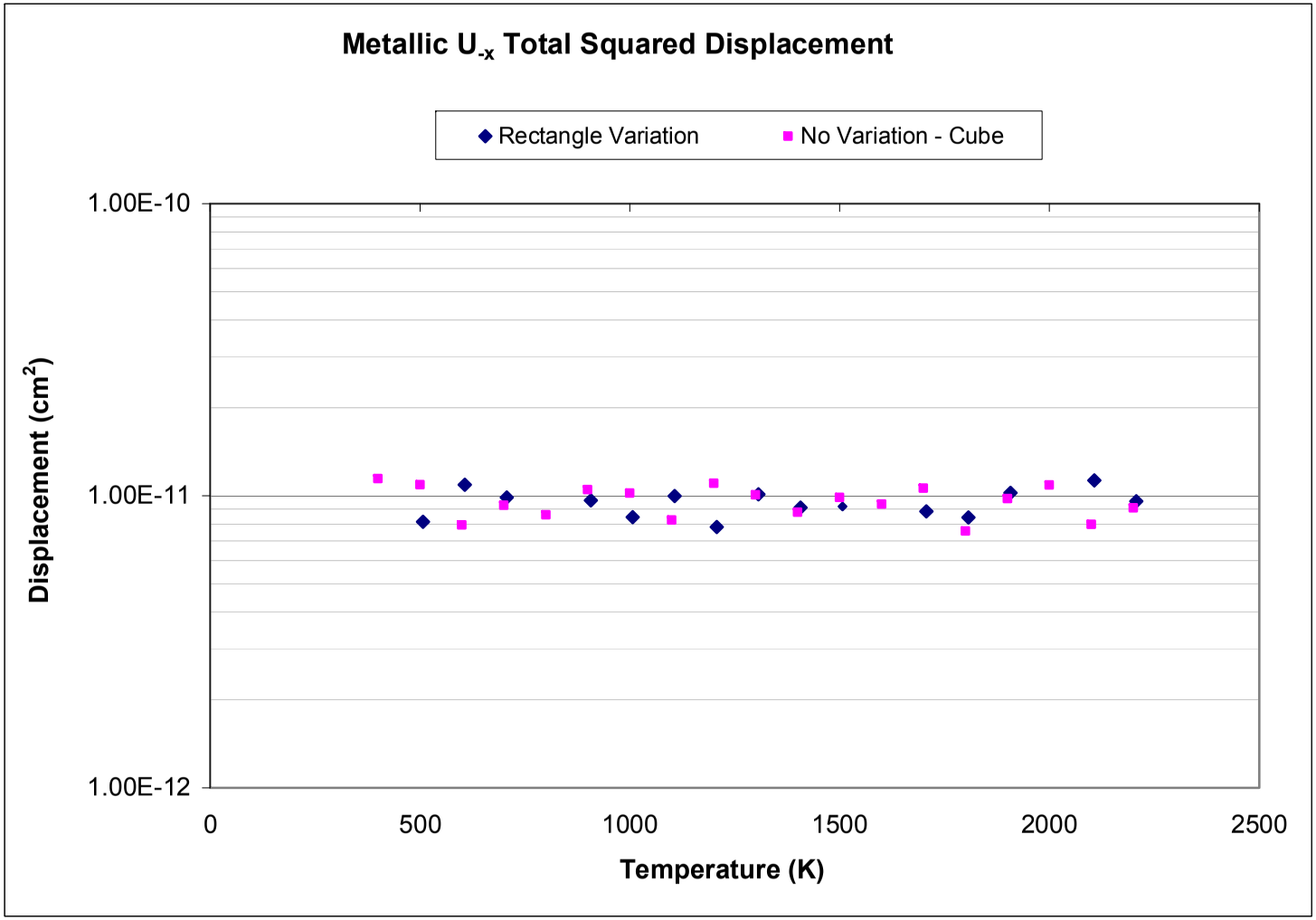

This figure compares the total squared displacement for uranium vacancies in metallic uranium between the 15x15x15 unit cell cube and the elongated rectangle model.

Table 1

UO_{2-x}

Equations of Best Fit Lines		
Type	Equation	R2 Value
Cube	y = 0.0072e-8341.7x	1
Rect	y = 0.011e-9075.4x	0.9815

This table shows that there is statistically no effect on diffusivity from enlarging the system from a 15x15x15 unit cube into an enlarged rectangle for the oxide system.

Table 2

U_{-x}

Equations of Best Fit Lines		
Type	Equation	R^2 Value
No Temp Variation	y = 0.0119e-15610x	0.9998
Temp Variation	y = 0.0143e-15942x	0.9998

This table shows that there is statistically no effect on diffusivity from enlarging the system from a 15x15x15 unit cube into an enlarged rectangle for the metallic system.

generated. This affect is present due to the periodic boundary conditions that exist in the model, which allow the small model to accurately simulate macroscopic bulk properties. The leading alternative method was to implement the high temperature value in the middle of the mesh grid and have all the boundaries at the same temperature – creating temperature humps across the system. There are two major disadvantages to this procedure. First, in order to have the proper temperature-gradient-delta value between fuel atoms, the maximum temperature would be half of the value that could be implemented into a full mesh gradient. Second, while the temperatures would be equivalent along the boundary, the derivatives would not be smooth throughout the mesh so there would still be discontinuities present. As such, this alternative process would have the same problem of cyclic temperature peaks and valleys and a discontinuous temperature derivative.

Every version of the model implemented periodic boundary conditions in order to simulate the behavior of the bulk material through the generation of an infinite lattice. As such, the size of the system did not necessarily need to be increased to model the material with the temperature gradient, however, this option was selected to maximize the temperature range present in the model, without distorting the temperature difference between neighboring fuel atoms.

There is no change in results with the implementation of the temperature gradient. The full range of temperature present in irradiated fuel cannot be obtained in the small system due to the cycling of the temperature values. Every period, the temperature values would cycle rather than continue its trend up or down. Even with an unrealistically large temperature gradient and significantly higher temperature deltas between fuel atoms, the

diffusion coefficient merely attains the value associated with the average of the temperature gradient's input values. This much larger temperature-delta is more analogous to a transient situation rather than steady-state operations. The implementation of the temperature gradient does increase the diffusion coefficient compared to a flat trial at the lower temperature without the gradient present.

A temperature gradient can act as a driving force on a material, causing thermal diffusion, especially when a concentration gradient is not present. Thermal diffusion transfers material from hot to cold regions. Even if there is only Brownian Motion present, the higher temperature values will cause a higher jump frequency in the hot zone that will garner a larger rate of transport to the cold zone than the cold zone can generate back to the hot region [1]. This results in the thermal flux from hot to cold and helps to explain why the central void forms in oxide fuel.

METALLIC FUEL MODEL

In addition to this uranium dioxide model, there is another model that consists of uranium interstitials and vacancies in a bcc metallic uranium lattice to model the gamma phase. The vacancy and interstitial concentrations varied from 1 part per thousand (~0.044% or three total species for this system size), 1%, 5%, 10%, and 20%. The results of this variation can be seen in Figures 14-17. Figures 14 and 16 show that the diffusivity calculated was unchanged even as the concentration of interstitials and vacancies varied, while Figures 15 and 17 show that as the concentration of interstitials and vacancies increased, the RMS displacement decreased.

Figure 14

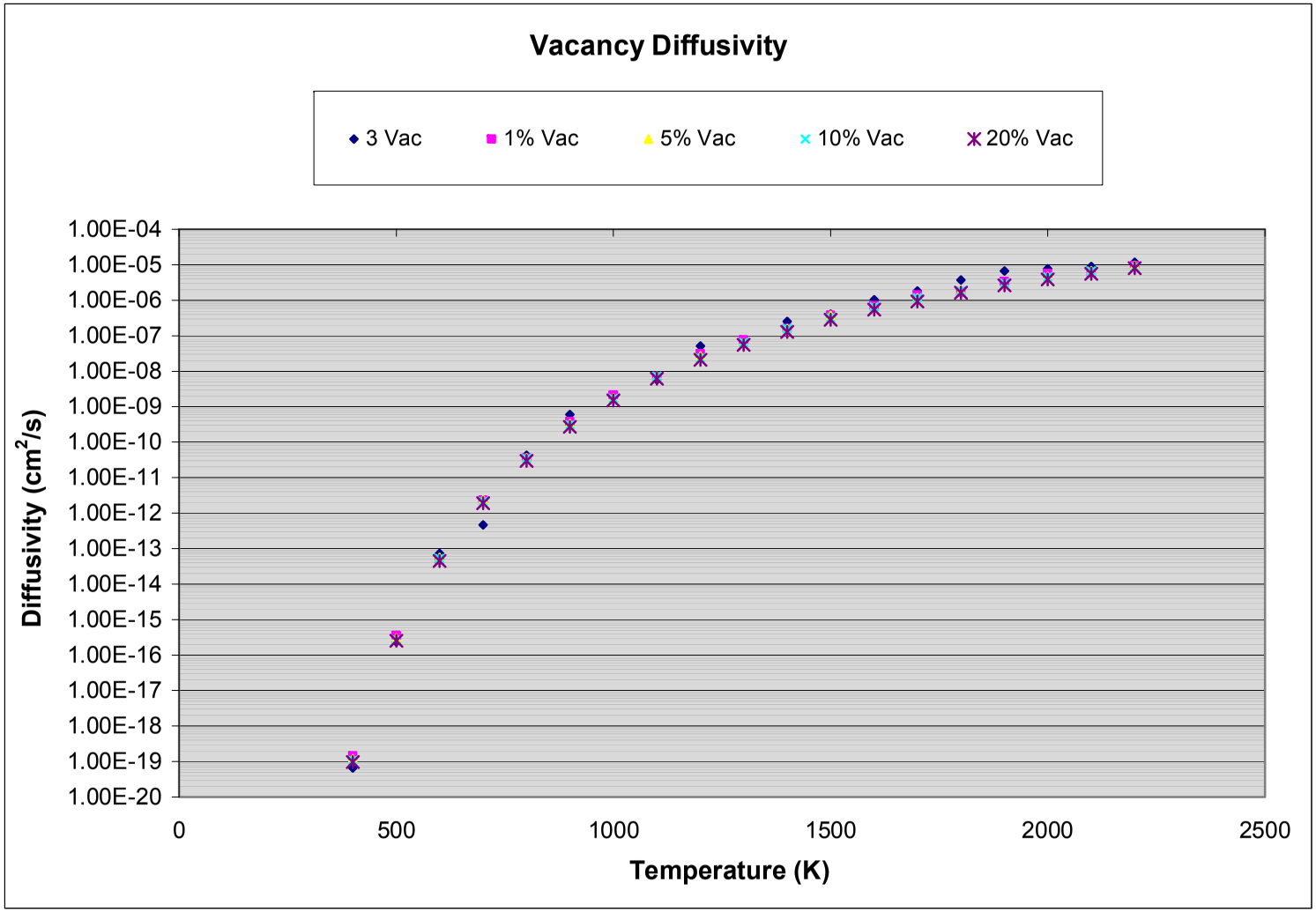

This figure shows the diffusivities of uranium vacancies in metallic uranium as the concentration of vacancies present varies.

Figure 15

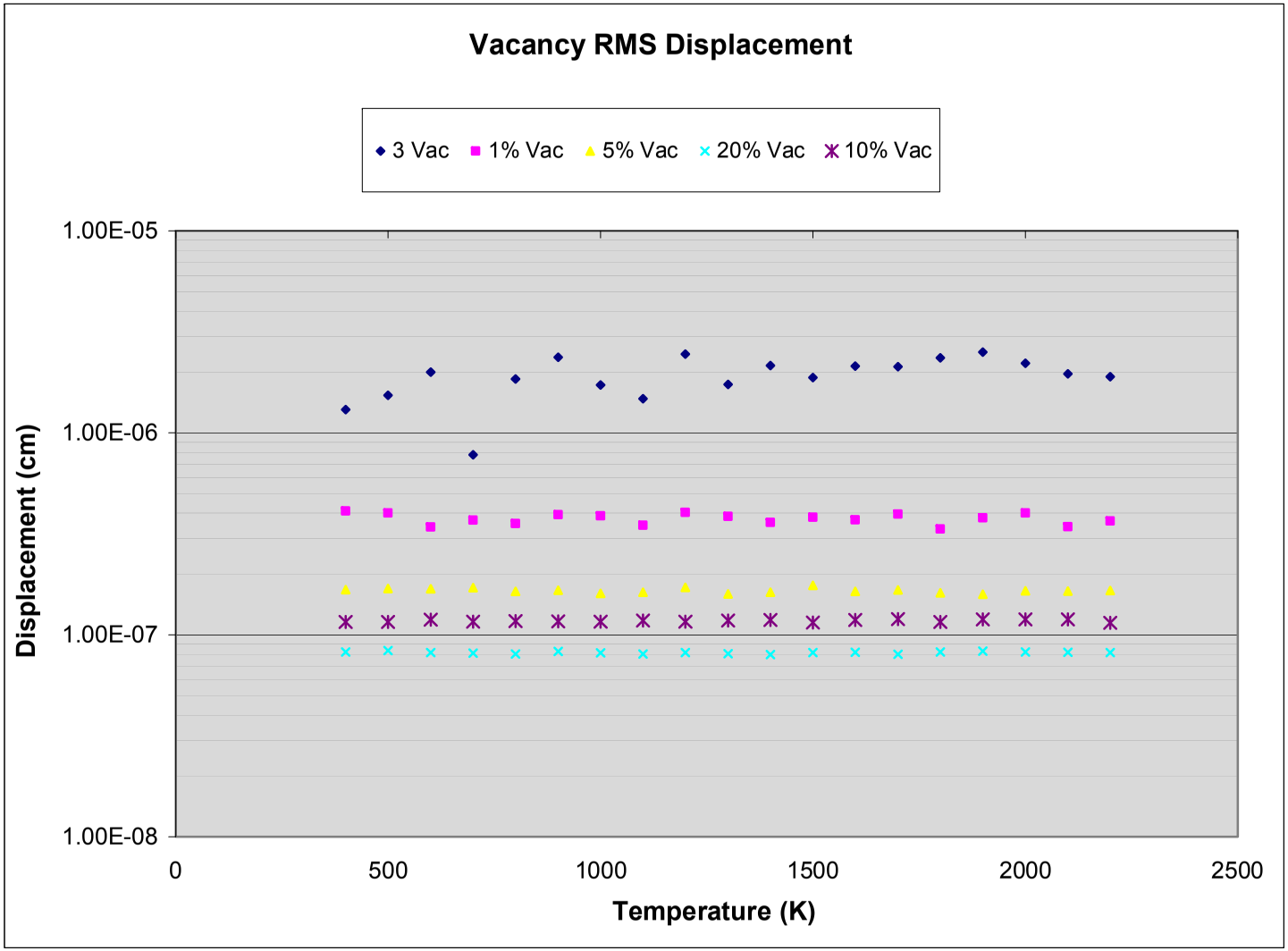

This figure shows the RMS displacement of uranium vacancies in metallic uranium as the concentration of vacancies present varies.

Figure 16

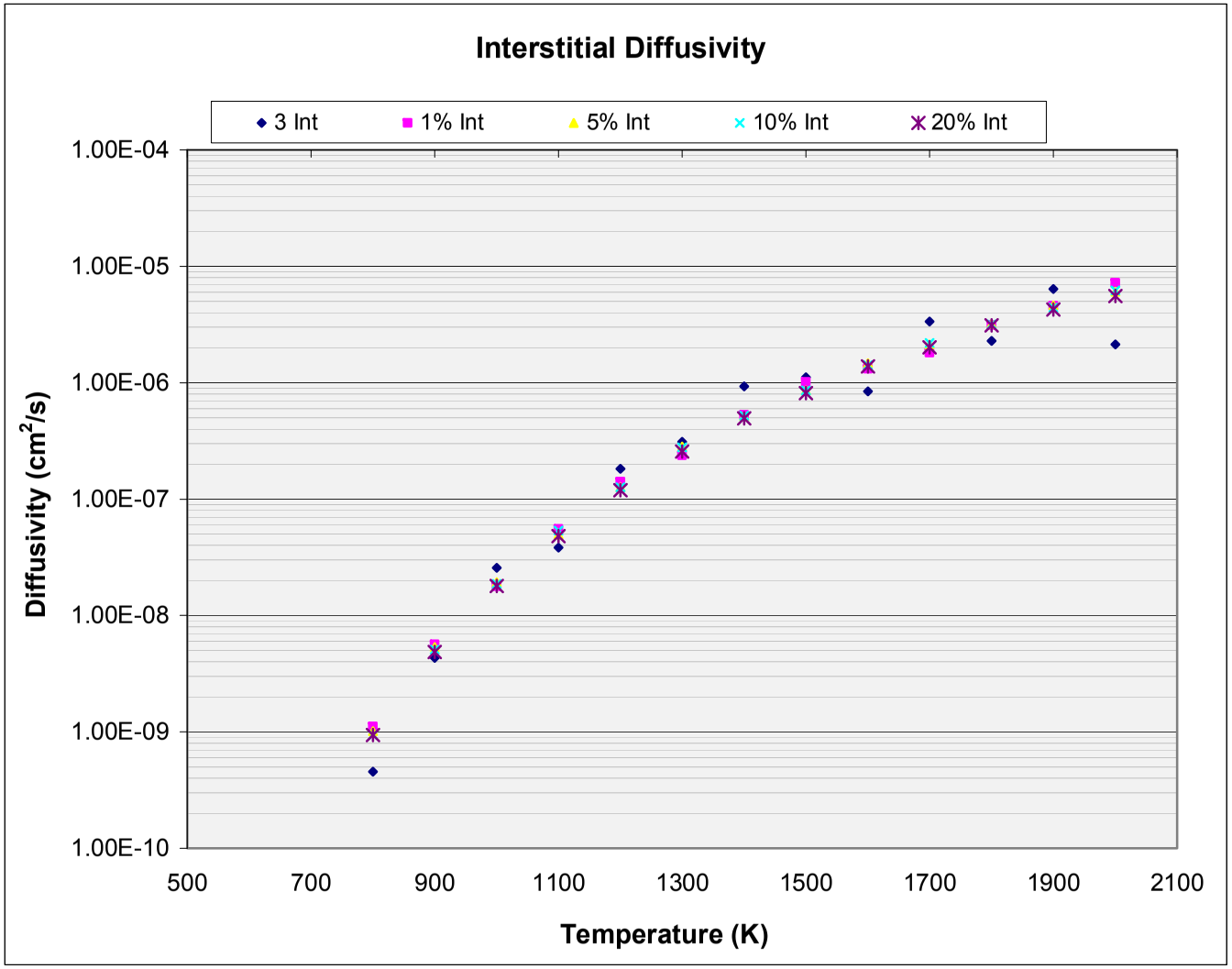

This figure shows the diffusivities of uranium interstitials in metallic uranium as the concentration of interstitials present varies.

Figure 17

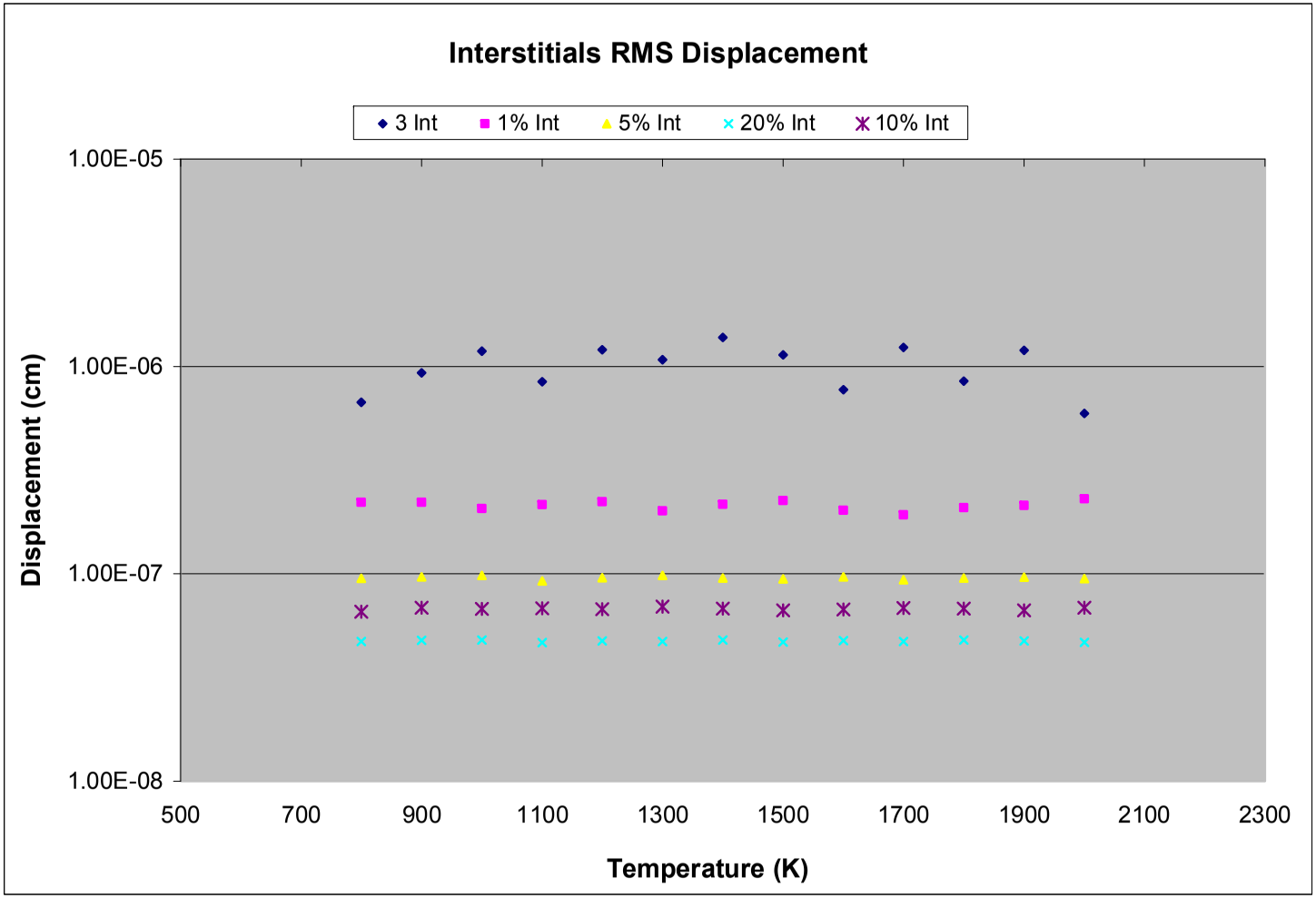

This figure shows the RMS displacement of uranium interstitials in metallic uranium as the concentration of interstitials present varies.

In this work, more vacancies mean fewer atoms in the lattice while the total number of lattice locations remains constant. Less atoms in the simulation result in fewer time steps for migration, hence there are fewer opportunities for movement. Therefore, the RMS displacement decreases, however, the diffusivity remains constant since the time also decreases maintaining the previous diffusivity value. Furthermore, there is no interaction between the vacancies to cluster and inhibit movement. Until the vacancies interact, there will be no change in diffusivity of the model. If a blocking mechanism was not implemented in the code, clustering of vacancies into voids could occur that would have an affect on the diffusivity.

As shown in Tables 3 and 4, and Figures 14 and 16 there is no change in the diffusivities. Tables 3 and 4 show the equations of the exponential trendlines in the form of Equation 3.8 for the variation of vacancies and interstitials respectively. While it is true that there is some change in the component values in Tables 3 and 4 as they relate to Equation 3.8, there is wide variation in experimentally determined diffusion coefficients [22, 37]. Investigations of gas atom migration in oxide fuel yielded values that vary widely, covering multiple orders of magnitude. These points highlight the non-unique parameters in the solutions chosen to fit a particular set of data. Additionally, the results generated are directly tied to the migration values or activation energies. Slight manipulation of those values could dramatically effect the results show different representations of reality. It is for this reason that it was imperative to attain accurate values.

It is worth noting that the full temperature range was undertaken as a comparison to the oxide system that has a much larger temperature range. Metallic fuel has a peak

Table 3

Vacancy Concentrations

	Equation	R^2
20%	y = 0.0096e-15651x	1
10%	y = 0.0114e-15683x	1
5%	y = 0.0114e-15632x	1
1%	y = 0.0119e-15610x	0.9998
3 Vac	y = 0.0235e-16209x	0.9975

This table shows that the diffusivities of the vacancies in metallic uranium are statistically the same even as the concentration of those vacancies varies widely.

Table 4

Interstitial Concentrations

	Equation	R^2
20%	y = 0.0019e-11605x	0.9999
10%	y = 0.0021e-11645x	0.9999
5%	y = 0.002e-11584x	0.9998
1%	y = 0.0019e-11505x	0.9985
3 Vac	y = 0.0023e-11860x	0.9674

This table shows that the diffusivities of the interstitials in metallic uranium are statistically the same even as the concentration of those interstitials varies widely.

operating temperature usually around 1060K and melts around 1350K. As such, the code results at higher temperature are likely to be erroneous when compared to experimental values since the inherent limitations of the model do not allow the fuel to melt thereby generating non-physical results.

INTERSTITIAL SENSITIVITY STUDY

A literature review was undertaken to determine what migration energy/activation energy should be used in the kMC simulations. Unfortunately, the value for interstitial migration energy varies widely as it did for vacancy migration energy. In fact, even after removing some of the outliers, there still existed a conservative range of 0.8 eV to 1.3 eV. This conservative range was modeled using intervals of 0.1 eV for both the fifteen unit cell cubes and the rectangles under identical conditions besides the aforementioned obvious variation. The results of this sensitivity study are shown in Figures 18-21. Figures 18 and 20 show the diffusivities of the different migration energy values for UO_{2+x} and metallic U_{+x} respectively while Figures 19 and 21 show the square of the total displacements for UO_{2+x} and metallic U_{+x} respectively. In Tables 5 and 6, the equations of best fit for the exponential trendlines are compared using the method of Equation of 3.8 to show that while there is not a significant difference between the fifteen unit cell cube system and the rectangular system, there is a significant difference in the results as the migration energy varies. The calculations are actually very sensitive to this parameter as shown in the tables and figures.

Figure 18

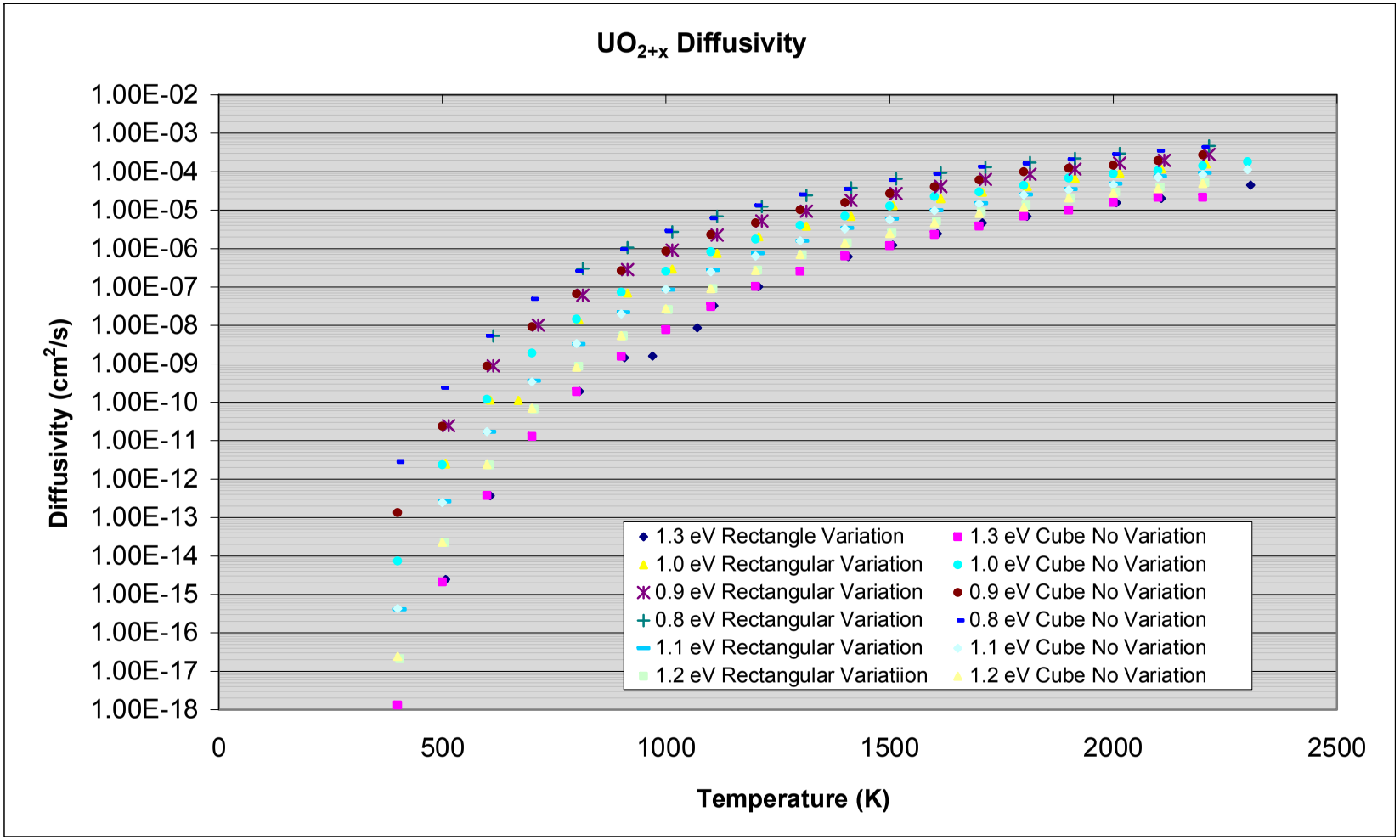

This figure shows the diffusivity results from a sensitivity study of migration energy values for the oxygen interstitials in uranium dioxide.

Figure 19

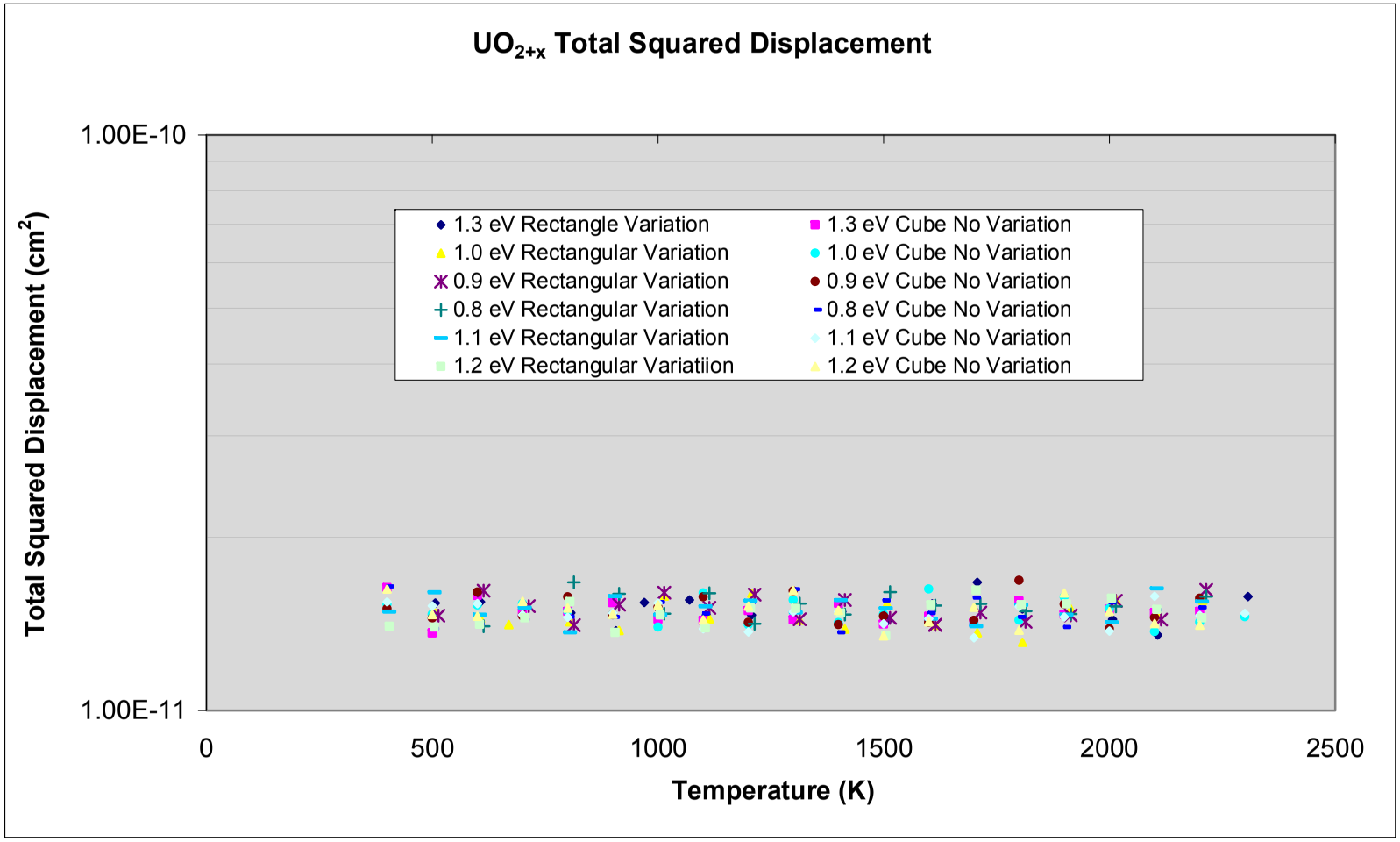

This figure shows the total squared displacement results from a sensitivity study of migration energy values for the oxygen interstitials in uranium dioxide.

Figure 20

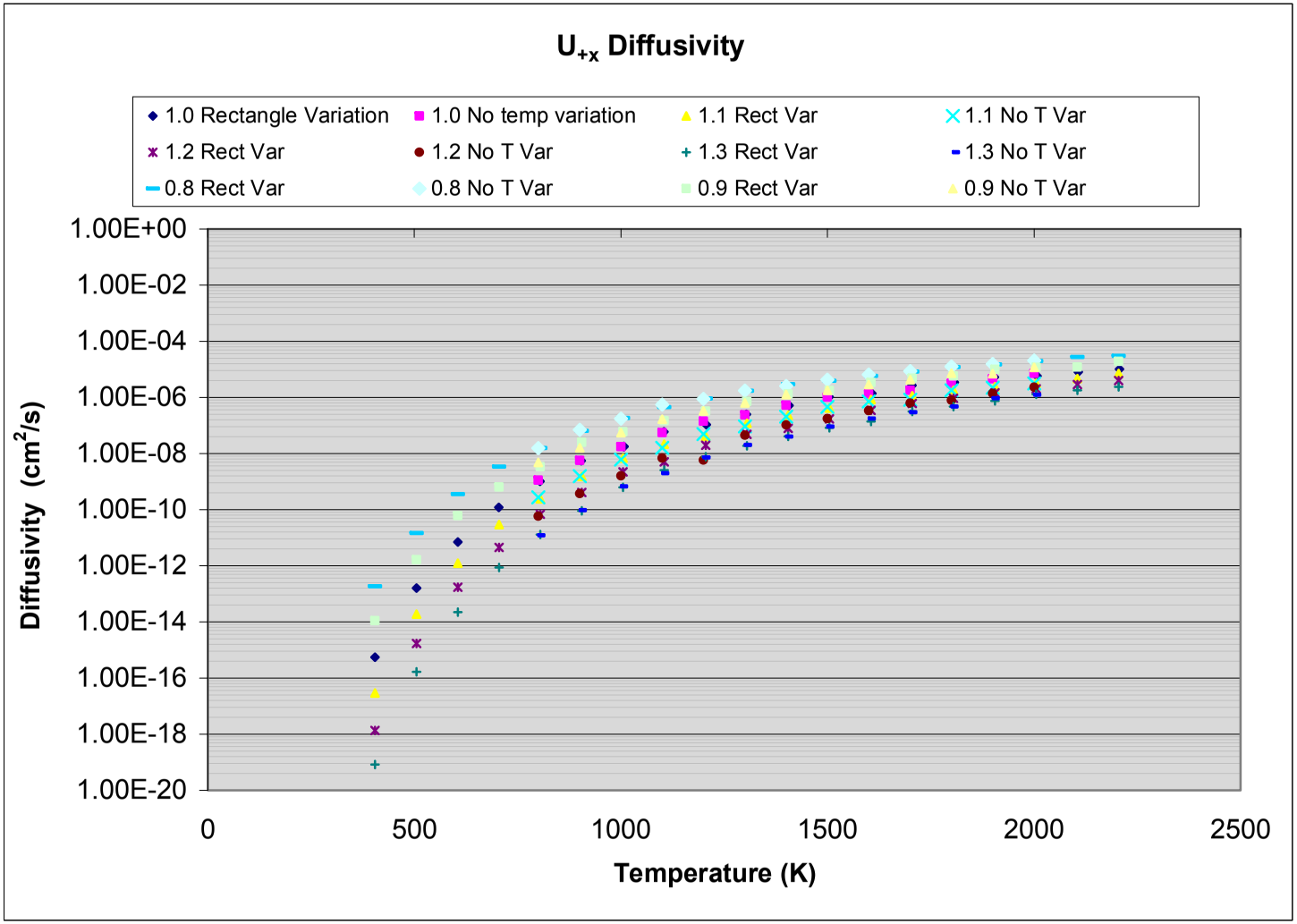

This figure shows the diffusivity results of a sensitivity study of migration energy values for uranium interstitials in metallic uranium.

Figure 21

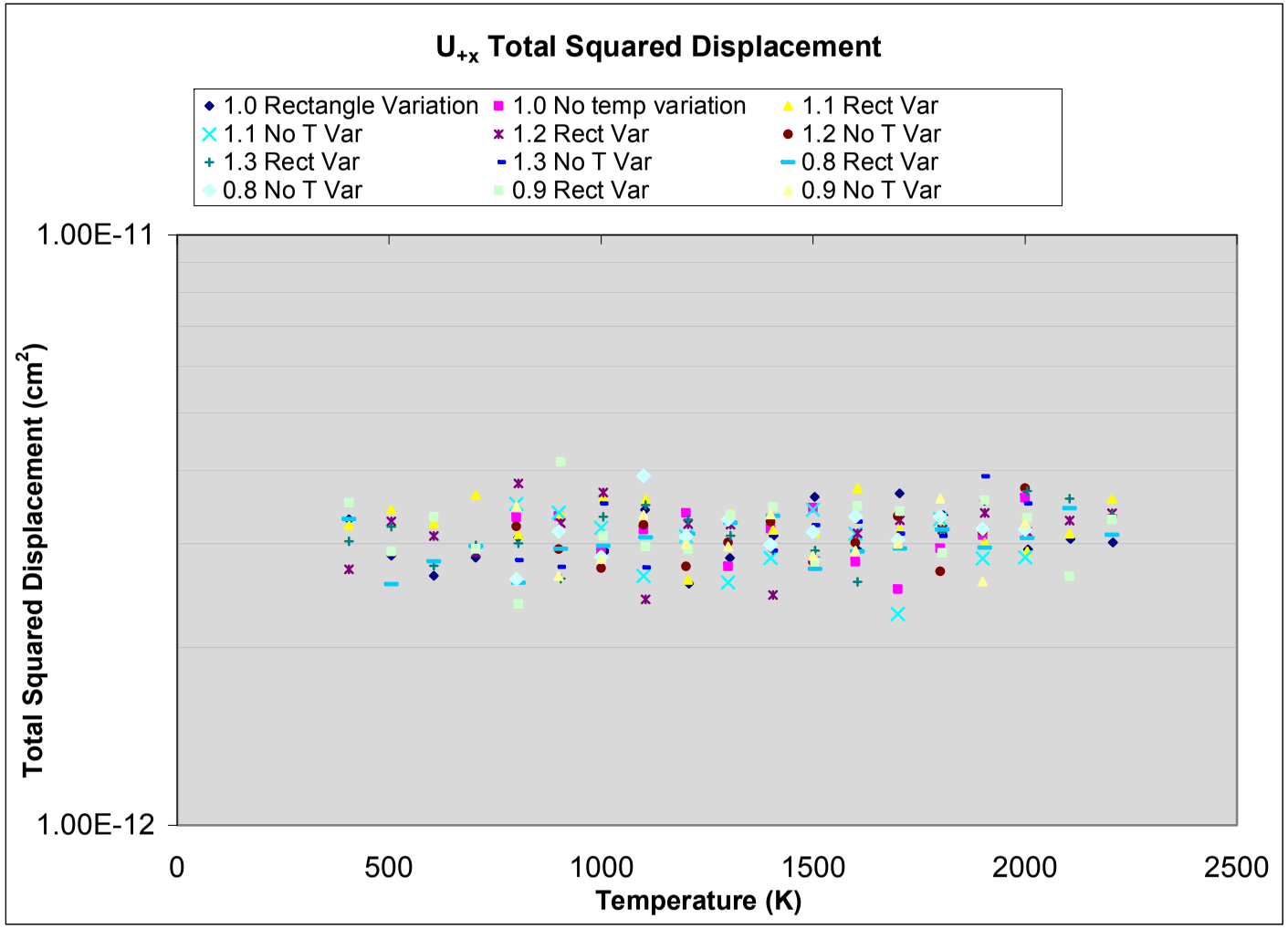

This figure shows the total squared displacement results of a sensitivity study of migration energy values for uranium interstitials in metallic uranium.

Table 5

Metallic U_{+x}

	Equation of Best Fit	R^2
1.0 Cube No Var	y = 0.0019e-11505x	0.9985
1.0 Rect Var	y = 0.0023e-11793x	0.9998
1.1 Cube No Var	y = 0.0016e-12513x	0.9985
1.1 Rect Var	y = 0.0023e-12913x	0.9998
1.2 Cube No Var	y = 0.0022e-14115x	0.9901
1.2 Rect Var	y = 0.0024e-14151x	0.9998
1.3 Cube No Var	y = 0.0026e-15350x	0.9994
1.3 Rect Var	y = 0.0024e-15346x	0.9999
0.9 Cube No Var	y = 0.002e-10449x	0.9983
0.9 Rect Var	y = 0.0022e-10579x	0.9995
0.8 Cube No Var	y = 0.0024e-9441.4x	0.9985
0.8 Rect Var	y = 0.0022e-9458.6x	0.9998

This table shows the effect on diffusivity for changing the migration energy barrier height for interstitials in the metallic system.

Table 6

UO_{2+x}

Energy	Type	Equation of Best Fit	R^2
0.8	Cube	y = 0.0287e-9269x	0.9999
0.8	Rect	y = 0.0348e-9572.2x	0.9997
0.9	Cube	y = 0.0292e-10438x	0.9999
0.9	Rect	y = 0.0342e-10756x	0.9998
1	Cube	y = 0.0287e-11590x	0.9999
1	Rect	y = 0.0377e-12124x	0.9941
1.1	Cube	y = 0.0278e-12731x	1
1.1	Rect	y = 0.0325e-12930x	1
1.2	Cube	y = 0.0282e-13890x	1
1.2	Rect	y = 0.0341e-14163x	1
1.3	Cube	y = 0.027e-15031x	0.9999
1.3	Rect	y = 0.031e-15384x	0.9976

This table shows the effect on diffusivity for changing the migration energy barrier height for interstitials in the oxide system.

COMPARISON OF SYSTEMS

Figure 22 shows the comparison of CeO_2 with and without La, UO_2, and U diffusivity plots with a vacancy concentration at 1%. This figure shows that in contrast to varying the concentration of vacancies or interstitials, modifying the species in the simulation itself does have an effect on the diffusivities with the CeO_2 system having the highest diffusivity values at a given temperature and the metallic uranium having the lowest diffusivities for any given temperature value. This result is not unexpected as the free migration velocity for oxide fuel is much greater than that of metallic fuel. The higher thermal conductivity reduces the maximum fuel temperature and temperature gradient in the fuel, thereby lowering the free migration velocity [1]. It should be noted that the metallic fuel should have a higher diffusivity than the diffusivity in oxide fuels if the comparison was uranium vacancies to uranium vacancies and not the oxygen vacancy diffusivity for oxide fuels and uranium vacancy diffusivity in metallic fuel [26].

Figure 23 shows this comparison with respect to the RMS displacement instead of the diffusivity. The Lanthanum has a big effect at lower temperatures, though at higher temperatures the effect is far less. Without the Lanthanum present, the CeO_2 and UO_2 systems appear nearly identical while the metallic uranium system has a RMS displacement value orders of magnitude higher. This is in stark contrast to the diffusivities where metallic uranium is much lower than the other systems. RMS displacement and total squared displacement are directly correlated so by application of Equation 3.5, the number of time steps required for the metallic system must be significantly greater than those of the oxide system. Whereas, the CeO_2 system uses less timesteps than the UO_2 system since both have about the same displacement values but different diffusivities.

Figure 22

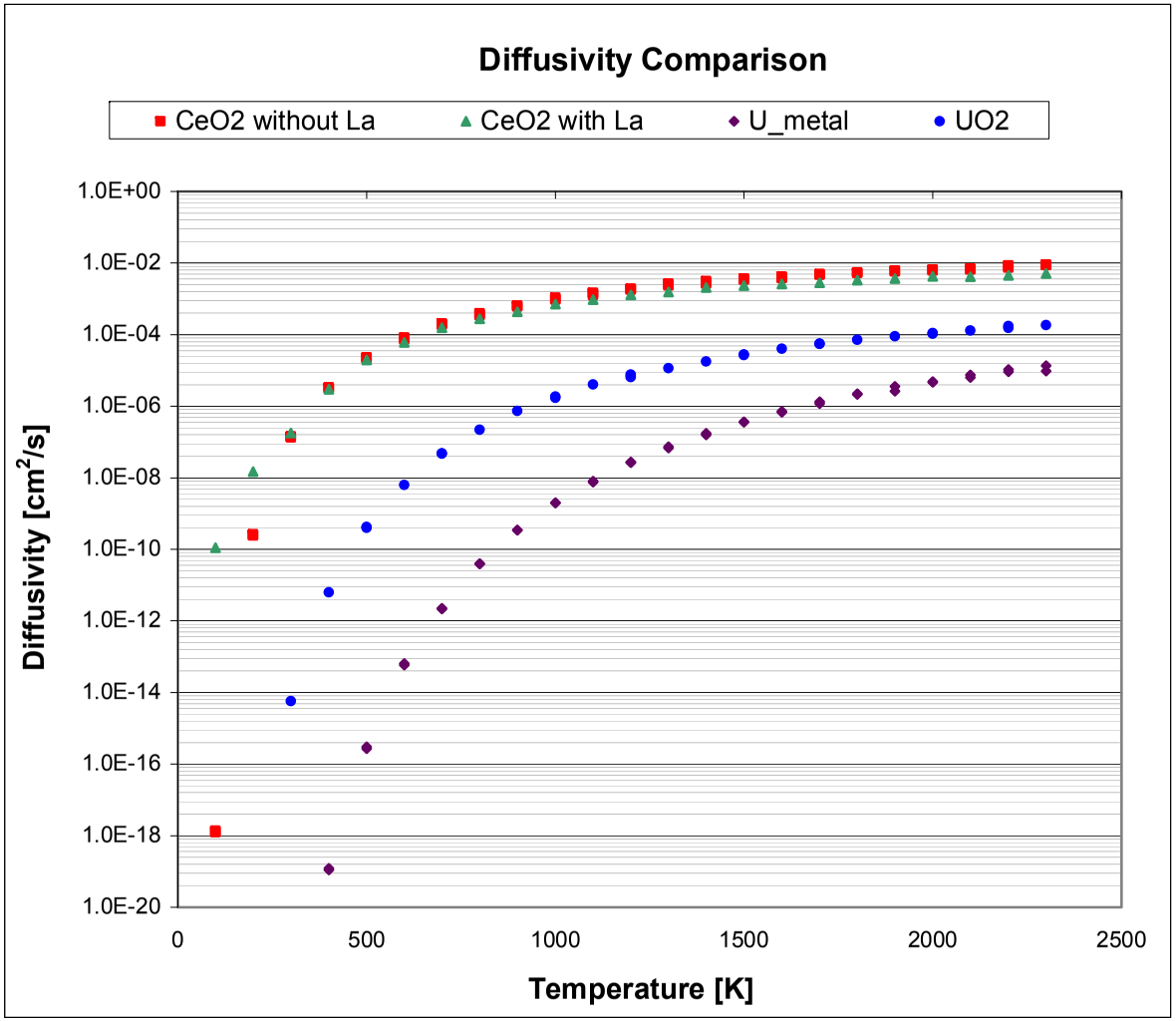

This figure compares diffusivities between 1% oxygen vacancies in oxide systems and 1% uranium vacancies in the metallic uranium system.

Figure 23

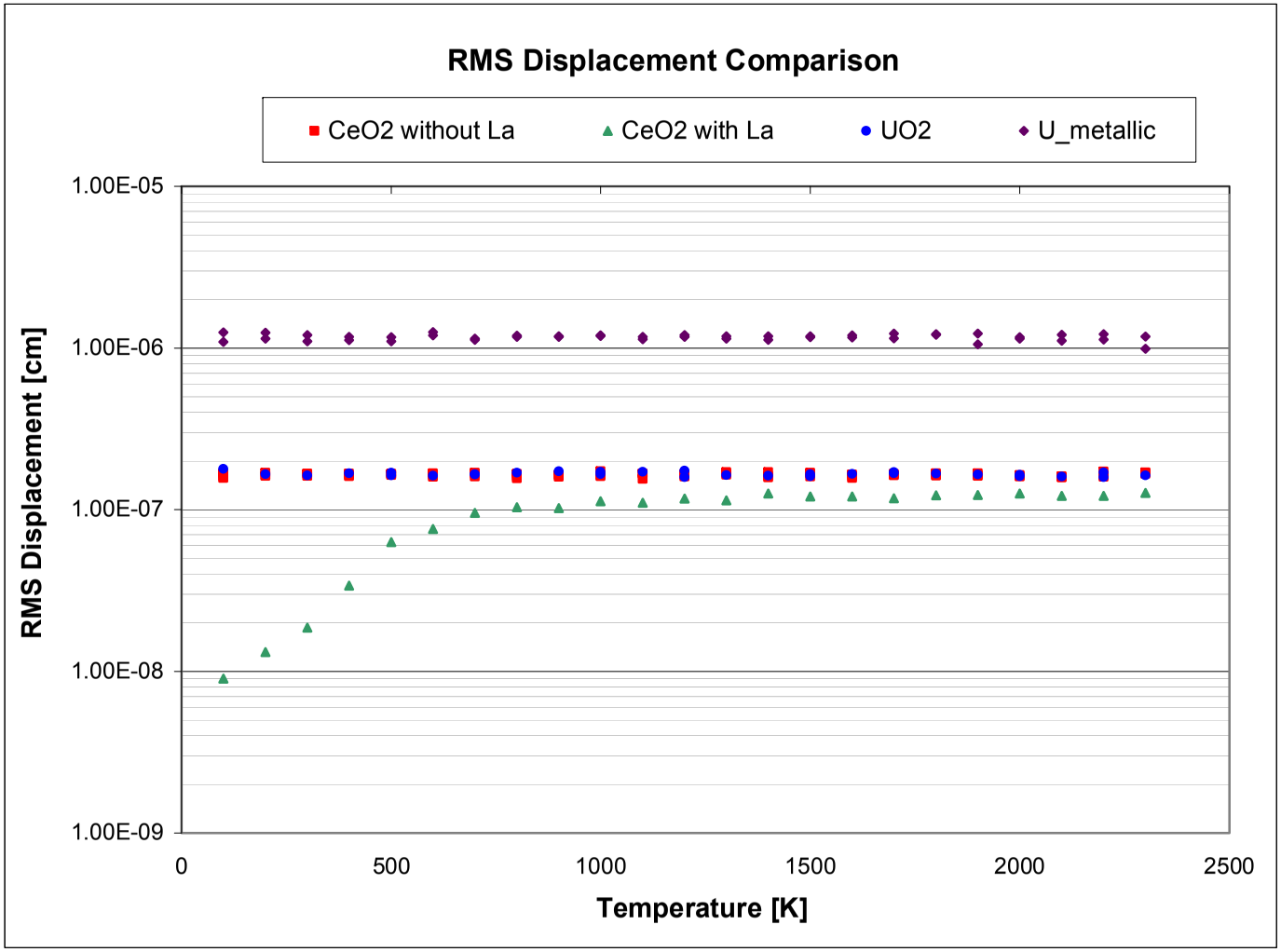

This figure compares RMS displacements between 1% oxygen vacancies in oxide systems and 1% uranium vacancies in the metallic uranium system.

Figures 24 and 25 show a comparison of interstitials to vacancies as concentrations of these species vary in the metallic uranium system. The vacancies show a higher displacement across the board while the interstitials maintain a higher diffusivity. This higher diffusivity of interstitials is expected, as the activation/migration energy for interstitials is lower than that of vacancies.

Figure 24

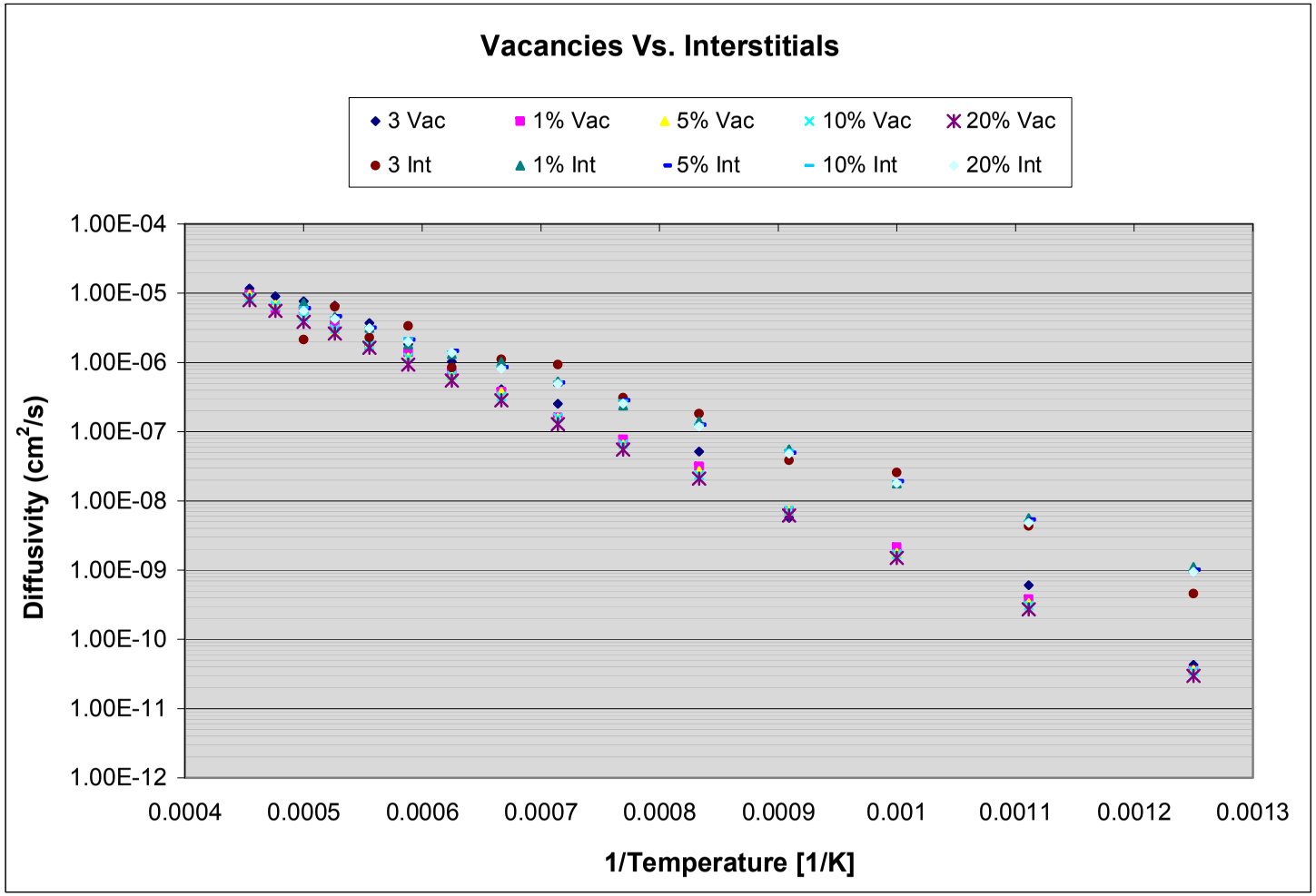

This figure shows the comparison of diffusivity between uranium vacancies and uranium interstitials in the metallic uranium system as the concentrations of those species vary.

Figure 25

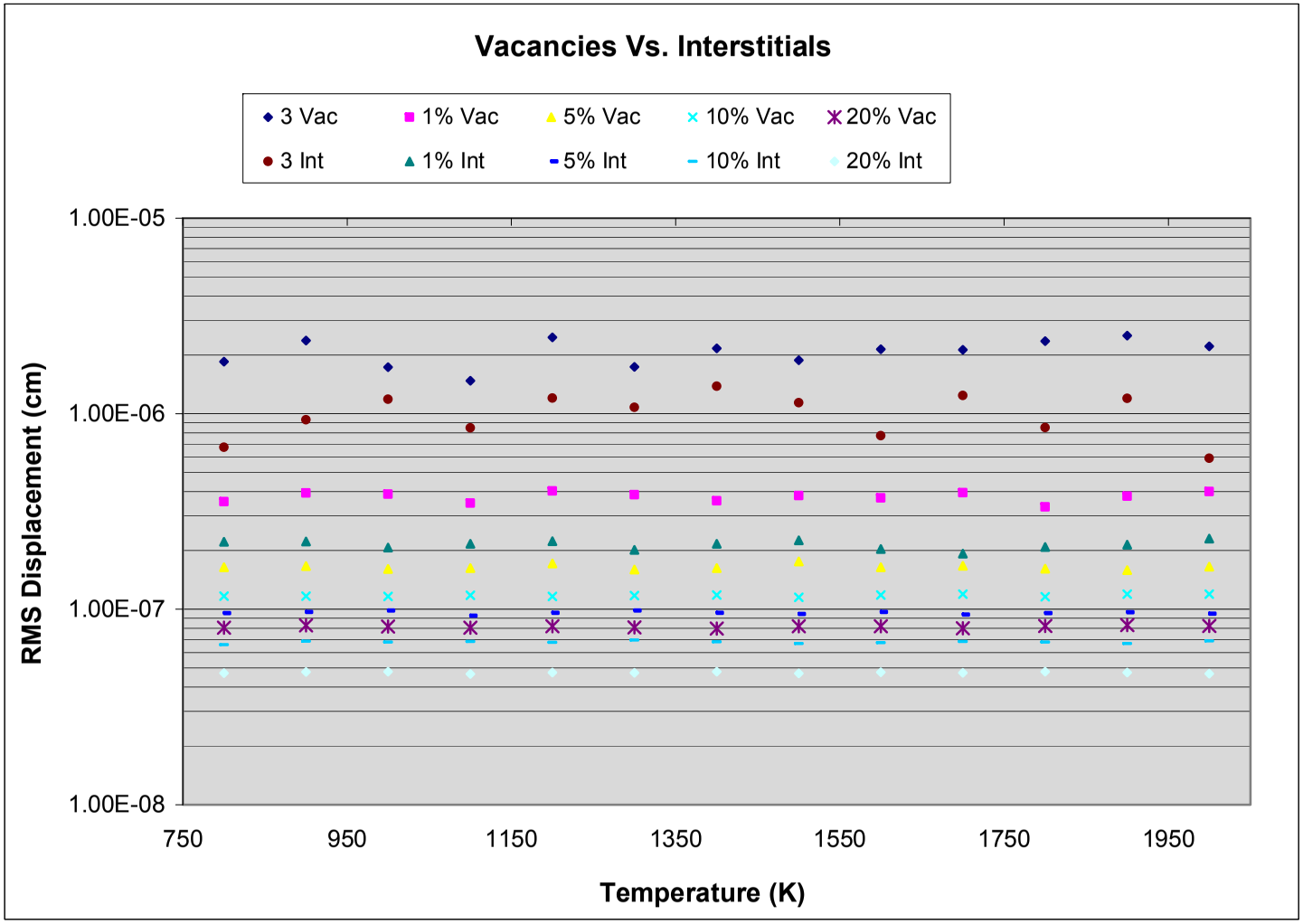

This figure shows the comparison of RMS displacement between uranium vacancies and uranium interstitials in the metallic uranium system as the concentrations of those species vary.

CHAPTER 4

MOLECULAR STATICS

GULP INTRODUCTION

The kMC code would be improved by increasing the types of events possible in the event catalog. Specifically through the addition of clustering and dissociation events that would allow the code to model void and cluster development in a scalable fashion. Unfortunately, a literature review showed that the potentials available were not acceptable for the task at hand. Therefore, new potentials were found through molecular static calculations because the quality of results generated in the kMC code are critically linked to the quality of the potentials used to describe the physical processes involved in the event catalog.

The General Utility Lattice Program (GULP) [43] creates and runs atomistic solid state simulations. Before running a defect energy calculation, the lattice system must be optimized under constant pressure, volume, temperature, and number of atoms. The calculation is undertaken through the relaxation of all atoms contained in the simulation. This relaxation is needed to offset the local disturbance created by the defects. Therefore, the enthalpy variation directly correlates to the internal energy variation.

The GULP code allows for lattice relaxation to occur to find not only the separation distance for the lattice under ideal conditions but also with defects. After determining the correct structure for the case under investigation, the code calculates the defect energy of the system. It is through the comparison of this defect energy that the activation energy barrier for migration is determined. Sample input files are found in Appendix A.

METHODS FOR COMPUTING DEFECT ENERGY

There are two methods for computing defect energies through molecular statics calculations. The first is the Mott-Littleton method (Catlow and Mackrodt 1982) that is based on separating the region into two concentric regions centered on the defect. In the first region, interactions are calculated using Born-Mayer-Huggins potentials. Outside this region, the interactions are not calculated. Molecular statics calculations routinely ignore interactions when the interatomic distances exceed a certain cut-off distance.

In the second method, the macroscopic solid is represented by a supercell (Leslie and Gillan, 1985) with periodic boundary conditions that generate an 'infinite' system eliminating surface effects. In this method, the defects have their own periodic images that could influence the other defect calculation through elastic and electrostatic interactions that can be mitigated though not ignored through careful selection of the energy cut-off distance. While these two methods are distinct, Leslie and Gillian, 1985, showed that when the supercell is large enough and a corrective term is applied for charge defects to account for the Madelung energy between defects and their periodic images, the two methods produce results within a hundredth of an electron volt. The Madelung energy term is a necessity since the electrostatic interactions between charged defects are very long-range phenomena that would require a prohibitively large supercell size [44].

The atomic configurations used in this work were a 3x3x3 supercell that consists of twenty seven unit cells for a total of 324 atoms, and a 4x4x4 supercell that consists of sixty four unit cells for a total of 768 atoms. This larger supercell configuration is an additional proof that the 3x3x3 supercell is sufficient to show accurate results. This selection is also

reinforced by literature, most prominently the Morelon paper [44], which was used for validation. Additionally, specific energy cut-offs were used since the GULP code automatically implements the Mott-Littleton method with defect calculations. The GULP code uses periodic boundary conditions. As such, either a very fine cut-off radius is required or a supercell is needed to prevent defects from interacting with each other. With the supercell, a larger allowance is given for the cut-off radius to prevent potential energy interactions from occurring as there is a larger distance between defect sites. This work uses the supercell method in addition to the Mott-Littleon method.

CALCULATION OF FINAL DEFECT ENERGY

Defects are put directly into the lattice structure to model the migration of a vacancy between two lattice locations. Both lattice locations are given vacancies and then an interstitial atom, of the same species as the vacancy in the lattice, is placed at a fixed position between the two vacancies. Through moving the interstitial position between the two lattice points containing vacancies, the affect of a single vacancy migrating between the two lattice positions is attained.

The activation energy is the difference between the ground vibrational state and the activated vibrational state – the atom or interstitial spends the majority of its time vibrating in the ground vibrational state known as the equilibrium position [1]. If the initial vibrational state and the final vibrational state are equal and symmetric, then the activation energy barrier to move from one lattice location to the other is equivalent to the reverse migration back to the original lattice location that the first migration step originated from. This translates into the kMC simulation as the activation energy for migration is independent of

the physical start or end locations of the jump since the barrier height imposed is identical regardless of orientation. In asymmetric systems, such as the migration next to an existing defect, this symmetry is not the case. As such, a different energy is needed for the clustering jump than the dissociation jump as the barrier heights and therefore the activation energy and hence the probabilities of the event occurring via the event catalog are not the same.

These potential energies are calculated based on the principle of cohesive energy in solids. Cohesive energy compares the states of a collection of atoms that differ only in the separation distance between the atoms. As the atoms are brought together from infinite separation, the energy decreases initially as the atoms attract each other, however, once the atoms become very close together a different result can be seen. The energy reaches a minimum value before sharply increasing under extremely close separation. The magnitude of this energy curve is the cohesive energy and the position denotes the separation distance for the solid [1]. Rather than bring the atoms together from an infinite separation distance as prescribed under the theory of cohesive energy in solids, the maximum separation distance is set at finite number ~12 Angstroms.

POTENTIALS

There are two categories of potentials: the rigid-ion and the shell models. The shell potential model accounts for atomic polarization effects in a simplified method while the rigid-ion potential model considers the ions to be non-deformable. The rigid-ion potential model was selected for multiple reasons including maintaining consistency with Morelon [44] as the simple single oxygen vacancy migration results were validated against Morelon [44] for benchmarking purposes. The rigid-ion potential model is a simplification of the

polarizable shell potential model that has been modified (Walker-Catlow 1981) to reproduce the grid parameters and static dielectric constant correctly. Rigid-ion potentials were used for the calculations rather than the shell potential model. The shell potential model includes the electron shells as springs, while the rigid-ion potential model only uses the nuclei. Rigid-ion potentials deemed to be just as accurate and significantly faster computationally. The pair potentials are different for each atomic pair. The uranium-oxygen interactions is governed by the standard form of the pair potentials, which is the addition of the Buckingham form to the Coulomb potential, $\frac{q_i q_j e^2}{4\pi\varepsilon_0}$, as shown in equation 4.1, where r is the distance between atoms i and j.

$$V_{ij}(r) = \frac{q_i q_j e^2}{4\pi\varepsilon_0} + A_{ij}\exp(-\frac{r}{p_{ij}}) - \frac{C_{ij}}{r^6} \tag{4.1}$$

The oxygen-oxygen interactions are governed by the Coulomb potential with the addition of a Buckingham form [29, 43, and 44] that includes the additional modification for very short distances. Specifically, the Buckingham-4 potential is used instead of the standard Buckingham and is shown in equation 4.2.

$$V_{ij}(r) = \frac{q_i q_j e^2}{4\pi\varepsilon_0} + \begin{cases} A_{ij}\exp(-\frac{r}{p_{ij}}), & \text{if } r \le r_1 \\ \text{fifth-degree polynomial}, & \text{if } r_1 < r \le r_{min} \\ \text{third-degree polynomial}, & \text{if } r_{min} < r \le r_2 \\ -\frac{C_{ij}}{r^6}, & \text{if } r > r_2 \end{cases} \tag{4.2}$$

While a zero short-range uranium-uranium interaction is assumed that is consistent with Morelon [44].

Different potentials are more suitable for different purposes. Morelon's potential more accurately describes dynamic calculations that have been undertaken and utilize rigid-ion potentials. The Morelon migration energy for vacancies in UO_2 was not utilized. Instead, the potential from Grimes [35] was selected, as it has been employed in past literature and has closer agreement with Matzke's experimental value.

VERIFICATION CALCULATION

The first calculation performed was a validation of single vacancy migration value against the Morelon [44] value to ensure that the results generated by the GULP code were accurate. Figure 26 shows the migration energy of an oxygen vacancy in the 444 supercell as the barrier height of the defect energy curve. The curve is symmetric so a detailed analysis was only done on one side of the curve since the other side is identical. This is only possible due to the symmetry of the single vacancy migration. Table 7 shows the migration values from both supercell configurations, 333 and 444, as well as the Morelon value for comparison.

OXYGEN PAIR

The next step was to add one stationary vacancy in the nearest neighbor location to the other migrating vacancy. Figure 27 shows the detailed migration energy of an oxygen vacancy in the 444 and 333 supercell structure superimposed on top of each other as the barrier height of the defect energy curve. This curve is not symmetric and as such, there are distinct barrier heights for the clustering action as well as for the action of dissociating from the cluster.

Figure 26

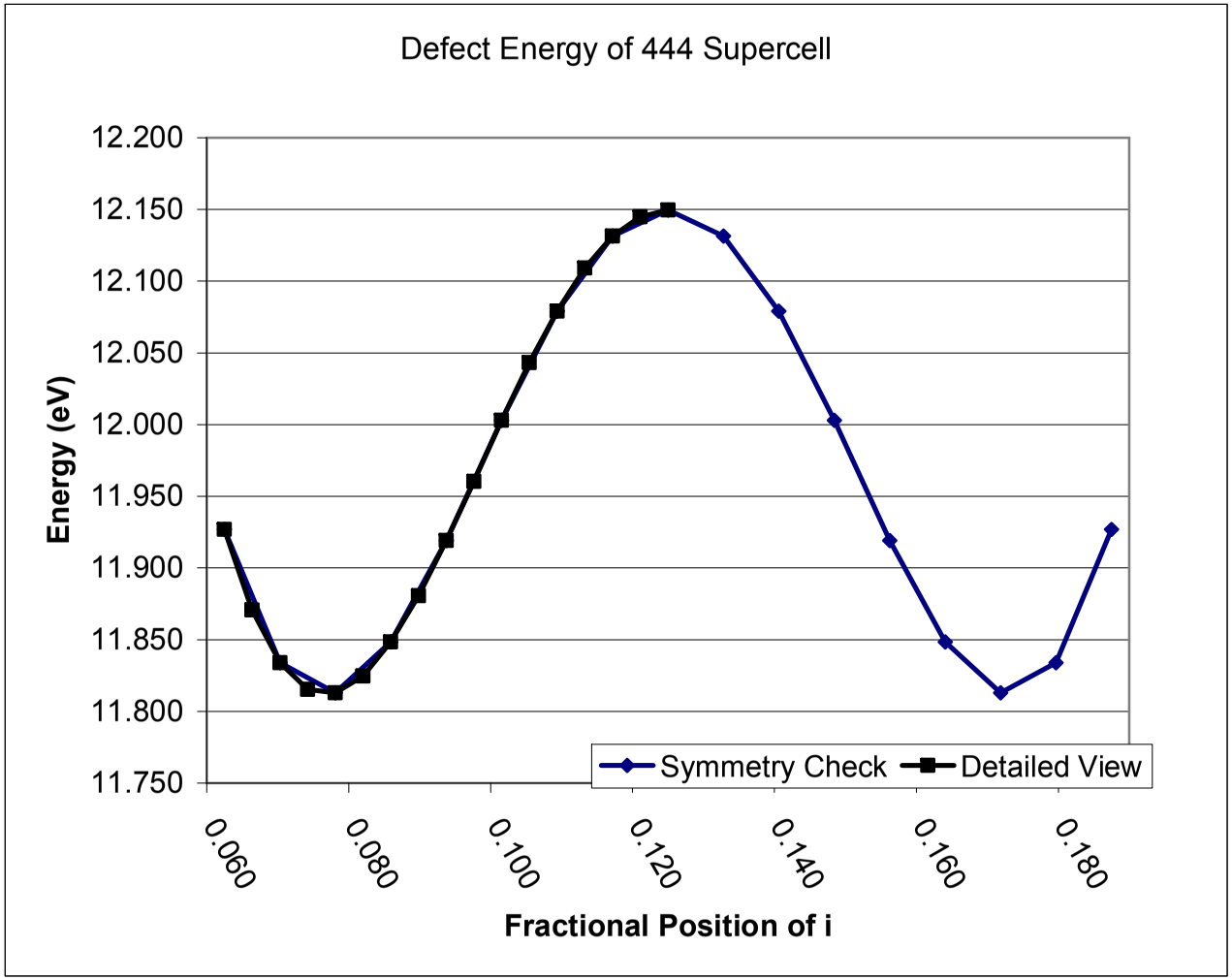

This figure shows the migration energy as the barrier height in defect energies for a single oxygen vacancy in uranium dioxide in the 444 supercell.

Figure 27

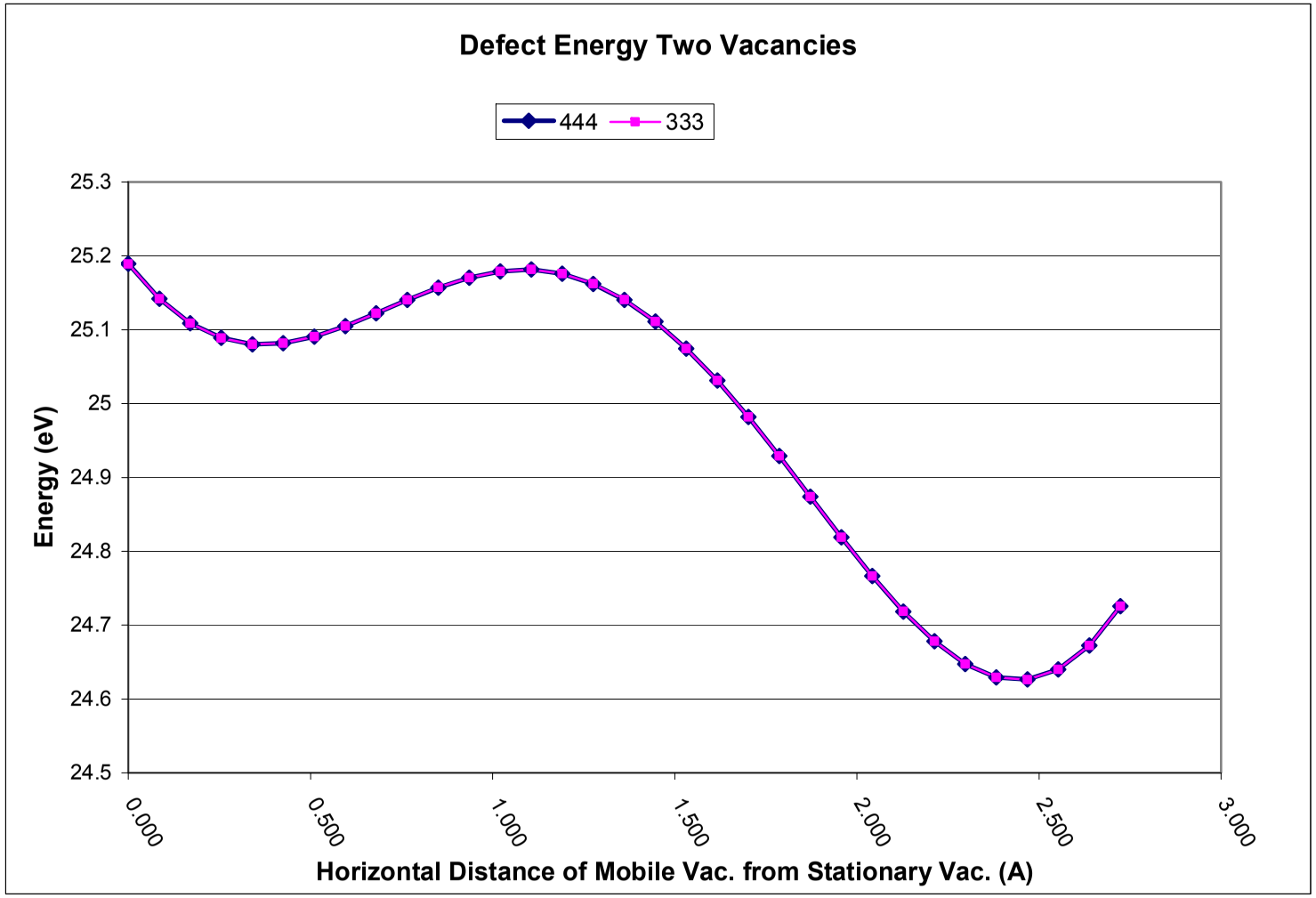

This figure shows the migration energy as the barrier height for the defect energy for a single migrating oxygen vacancy with a stationary oxygen vacancy present in the uranium dioxide system for both 333 and 444 supercells.

Table 7

Single Vacancy Migration Energy

Size of Supercell	Barrier Height (eV)
333	0.3416
444	0.3366
Morelon [44]	0.33

This table shows the migration values of the single vacancy migration in the 333 and 444 supercells as well as the equivalent value used in the validation source.

These two barrier heights are shown in Table 8. Another important thing to note from Figure 27 is that the total defect energy of the system calculated has dramatically increased. The defect energy range in Figure 26 varied between 11.813 eV and 12.150 eV while the defect energy range in Figure 27 ranges between 24.6262 eV and 25.189 eV. This overall system energy increase is attributed to the stress field that the additional vacancy has added to the system. Moreover, the defect energy appears to be decreasing as distance from the stationary vacancy increases, however, the energy spikes as it approaches the next nodal location. As such, the question arose of what this defect energy curve would look like if it were extended out to another nodal location away from the stationary defect.

Figure 28 shows the superposition of the two detailed supercell results. The spike that occurred as the vacancy approached the nodal location in Figure 27 can now be seen to be a local maximum. The total defect energy continues to decrease as the distance from the stationary vacancy increases, which supports the aforementioned theory that this increase in defect energy is caused by the additional point defect. Unfortunately, this also creates some discrepancies between the two figures when comparing the same region. In order to accurately model the migration of a vacancy from two nodal points away from the stationary vacancy, an additional vacancy and interstitial were introduced. In Figure 28, the range of the defect energy of the nearest nodal region is now 24.790 eV to 25.413 eV. This overall system increase may be caused by the addition of the additional vacancy and interstitial now present in the system even though limited to the other, more distant, node. The net affect is a single vacancy migrating to the stationary vacancy, however, physically a vacancy is introduced

Table 8

Single Vacancy Migration Energy with Stationary Vacancy at Nearest Neighbor

Size of Supercell	Barrier Height for Clustering (eV)	Barrier Height for Dissociation (eV)
333	0.5552	0.1012
444	0.5629	0.1088

This table shows the clustering and dissociate values for a single oxygen vacancy in the 333 and 444 supercells with another oxygen vacancy stationary.

Figure 28

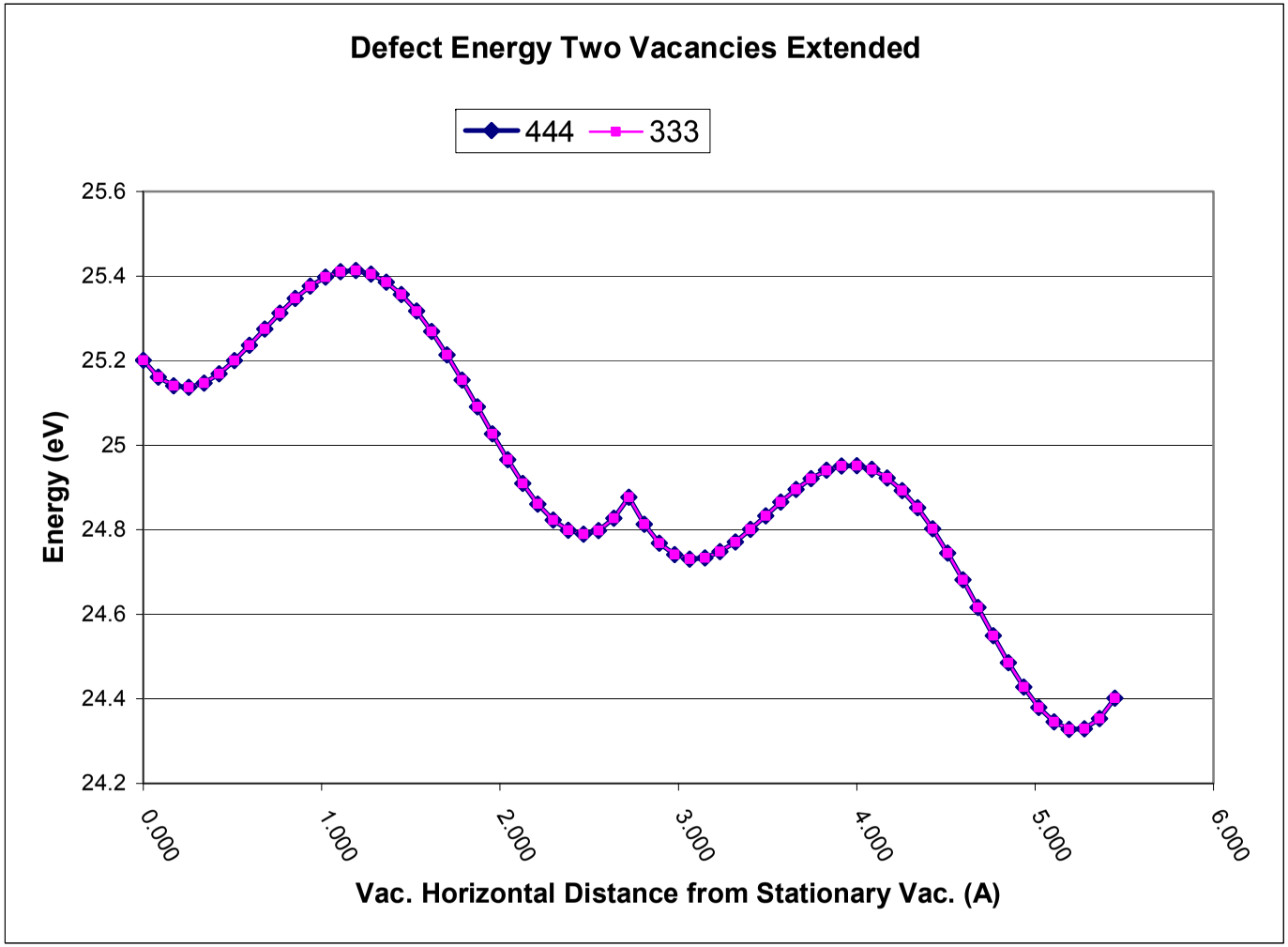

This figure shows the migration energy as the barrier height for the defect energy for a single migrating oxygen vacancy with a stationary oxygen vacancy present in the uranium dioxide system across two nodal distances for both 333 and 444 supercells.

two nodal points away, one nodal point away and at the nearest neighbor location while interstitials are fixed onto the nearest neighbor location and the lattice location one nodal point away. As these interstitials migrate one by one to the further lattice location node, the vacancy migrates closer to the stationary defect. This is also the method used in the single vacancy migration.

The various dislocation and clustering migration energies are shown in Table 9 as the barrier heights. It can be seen that this alteration not only increases the range of energy in the system but also increased the barrier height requirement for both clustering and dissociation through the comparison of Tables 8 and 9. In the case of the extended trial, the results are identical for both the 333 and 444 supercell results. A 0.4028 eV difference is seen between the dissociation and clustering energies for the further away nodal point and a .3472 eV difference is shown for the energies of the nearest nodal point. This energy difference for the two supercells is nearly identical for the single nodal scenario yielding 0.4541 eV for the 444 supercell and 0.4540 eV for the 333 supercell.

ALTERNATIVE THEORY TEST

An alternative to the point defect long range stress effect was proposed – the system energy increase was caused and then amplified by the local charge imbalance rather than the stress of additional defects in the otherwise perfect lattice. A stationary uranium vacancy was added in a nearest neighbor location between the previous stationary oxygen vacancy and the nearest lattice location for the mobile vacancy. The result of this addition is that the code is now modeling a Schottky defect, a neutral trivacancy, rather than an oxygen divacancy. While the charge imbalance was effectively neutralized, the defect energy calculated in the

Table 9

Barrier Heights for Migration Across Two Lattice Nodes

	First Nodal		Second Nodal		Bi-Nodal	
Supercell	Dissociation (eV)	Cluster (eV)	Dissociation (eV)	Cluster (eV)	Dissociation (eV)	Cluster (eV)
333	0.2762	0.6234	0.2212	0.6240	0.0876	0.1464
444	0.2762	0.6234	0.2212	0.6240	0.0872	0.1461

This table shows the clustering and dissociate values for a single oxygen vacancy in the 333 and 444 supercells with another oxygen vacancy stationary. Additionally, this comparison is across two nodal distances and it also shows the barrier height at the middle nodal location.

system dramatically increased due to the much larger point defect creating a significantly larger stress on the system. Interstitials and vacancies on the oxygen sublattice affect only the anion sublattice while studies [44] indicate that an uranium defect would perturb both sublattices. The energy needed for this would be significantly greater than that needed to only perturb the oxygen sublattice. As such, the previous scenarios only focused on perturbations to the oxygen sublattice.

Figure 29 shows the migration energy as the barrier height of the defect energy for a single migrating oxygen vacancy with a stationary oxygen and uranium vacancy present. The overall trend of the curve closely matches those of the oxygen only studies, however, there are two major differences. First, as previously mentioned the overall system energy is dramatically higher and second, there are stand-alone extreme maximum values. Further research is needed to confirm that these are non-physical results that the code has generated due to some limitation of the code. The evidence for that statement is that these extreme outliers do not occur at the same physical distance from the uranium or oxygen atoms, while a couple of the outliers occur at identical horizontal locations, the majority do not. The physical distance is measured from a fixed location, the stationary oxygen vacancy, in the supercell models. Table 10 shows the barrier height energy that corresponds to the migration energy for the oxygen vacancy as it dissociates and clusters around the stationary oxygen vacancy with the presence of the nearby stationary uranium vacancy.

The table shows these values when including the outliers as well as without including the outliers. This comparison was only undertaken through the first nodal location. While there is a significant difference between the 333 and 444 supercell results with the outliers included, the results without the outliers are statistically the same. This is further evidence

Figure 29

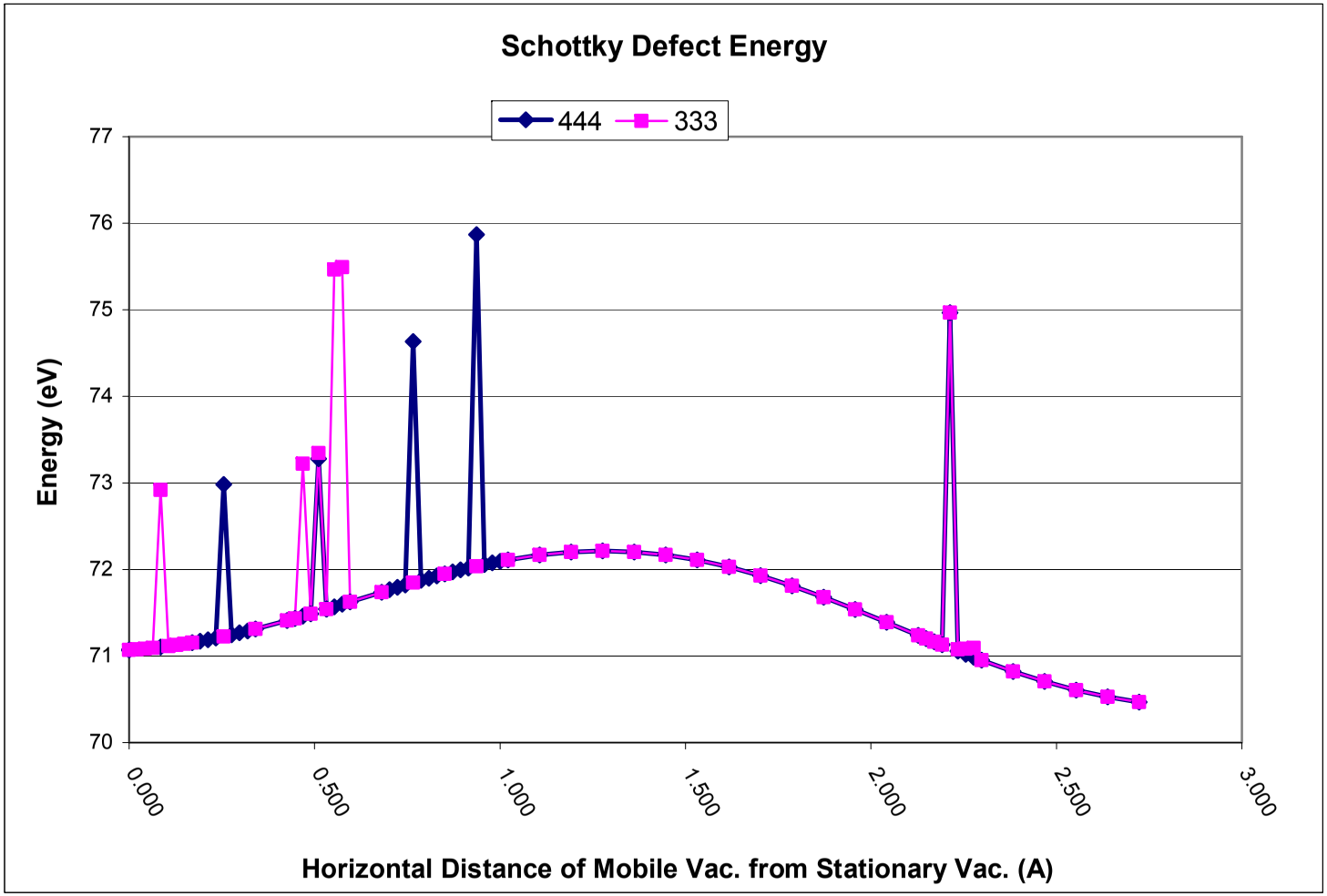

This figure shows the migration energy as the barrier height of the defect energy for a single migrating oxygen vacancy with stationary oxygen and uranium vacancies present for both 333 and 444 supercells.

Table 10

Barrier Heights for Migration with Uranium Vacancy Present

	With Outliers		Without Outliers	
Supercell	Dissociation (eV)	Cluster (eV)	Dissociation (eV)	Cluster (eV)
333	4.4234	4.9658	1.1445	1.7460
444	4.7997	5.4012	1.1445	1.7460

This table shows the barrier height energies for the 333 and 444 supercells that correspond to the dissociation and clustering activation energies for a single migrating oxygen vacancy with a stationary oxygen and uranium vacancy present.

that the outliers represent a non-physical result. The difference between the dissociation and clustering barrier heights in the case without the outliers is 0.6015 eV, which is similar to the difference displayed in the previous cases that lacked the addition of the uranium vacancy.

CHAPTER 5

CONCLUSION

The goal of this work has been the development of a predictive fuel modeling code. To that end, kinetic Monte Carlo studies were undertaken to calculate and compare diffusivities of point defects in a variety of nuclear fuels and a nuclear fuel surrogate so that a more complete understanding of the structure and properties could be developed on an atomistic level as they control the bulk properties of the material. The species' diffusivity depends on numerous variables that are intrinsically linked. The measured diffusivities were studied as various system variables were altered to determine their effect on the diffusivity calculated by the system. In the field of fuel performance modeling, the diffusivity is most sensitive to the activation energy of the barrier height used for migration events. As such, the kMC diffusivity results shown are inextricably linked to the migration energies selected for the rate equation.

It was for this reason that, in the second part of this work, molecular static calculations were undertaken to gather the activation barrier energies required for the kMC event catalog to expand and include events beyond simple migration events. The goal is for the event catalog to include dissociation and clustering effects so that a more complete picture of bubble formation and movement could be undertaken. During these molecular statics calculations, it was observed that the accumulation of supplemental point defects into the model, to replicate the process of clustering and dissociation, dramatically increased the overall energy of the system due to the long range stress affect the defects caused in the system. This affect is by far the most prominent, dominating the effect of local

electroneutrality that was tested by adding a uranium atom vacancy to create the neutral trivacancy.

Additionally, the diffusivities calculated were compared to their analytical equivalents through use of the classical diffusion equation. Results for both the diffusivities and migration energies fall within the broad range as depicted across literature. This work is in conjunction with other graduate students and national laboratories of the study of existing fuel code methodologies and implementation of a predictive fuel code for the future.

CHAPTER 6

FUTURE WORK

Additional computational and experimental work can be undertaken to further explore the results from this investigation. Some such simulations include supplementing the kMC event catalog to include additional possible action steps for clustering and dissociation events. The ideal scenario allowing for the growth and movement of a void or cluster without limitations on the size of the void or cluster, rather each individual atom or defect composing the void or cluster would be treated individually. This would prevent clusters or voids from growing to a set size and becoming immobile. More molecular statics calculations could be undertaken using the polarizable shell potential model rather than the rigid-ion potential model to give a more complex and likely accurate barrier height for activation energies. The integration of these scales levels to allow important information to be passed up the ladder along with the uncertainties of each calculation would generate a code that could reach a level of precision currently unavailable in models of any scale.

Furthermore, another temperature gradient study could be carried out through the addition of a new term to the activation energy in the rate equation rather than the implementation of a variant temperature to simulate a gradient. The addition of impurity species as interstitial atoms would be a concrete step toward modeling fission cascades. In addition to the inclusion of other sinks such as grain boundaries, the impurity atoms act as a sink for the point defects inhibiting diffusion as well as pinning dislocation lines to restrain their climb. The gas atoms most suitable for incorporation are the chemically inert noble gases: He, Kr, and Xe. Their chemical inertness prevents them from directly interacting with the fuel to create new chemical species and alter the delicate fuel stoichiometry - rather the

gas atoms precipitate as small bubbles [22]. Another step would be to add mechanisms for interstitial movement and allow for the lower energy configuration of the Willis Cluster to be formed sharing a single lattice location. A big step toward the physical accuracy of this will be to modify the blocking mechanism, thereby allowing recombination events to occur. A method for initiating recombination would be to allow for the interstitial atom and vacancy to recombine if they attain a specific distance – likely closer than nearest neighbor distance analogous to the radius of interaction proposed for clustering and dissociation.

Longer time lengths and physical lengths of models will allow for more meaningful clustering to occur. Diffusivity is highly dependent on stoichiometry of both uranium and oxygen. Allowing the stoichiometry to change over the course of the scenario would be a concrete action toward the addition of fission chains that would allow the fuel code to actively create fission events and consider burnup. The key steps in such a fission cascade would be the collision event, the thermal spike, quenching, and annealing.

APPENDIX A

REPRESENTATIVE INPUT FILES

KMC Configuration Input File UO_{2-x}

<configuration>
<boltzmann_constant>**8.61738e-5**</boltzmann_constant>
<cluster_radius>**9**</cluster_radius>
<dimensions>
<x>**15**</x>
<y>**15**</y>
<z>**15**</z>
</dimensions>
<initial_populations>
<population>
<count>**270**</count>
<entity>**tet_vacancy**</entity>
</population>
</initial_populations>
<lattice_parameter>**5.464e-8**</lattice_parameter>
<lattice_type>**face_centered_cubic**</lattice_type>
<rng_seed>**0**</rng_seed>
<simulation_steps>**10000**</simulation_steps>
<temperature>**2100**</temperature>
</configuration>

KMC Actions Input File UO_{2-x}

```
- <actions>
- <action>
  <cluster>0</cluster>
- <direction>
  <x>0</x>
  <y>0</y>
  <z>2</z>
    </direction>
  <energy>0.72</energy>
  <entity>tet_vacancy</entity>
  <frequency>1.0e13</frequency>
  <sublattice>tetrahedral</sublattice>
  <type>migration</type>
    </action>
- <action>
  <cluster>0</cluster>
- <direction>
  <x>0</x>
  <y>0</y>
  <z>-2</z>
    </direction>
  <energy>0.72</energy>
  <entity>tet_vacancy</entity>
  <frequency>1.0e13</frequency>
  <sublattice>tetrahedral</sublattice>
  <type>migration</type>
    </action>
- <action>
  <cluster>0</cluster>
- <direction>
  <x>0</x>
  <y>2</y>
  <z>0</z>
    </direction>
  <energy>0.72</energy>
  <entity>tet_vacancy</entity>
  <frequency>1.0e13</frequency>
  <sublattice>tetrahedral</sublattice>
  <type>migration</type>
    </action>
- <action>
  <cluster>0</cluster>
- <direction>
  <x>0</x>
  <y>-2</y>
  <z>0</z>
    </direction>
```

(Continued) kMC Actions Input File UO_{2-x}

```
<energy>0.72</energy>
<entity>tet_vacancy</entity>
<frequency>1.0e13</frequency>
<sublattice>tetrahedral</sublattice>
<type>migration</type>
  </action>
- <action>
<cluster>0</cluster>
- <direction>
<x>2</x>
<y>0</y>
<z>0</z>
  </direction>
<energy>0.72</energy>
<entity>tet_vacancy</entity>
<frequency>1.0e13</frequency>
<sublattice>tetrahedral</sublattice>
<type>migration</type>
  </action>
- <action>
<cluster>0</cluster>
- <direction>
<x>-2</x>
<y>0</y>
<z>0</z>
  </direction>
<energy>0.72</energy>
<entity>tet_vacancy</entity>
<frequency>1.0e13</frequency>
<sublattice>tetrahedral</sublattice>
<type>migration</type>
  </action>
  </actions>
```

KMC Entities Input File UO_{2-x}

```
- <root>
- <entities>
- <entity>
  <name>tet_vacancy</name>
  <sublattice>tetrahedral</sublattice>
    </entity>
    </entities>
  <clusters />
    </root>
```

kMC Configuration Input File U_{+x} with Temperature Gradient

```
- <configuration>
  <boltzmann_constant>8.61738e-5</boltzmann_constant>
  <cluster_radius>9</cluster_radius>
- <dimensions>
  <x>800</x>
  <y>15</y>
  <z>15</z>
    </dimensions>
- <initial_populations>
- <population>
  <count>68</count>
  <entity>oct_uranium</entity>
    </population>
    </initial_populations>
  <lattice_parameter>3.54e-8</lattice_parameter>
  <lattice_type>body_centered_cubic</lattice_type>
  <rng_seed>0</rng_seed>
  <simulation_steps>10001</simulation_steps>
  <temperature>2200</temperature>
  <temperatureX>2210</temperatureX>
    </configuration>
```

kMC Actions Input File U_{+x} with Temperature Gradient

```
- <actions>
- <action>
  <type>migration</type>
  <entity>oct_uranium</entity>
  <cluster>0</cluster>
  <sublattice>octahedral</sublattice>
  <energy>1.20</energy>
  <frequency>1.0e13</frequency>
- <direction>
  <x>2</x>
  <y>0</y>
  <z>0</z>
    </direction>
    </action>
- <action>
  <type>migration</type>
  <entity>oct_uranium</entity>
  <cluster>0</cluster>
  <sublattice>octahedral</sublattice>
  <energy>1.20</energy>
  <frequency>1.0e13</frequency>
- <direction>
  <x>-2</x>
  <y>0</y>
  <z>0</z>
    </direction>
    </action>
- <action>
  <type>migration</type>
  <entity>oct_uranium</entity>
  <cluster>0</cluster>
  <sublattice>octahedral</sublattice>
  <energy>1.20</energy>
  <frequency>1.0e13</frequency>
- <direction>
  <x>0</x>
  <y>2</y>
  <z>0</z>
    </direction>
    </action>
- <action>
  <type>migration</type>
  <entity>oct_uranium</entity>
  <cluster>0</cluster>
  <sublattice>octahedral</sublattice>
  <energy>1.20</energy>
  <frequency>1.0e13</frequency>
```

(Continued) kMC Actions Input File U_{+x} with Temperature Gradient

```
- <direction>
  <x>0</x>
  <y>-2</y>
  <z>0</z>
    </direction>
    </action>
- <action>
  <type>migration</type>
  <entity>oct_uranium</entity>
  <cluster>0</cluster>
  <sublattice>octahedral</sublattice>
  <energy>1.20</energy>
  <frequency>1.0e13</frequency>
- <direction>
  <x>0</x>
  <y>0</y>
  <z>2</z>
    </direction>
    </action>
- <action>
  <type>migration</type>
  <entity>oct_uranium</entity>
  <cluster>0</cluster>
  <sublattice>octahedral</sublattice>
  <energy>1.20</energy>
  <frequency>1.0e13</frequency>
- <direction>
  <x>0</x>
  <y>0</y>
  <z>-2</z>
    </direction>
    </action>
    </actions>
```

kMC Entities Input File U_{+x} with Temperature Gradient

```
- <root>
- <entities>
- <entity>
  <name>oct_uranium</name>
  <sublattice>octahedral</sublattice>
    </entity>
    </entities>
  <clusters />
    </root>
```

GULP Defect Calculation Input File

```
#
# Keywords:
#
bulk_nooptimise defect cartesian full
#
# Options:
#
title
Morelon potential for UO2
end

# Cell Structure
cell
   16.339883  16.339883  16.339883  90.000000  90.000000  90.000000
fractional
U     core 0.0000000 0.0000000 0.0000000 3.22725200 1.00000 0.00000
U     core 1.0000000 1.0000000 0.3333333 3.22725200 1.00000 0.00000
U     core 1.0000000 1.0000000 0.6666667 3.22725200 1.00000 0.00000
U     core 1.0000000 0.3333333 1.0000000 3.22725200 1.00000 0.00000
U     core 1.0000000 0.3333333 0.3333333 3.22725200 1.00000 0.00000
U     core 1.0000000 0.3333333 0.6666667 3.22725200 1.00000 0.00000
U     core 1.0000000 0.6666667 1.0000000 3.22725200 1.00000 0.00000
U     core 1.0000000 0.6666667 0.3333333 3.22725200 1.00000 0.00000
U     core 1.0000000 0.6666667 0.6666667 3.22725200 1.00000 0.00000
U     core 0.3333333 1.0000000 1.0000000 3.22725200 1.00000 0.00000
U     core 0.3333333 1.0000000 0.3333333 3.22725200 1.00000 0.00000
U     core 0.3333333 1.0000000 0.6666667 3.22725200 1.00000 0.00000
U     core 0.3333333 0.3333333 0.0000000 3.22725200 1.00000 0.00000
U     core 0.3333333 0.3333333 0.3333333 3.22725200 1.00000 0.00000
U     core 0.3333333 0.3333333 0.6666667 3.22725200 1.00000 0.00000
U     core 0.3333333 0.6666667 1.0000000 3.22725200 1.00000 0.00000
U     core 0.3333333 0.6666667 0.3333333 3.22725200 1.00000 0.00000
U     core 0.3333333 0.6666667 0.6666667 3.22725200 1.00000 0.00000
U     core 0.6666667 1.0000000 1.0000000 3.22725200 1.00000 0.00000
U     core 0.6666667 1.0000000 0.3333333 3.22725200 1.00000 0.00000
U     core 0.6666667 1.0000000 0.6666667 3.22725200 1.00000 0.00000
U     core 0.6666667 0.3333333 0.0000000 3.22725200 1.00000 0.00000
U     core 0.6666667 0.3333333 0.3333333 3.22725200 1.00000 0.00000
U     core 0.6666667 0.3333333 0.6666667 3.22725200 1.00000 0.00000
U     core 0.6666667 0.6666667 1.0000000 3.22725200 1.00000 0.00000
U     core 0.6666667 0.6666667 0.3333333 3.22725200 1.00000 0.00000
U     core 0.6666667 0.6666667 0.6666667 3.22725200 1.00000 0.00000
U     core 1.0000000 0.1666667 0.1666667 3.22725200 1.00000 0.00000
U     core 1.0000000 0.1666667 0.5000000 3.22725200 1.00000 0.00000
U     core 1.0000000 0.1666667 0.8333333 3.22725200 1.00000 0.00000
U     core 1.0000000 0.5000000 0.1666667 3.22725200 1.00000 0.00000
U     core 1.0000000 0.5000000 0.5000000 3.22725200 1.00000 0.00000
U     core 1.0000000 0.5000000 0.8333333 3.22725200 1.00000 0.00000
U     core 1.0000000 0.8333333 0.1666667 3.22725200 1.00000 0.00000
U     core 1.0000000 0.8333333 0.5000000 3.22725200 1.00000 0.00000
U     core 1.0000000 0.8333333 0.8333333 3.22725200 1.00000 0.00000
U     core 0.3333333 0.1666667 0.1666667 3.22725200 1.00000 0.00000
U     core 0.3333333 0.1666667 0.5000000 3.22725200 1.00000 0.00000
U     core 0.3333333 0.1666667 0.8333333 3.22725200 1.00000 0.00000
```

(Continued) GULP Defect Calculation Input File

```
U     core 0.3333333 0.5000000 0.1666667 3.22725200 1.00000 0.00000
U     core 0.3333333 0.5000000 0.5000000 3.22725200 1.00000 0.00000
U     core 0.3333333 0.5000000 0.8333333 3.22725200 1.00000 0.00000
U     core 0.3333333 0.8333333 0.1666667 3.22725200 1.00000 0.00000
U     core 0.3333333 0.8333333 0.5000000 3.22725200 1.00000 0.00000
U     core 0.3333333 0.8333333 0.8333333 3.22725200 1.00000 0.00000
U     core 0.6666667 0.1666667 0.1666667 3.22725200 1.00000 0.00000
U     core 0.6666667 0.1666667 0.5000000 3.22725200 1.00000 0.00000
U     core 0.6666667 0.1666667 0.8333333 3.22725200 1.00000 0.00000
U     core 0.6666667 0.5000000 0.1666667 3.22725200 1.00000 0.00000
U     core 0.6666667 0.5000000 0.5000000 3.22725200 1.00000 0.00000
U     core 0.6666667 0.5000000 0.8333333 3.22725200 1.00000 0.00000
U     core 0.6666667 0.8333333 0.1666667 3.22725200 1.00000 0.00000
U     core 0.6666667 0.8333333 0.5000000 3.22725200 1.00000 0.00000
U     core 0.6666667 0.8333333 0.8333333 3.22725200 1.00000 0.00000
U     core 0.1666667 1.0000000 0.1666667 3.22725200 1.00000 0.00000
U     core 0.1666667 1.0000000 0.5000000 3.22725200 1.00000 0.00000
U     core 0.1666667 1.0000000 0.8333333 3.22725200 1.00000 0.00000
U     core 0.1666667 0.3333333 0.1666667 3.22725200 1.00000 0.00000
U     core 0.1666667 0.3333333 0.5000000 3.22725200 1.00000 0.00000
U     core 0.1666667 0.3333333 0.8333333 3.22725200 1.00000 0.00000
U     core 0.1666667 0.6666667 0.1666667 3.22725200 1.00000 0.00000
U     core 0.1666667 0.6666667 0.5000000 3.22725200 1.00000 0.00000
U     core 0.1666667 0.6666667 0.8333333 3.22725200 1.00000 0.00000
U     core 0.5000000 1.0000000 0.1666667 3.22725200 1.00000 0.00000
U     core 0.5000000 1.0000000 0.5000000 3.22725200 1.00000 0.00000
U     core 0.5000000 1.0000000 0.8333333 3.22725200 1.00000 0.00000
U     core 0.5000000 0.3333333 0.1666667 3.22725200 1.00000 0.00000
U     core 0.5000000 0.3333333 0.5000000 3.22725200 1.00000 0.00000
U     core 0.5000000 0.3333333 0.8333333 3.22725200 1.00000 0.00000
U     core 0.5000000 0.6666667 0.1666667 3.22725200 1.00000 0.00000
U     core 0.5000000 0.6666667 0.5000000 3.22725200 1.00000 0.00000
U     core 0.5000000 0.6666667 0.8333333 3.22725200 1.00000 0.00000
U     core 0.8333333 1.0000000 0.1666667 3.22725200 1.00000 0.00000
U     core 0.8333333 1.0000000 0.5000000 3.22725200 1.00000 0.00000
U     core 0.8333333 1.0000000 0.8333333 3.22725200 1.00000 0.00000
U     core 0.8333333 0.3333333 0.1666667 3.22725200 1.00000 0.00000
U     core 0.8333333 0.3333333 0.5000000 3.22725200 1.00000 0.00000
U     core 0.8333333 0.3333333 0.8333333 3.22725200 1.00000 0.00000
U     core 0.8333333 0.6666667 0.1666667 3.22725200 1.00000 0.00000
U     core 0.8333333 0.6666667 0.5000000 3.22725200 1.00000 0.00000
U     core 0.8333333 0.6666667 0.8333333 3.22725200 1.00000 0.00000
U     core 0.1666667 0.1666667 1.0000000 3.22725200 1.00000 0.00000
U     core 0.1666667 0.1666667 0.3333333 3.22725200 1.00000 0.00000
U     core 0.1666667 0.1666667 0.6666667 3.22725200 1.00000 0.00000
U     core 0.1666667 0.5000000 1.0000000 3.22725200 1.00000 0.00000
U     core 0.1666667 0.5000000 0.3333333 3.22725200 1.00000 0.00000
U     core 0.1666667 0.5000000 0.6666667 3.22725200 1.00000 0.00000
U     core 0.1666667 0.8333333 1.0000000 3.22725200 1.00000 0.00000
U     core 0.1666667 0.8333333 0.3333333 3.22725200 1.00000 0.00000
U     core 0.1666667 0.8333333 0.6666667 3.22725200 1.00000 0.00000
U     core 0.5000000 0.1666667 0.0000000 3.22725200 1.00000 0.00000
U     core 0.5000000 0.1666667 0.3333333 3.22725200 1.00000 0.00000
U     core 0.5000000 0.1666667 0.6666667 3.22725200 1.00000 0.00000
```

(Continued) GULP Defect Calculation Input File

```
U     core 0.5000000 0.5000000 0.0000000 3.22725200 1.00000 0.00000
U     core 0.5000000 0.5000000 0.3333333 3.22725200 1.00000 0.00000
U     core 0.5000000 0.5000000 0.6666667 3.22725200 1.00000 0.00000
U     core 0.5000000 0.8333333 1.0000000 3.22725200 1.00000 0.00000
U     core 0.5000000 0.8333333 0.3333333 3.22725200 1.00000 0.00000
U     core 0.5000000 0.8333333 0.6666667 3.22725200 1.00000 0.00000
U     core 0.8333333 0.1666667 1.0000000 3.22725200 1.00000 0.00000
U     core 0.8333333 0.1666667 0.3333333 3.22725200 1.00000 0.00000
U     core 0.8333333 0.1666667 0.6666667 3.22725200 1.00000 0.00000
U     core 0.8333333 0.5000000 1.0000000 3.22725200 1.00000 0.00000
U     core 0.8333333 0.5000000 0.3333333 3.22725200 1.00000 0.00000
U     core 0.8333333 0.5000000 0.6666667 3.22725200 1.00000 0.00000
U     core 0.8333333 0.8333333 1.0000000 3.22725200 1.00000 0.00000
U     core 0.8333333 0.8333333 0.3333333 3.22725200 1.00000 0.00000
U     core 0.8333333 0.8333333 0.6666667 3.22725200 1.00000 0.00000
O     core 0.0833333 0.0833333 0.0833333 -1.6136260 1.00000 0.00000
O     core 0.0833333 0.0833333 0.4166666 -1.6136260 1.00000 0.00000
O     core 0.0833333 0.0833333 0.7500000 -1.6136260 1.00000 0.00000
O     core 0.0833333 0.4166666 0.0833333 -1.6136260 1.00000 0.00000
O     core 0.0833333 0.4166666 0.4166666 -1.6136260 1.00000 0.00000
O     core 0.0833333 0.4166666 0.7500000 -1.6136260 1.00000 0.00000
O     core 0.0833333 0.7500000 0.0833333 -1.6136260 1.00000 0.00000
O     core 0.0833333 0.7500000 0.4166666 -1.6136260 1.00000 0.00000
O     core 0.0833333 0.7500000 0.7500000 -1.6136260 1.00000 0.00000
O     core 0.4166666 0.0833333 0.0833333 -1.6136260 1.00000 0.00000
O     core 0.4166666 0.0833333 0.4166666 -1.6136260 1.00000 0.00000
O     core 0.4166666 0.0833333 0.7500000 -1.6136260 1.00000 0.00000
O     core 0.4166666 0.4166666 0.0833333 -1.6136260 1.00000 0.00000
O     core 0.4166666 0.4166666 0.4166666 -1.6136260 1.00000 0.00000
O     core 0.4166666 0.4166666 0.7500000 -1.6136260 1.00000 0.00000
O     core 0.4166666 0.7500000 0.0833333 -1.6136260 1.00000 0.00000
O     core 0.4166666 0.7500000 0.4166666 -1.6136260 1.00000 0.00000
O     core 0.4166666 0.7500000 0.7500000 -1.6136260 1.00000 0.00000
O     core 0.7500000 0.0833333 0.0833333 -1.6136260 1.00000 0.00000
O     core 0.7500000 0.0833333 0.4166666 -1.6136260 1.00000 0.00000
O     core 0.7500000 0.0833333 0.7500000 -1.6136260 1.00000 0.00000
O     core 0.7500000 0.4166666 0.0833333 -1.6136260 1.00000 0.00000
O     core 0.7500000 0.4166666 0.4166666 -1.6136260 1.00000 0.00000
O     core 0.7500000 0.4166666 0.7500000 -1.6136260 1.00000 0.00000
O     core 0.7500000 0.7500000 0.0833333 -1.6136260 1.00000 0.00000
O     core 0.7500000 0.7500000 0.4166666 -1.6136260 1.00000 0.00000
O     core 0.7500000 0.7500000 0.7500000 -1.6136260 1.00000 0.00000
O     core 0.0833333 0.2500000 0.2500000 -1.6136260 1.00000 0.00000
O     core 0.0833333 0.2500000 0.5833333 -1.6136260 1.00000 0.00000
O     core 0.0833333 0.2500000 0.9166666 -1.6136260 1.00000 0.00000
O     core 0.0833333 0.5833333 0.2500000 -1.6136260 1.00000 0.00000
O     core 0.0833333 0.5833333 0.5833333 -1.6136260 1.00000 0.00000
O     core 0.0833333 0.5833333 0.9166666 -1.6136260 1.00000 0.00000
O     core 0.0833333 0.9166666 0.2500000 -1.6136260 1.00000 0.00000
O     core 0.0833333 0.9166666 0.5833333 -1.6136260 1.00000 0.00000
O     core 0.0833333 0.9166666 0.9166666 -1.6136260 1.00000 0.00000
O     core 0.4166666 0.2500000 0.2500000 -1.6136260 1.00000 0.00000
O     core 0.4166666 0.2500000 0.5833333 -1.6136260 1.00000 0.00000
O     core 0.4166666 0.2500000 0.9166666 -1.6136260 1.00000 0.00000
```

(Continued) GULP Defect Calculation Input File

```
O     core 0.4166666 0.5833333 0.2500000 -1.6136260 1.00000 0.00000
O     core 0.4166666 0.5833333 0.5833333 -1.6136260 1.00000 0.00000
O     core 0.4166666 0.5833333 0.9166666 -1.6136260 1.00000 0.00000
O     core 0.4166666 0.9166666 0.2500000 -1.6136260 1.00000 0.00000
O     core 0.4166666 0.9166666 0.5833333 -1.6136260 1.00000 0.00000
O     core 0.4166666 0.9166666 0.9166666 -1.6136260 1.00000 0.00000
O     core 0.7500000 0.2500000 0.2500000 -1.6136260 1.00000 0.00000
O     core 0.7500000 0.2500000 0.5833333 -1.6136260 1.00000 0.00000
O     core 0.7500000 0.2500000 0.9166666 -1.6136260 1.00000 0.00000
O     core 0.7500000 0.5833333 0.2500000 -1.6136260 1.00000 0.00000
O     core 0.7500000 0.5833333 0.5833333 -1.6136260 1.00000 0.00000
O     core 0.7500000 0.5833333 0.9166666 -1.6136260 1.00000 0.00000
O     core 0.7500000 0.9166666 0.2500000 -1.6136260 1.00000 0.00000
O     core 0.7500000 0.9166666 0.5833333 -1.6136260 1.00000 0.00000
O     core 0.7500000 0.9166666 0.9166666 -1.6136260 1.00000 0.00000
O     core 0.2500000 0.0833333 0.2500000 -1.6136260 1.00000 0.00000
O     core 0.2500000 0.0833333 0.5833333 -1.6136260 1.00000 0.00000
O     core 0.2500000 0.0833333 0.9166666 -1.6136260 1.00000 0.00000
O     core 0.2500000 0.4166666 0.2500000 -1.6136260 1.00000 0.00000
O     core 0.2500000 0.4166666 0.5833333 -1.6136260 1.00000 0.00000
O     core 0.2500000 0.4166666 0.9166666 -1.6136260 1.00000 0.00000
O     core 0.2500000 0.7500000 0.2500000 -1.6136260 1.00000 0.00000
O     core 0.2500000 0.7500000 0.5833333 -1.6136260 1.00000 0.00000
O     core 0.2500000 0.7500000 0.9166666 -1.6136260 1.00000 0.00000
O     core 0.5833333 0.0833333 0.2500000 -1.6136260 1.00000 0.00000
O     core 0.5833333 0.0833333 0.5833333 -1.6136260 1.00000 0.00000
O     core 0.5833333 0.0833333 0.9166666 -1.6136260 1.00000 0.00000
O     core 0.5833333 0.4166666 0.2500000 -1.6136260 1.00000 0.00000
O     core 0.5833333 0.4166666 0.5833333 -1.6136260 1.00000 0.00000
O     core 0.5833333 0.4166666 0.9166666 -1.6136260 1.00000 0.00000
O     core 0.5833333 0.7500000 0.2500000 -1.6136260 1.00000 0.00000
O     core 0.5833333 0.7500000 0.5833333 -1.6136260 1.00000 0.00000
O     core 0.5833333 0.7500000 0.9166666 -1.6136260 1.00000 0.00000
O     core 0.9166666 0.0833333 0.2500000 -1.6136260 1.00000 0.00000
O     core 0.9166666 0.0833333 0.5833333 -1.6136260 1.00000 0.00000
O     core 0.9166666 0.0833333 0.9166666 -1.6136260 1.00000 0.00000
O     core 0.9166666 0.4166666 0.2500000 -1.6136260 1.00000 0.00000
O     core 0.9166666 0.4166666 0.5833333 -1.6136260 1.00000 0.00000
O     core 0.9166666 0.4166666 0.9166666 -1.6136260 1.00000 0.00000
O     core 0.9166666 0.7500000 0.2500000 -1.6136260 1.00000 0.00000
O     core 0.9166666 0.7500000 0.5833333 -1.6136260 1.00000 0.00000
O     core 0.9166666 0.7500000 0.9166666 -1.6136260 1.00000 0.00000
O     core 0.2500000 0.2500000 0.0833333 -1.6136260 1.00000 0.00000
O     core 0.2500000 0.2500000 0.4166666 -1.6136260 1.00000 0.00000
O     core 0.2500000 0.2500000 0.7500000 -1.6136260 1.00000 0.00000
O     core 0.2500000 0.5833333 0.0833333 -1.6136260 1.00000 0.00000
O     core 0.2500000 0.5833333 0.4166666 -1.6136260 1.00000 0.00000
O     core 0.2500000 0.5833333 0.7500000 -1.6136260 1.00000 0.00000
O     core 0.2500000 0.9166666 0.0833333 -1.6136260 1.00000 0.00000
O     core 0.2500000 0.9166666 0.4166666 -1.6136260 1.00000 0.00000
O     core 0.2500000 0.9166666 0.7500000 -1.6136260 1.00000 0.00000
O     core 0.5833333 0.2500000 0.0833333 -1.6136260 1.00000 0.00000
O     core 0.5833333 0.2500000 0.4166666 -1.6136260 1.00000 0.00000
O     core 0.5833333 0.2500000 0.7500000 -1.6136260 1.00000 0.00000
```

(Continued) GULP Defect Calculation Input File

```
O     core 0.5833333 0.5833333 0.0833333 -1.6136260 1.00000 0.00000
O     core 0.5833333 0.5833333 0.4166666 -1.6136260 1.00000 0.00000
O     core 0.5833333 0.5833333 0.7500000 -1.6136260 1.00000 0.00000
O     core 0.5833333 0.9166666 0.0833333 -1.6136260 1.00000 0.00000
O     core 0.5833333 0.9166666 0.4166666 -1.6136260 1.00000 0.00000
O     core 0.5833333 0.9166666 0.7500000 -1.6136260 1.00000 0.00000
O     core 0.9166666 0.2500000 0.0833333 -1.6136260 1.00000 0.00000
O     core 0.9166666 0.2500000 0.4166666 -1.6136260 1.00000 0.00000
O     core 0.9166666 0.2500000 0.7500000 -1.6136260 1.00000 0.00000
O     core 0.9166666 0.5833333 0.0833333 -1.6136260 1.00000 0.00000
O     core 0.9166666 0.5833333 0.4166666 -1.6136260 1.00000 0.00000
O     core 0.9166666 0.5833333 0.7500000 -1.6136260 1.00000 0.00000
O     core 0.9166666 0.9166666 0.0833333 -1.6136260 1.00000 0.00000
O     core 0.9166666 0.9166666 0.4166666 -1.6136260 1.00000 0.00000
O     core 0.9166666 0.9166666 0.7500000 -1.6136260 1.00000 0.00000
O     core 0.2500000 0.2500000 0.2500000 -1.6136260 1.00000 0.00000
O     core 0.2500000 0.2500000 0.5833333 -1.6136260 1.00000 0.00000
O     core 0.2500000 0.2500000 0.9166666 -1.6136260 1.00000 0.00000
O     core 0.2500000 0.5833333 0.2500000 -1.6136260 1.00000 0.00000
O     core 0.2500000 0.5833333 0.5833333 -1.6136260 1.00000 0.00000
O     core 0.2500000 0.5833333 0.9166666 -1.6136260 1.00000 0.00000
O     core 0.2500000 0.9166666 0.2500000 -1.6136260 1.00000 0.00000
O     core 0.2500000 0.9166666 0.5833333 -1.6136260 1.00000 0.00000
O     core 0.2500000 0.9166666 0.9166666 -1.6136260 1.00000 0.00000
O     core 0.5833333 0.2500000 0.2500000 -1.6136260 1.00000 0.00000
O     core 0.5833333 0.2500000 0.5833333 -1.6136260 1.00000 0.00000
O     core 0.5833333 0.2500000 0.9166666 -1.6136260 1.00000 0.00000
O     core 0.5833333 0.5833333 0.2500000 -1.6136260 1.00000 0.00000
O     core 0.5833333 0.5833333 0.5833333 -1.6136260 1.00000 0.00000
O     core 0.5833333 0.5833333 0.9166666 -1.6136260 1.00000 0.00000
O     core 0.5833333 0.9166666 0.2500000 -1.6136260 1.00000 0.00000
O     core 0.5833333 0.9166666 0.5833333 -1.6136260 1.00000 0.00000
O     core 0.5833333 0.9166666 0.9166666 -1.6136260 1.00000 0.00000
O     core 0.9166666 0.2500000 0.2500000 -1.6136260 1.00000 0.00000
O     core 0.9166666 0.2500000 0.5833333 -1.6136260 1.00000 0.00000
O     core 0.9166666 0.2500000 0.9166666 -1.6136260 1.00000 0.00000
O     core 0.9166666 0.5833333 0.2500000 -1.6136260 1.00000 0.00000
O     core 0.9166666 0.5833333 0.5833333 -1.6136260 1.00000 0.00000
O     core 0.9166666 0.5833333 0.9166666 -1.6136260 1.00000 0.00000
O     core 0.9166666 0.9166666 0.2500000 -1.6136260 1.00000 0.00000
O     core 0.9166666 0.9166666 0.5833333 -1.6136260 1.00000 0.00000
O     core 0.9166666 0.9166666 0.9166666 -1.6136260 1.00000 0.00000
O     core 0.2500000 0.0833333 0.0833333 -1.6136260 1.00000 0.00000
O     core 0.2500000 0.0833333 0.4166666 -1.6136260 1.00000 0.00000
O     core 0.2500000 0.0833333 0.7500000 -1.6136260 1.00000 0.00000
O     core 0.2500000 0.4166666 0.0833333 -1.6136260 1.00000 0.00000
O     core 0.2500000 0.4166666 0.4166666 -1.6136260 1.00000 0.00000
O     core 0.2500000 0.4166666 0.7500000 -1.6136260 1.00000 0.00000
O     core 0.2500000 0.7500000 0.0833333 -1.6136260 1.00000 0.00000
O     core 0.2500000 0.7500000 0.4166666 -1.6136260 1.00000 0.00000
O     core 0.2500000 0.7500000 0.7500000 -1.6136260 1.00000 0.00000
O     core 0.5833333 0.0833333 0.0833333 -1.6136260 1.00000 0.00000
O     core 0.5833333 0.0833333 0.4166666 -1.6136260 1.00000 0.00000
O     core 0.5833333 0.0833333 0.7500000 -1.6136260 1.00000 0.00000
```

(Continued) GULP Defect Calculation Input File

```
O     core 0.5833333 0.4166666 0.0833333 -1.6136260 1.00000 0.00000
O     core 0.5833333 0.4166666 0.4166666 -1.6136260 1.00000 0.00000
O     core 0.5833333 0.4166666 0.7500000 -1.6136260 1.00000 0.00000
O     core 0.5833333 0.7500000 0.0833333 -1.6136260 1.00000 0.00000
O     core 0.5833333 0.7500000 0.4166666 -1.6136260 1.00000 0.00000
O     core 0.5833333 0.7500000 0.7500000 -1.6136260 1.00000 0.00000
O     core 0.9166666 0.0833333 0.0833333 -1.6136260 1.00000 0.00000
O     core 0.9166666 0.0833333 0.4166666 -1.6136260 1.00000 0.00000
O     core 0.9166666 0.0833333 0.7500000 -1.6136260 1.00000 0.00000
O     core 0.9166666 0.4166666 0.0833333 -1.6136260 1.00000 0.00000
O     core 0.9166666 0.4166666 0.4166666 -1.6136260 1.00000 0.00000
O     core 0.9166666 0.4166666 0.7500000 -1.6136260 1.00000 0.00000
O     core 0.9166666 0.7500000 0.0833333 -1.6136260 1.00000 0.00000
O     core 0.9166666 0.7500000 0.4166666 -1.6136260 1.00000 0.00000
O     core 0.9166666 0.7500000 0.7500000 -1.6136260 1.00000 0.00000
O     core 0.0833333 0.2500000 0.0833333 -1.6136260 1.00000 0.00000
O     core 0.0833333 0.2500000 0.4166666 -1.6136260 1.00000 0.00000
O     core 0.0833333 0.2500000 0.7500000 -1.6136260 1.00000 0.00000
O     core 0.0833333 0.5833333 0.0833333 -1.6136260 1.00000 0.00000
O     core 0.0833333 0.5833333 0.4166666 -1.6136260 1.00000 0.00000
O     core 0.0833333 0.5833333 0.7500000 -1.6136260 1.00000 0.00000
O     core 0.0833333 0.9166666 0.0833333 -1.6136260 1.00000 0.00000
O     core 0.0833333 0.9166666 0.4166666 -1.6136260 1.00000 0.00000
O     core 0.0833333 0.9166666 0.7500000 -1.6136260 1.00000 0.00000
O     core 0.4166666 0.2500000 0.0833333 -1.6136260 1.00000 0.00000
O     core 0.4166666 0.2500000 0.4166666 -1.6136260 1.00000 0.00000
O     core 0.4166666 0.2500000 0.7500000 -1.6136260 1.00000 0.00000
O     core 0.4166666 0.5833333 0.0833333 -1.6136260 1.00000 0.00000
O     core 0.4166666 0.5833333 0.4166666 -1.6136260 1.00000 0.00000
O     core 0.4166666 0.5833333 0.7500000 -1.6136260 1.00000 0.00000
O     core 0.4166666 0.9166666 0.0833333 -1.6136260 1.00000 0.00000
O     core 0.4166666 0.9166666 0.4166666 -1.6136260 1.00000 0.00000
O     core 0.4166666 0.9166666 0.7500000 -1.6136260 1.00000 0.00000
O     core 0.7500000 0.2500000 0.0833333 -1.6136260 1.00000 0.00000
O     core 0.7500000 0.2500000 0.4166666 -1.6136260 1.00000 0.00000
O     core 0.7500000 0.2500000 0.7500000 -1.6136260 1.00000 0.00000
O     core 0.7500000 0.5833333 0.0833333 -1.6136260 1.00000 0.00000
O     core 0.7500000 0.5833333 0.4166666 -1.6136260 1.00000 0.00000
O     core 0.7500000 0.5833333 0.7500000 -1.6136260 1.00000 0.00000
O     core 0.7500000 0.9166666 0.0833333 -1.6136260 1.00000 0.00000
O     core 0.7500000 0.9166666 0.4166666 -1.6136260 1.00000 0.00000
O     core 0.7500000 0.9166666 0.7500000 -1.6136260 1.00000 0.00000
O     core 0.0833333 0.0833333 0.2500000 -1.6136260 1.00000 0.00000
O     core 0.0833333 0.0833333 0.5833333 -1.6136260 1.00000 0.00000
O     core 0.0833333 0.0833333 0.9166666 -1.6136260 1.00000 0.00000
O     core 0.0833333 0.4166666 0.2500000 -1.6136260 1.00000 0.00000
O     core 0.0833333 0.4166666 0.5833333 -1.6136260 1.00000 0.00000
O     core 0.0833333 0.4166666 0.9166666 -1.6136260 1.00000 0.00000
O     core 0.0833333 0.7500000 0.2500000 -1.6136260 1.00000 0.00000
O     core 0.0833333 0.7500000 0.5833333 -1.6136260 1.00000 0.00000
O     core 0.0833333 0.7500000 0.9166666 -1.6136260 1.00000 0.00000
O     core 0.4166666 0.0833333 0.2500000 -1.6136260 1.00000 0.00000
O     core 0.4166666 0.0833333 0.5833333 -1.6136260 1.00000 0.00000
O     core 0.4166666 0.0833333 0.9166666 -1.6136260 1.00000 0.00000
```

(Continued) GULP Defect Calculation Input File

```
O     core 0.4166666 0.4166666 0.2500000 -1.6136260 1.00000 0.00000
O     core 0.4166666 0.4166666 0.5833333 -1.6136260 1.00000 0.00000
O     core 0.4166666 0.4166666 0.9166666 -1.6136260 1.00000 0.00000
O     core 0.4166666 0.7500000 0.2500000 -1.6136260 1.00000 0.00000
O     core 0.4166666 0.7500000 0.5833333 -1.6136260 1.00000 0.00000
O     core 0.4166666 0.7500000 0.9166666 -1.6136260 1.00000 0.00000
O     core 0.7500000 0.0833333 0.2500000 -1.6136260 1.00000 0.00000
O     core 0.7500000 0.0833333 0.5833333 -1.6136260 1.00000 0.00000
O     core 0.7500000 0.0833333 0.9166666 -1.6136260 1.00000 0.00000
O     core 0.7500000 0.4166666 0.2500000 -1.6136260 1.00000 0.00000
O     core 0.7500000 0.4166666 0.5833333 -1.6136260 1.00000 0.00000
O     core 0.7500000 0.4166666 0.9166666 -1.6136260 1.00000 0.00000
O     core 0.7500000 0.7500000 0.2500000 -1.6136260 1.00000 0.00000
O     core 0.7500000 0.7500000 0.5833333 -1.6136260 1.00000 0.00000
O     core 0.7500000 0.7500000 0.9166666 -1.6136260 1.00000 0.00000

# Defect information
centre  0.0833333 0.0833333 0.1666667
size  12.0000  23.0000
vacancy  0.0833333 0.0833333 0.0833333
vacancy  0.0833333 0.0833333 0.2500000
interstitial O 0.0833333 0.0833333 0.1875000 fix xyz

# Short Range Potentials
buck
O     U    566.498     0.42056    0.0000      0.00 12.00
buck4
O     O    11272.6     0.1363     134.00      1.2 2.1 2.6 12.00
```

GULP System Optimization Input File

```
#
# Keywords:
#
opti conp cartesian full
#
# Options:
#
title
Morelon potential for UO2
end

# Cell Structure
cell
   5.464   5.464   5.464  90.000000  90.000000  90.000000
fractional
U     core 0.000000 0.000000 0.000000 3.227252  1.00000 0.00000
O     core 0.250000 0.250000 0.250000 -1.613626 1.00000 0.00000
space
225
supercell
3 3 3

# Defect information
centre  0.5000 0.2500 0.2500
size  12.0000  23.0000
vacancy  0.250000 0.750000 0.250000
vacancy  0.250000 0.250000 0.250000
vacancy  0.750000 0.250000 0.250000
interstitial O 0.250000 0.250000 0.250000 fix xyz

# Short Range Potentials
buck
O     U    566.498     0.42056    0.0000      0.00 12.00
buck4
O     O    11272.6     0.1363     134.00      1.2 2.1 2.6 12.00

dump UO2_Opti.dump
```

REFERENCES

[1] Olander, D.R. *Fundamental Aspects of Nuclear Reactor Fuel Elements*. Springfield, VA: National Technical Information Service, 1976.

[2] Koch, L.J. *Experimental Breeder Reactor-II (EBR-II).* Argonne National Laboratory 2008.

[3] Kagana, G. and REST, J. "A Physical Description of Fission Product Behavior in Fuels for Advanced Power Reactors." ANL-07/24.

[4] Walker, C.T. et al. "Concerning the Microstructure Changes that occur at the Surface of UO_2 pellets on Irradiation to High Burnup." *Journal of Nuclear Materials* 188 (1992) 73-79.

[5] Thomas, L.E., Beyer, C.E., and Charlot, L.A.. "Microstructural Analysis of LWR Spent Fuels at High Burnup." *Journal of Nuclear Materials* 188 (1992) 80-89.

[6] Rest, J. "Kinetics of Fission-Gas-Bubble-Nucleated Void Swelling of the Alpha-Uranium Phase of Irradiated U-Zr and U-Pu-Zr Fuel." *Journal of Nuclear Materials* 207 (1993) 192-204.

[7] Mansur, L.K. and Coghlan, W.A. "Mechanisms of Helium Interactions with Radiation Effects in Metals and Alloys: A Review." *Journal of Nuclear Materials* 119 (1983) 1-25.

[8] Glasstone, S. and Sesonske, A. *Nuclear Reactor Engineering. Reactor Design Basics.* Springer, New York, 1994.

[9] Turnbull, J.A. and Friskney, C.A. "The Release of Fission Products from Nuclear Fuel During Irradiation by Both Lattice and Grain Boundary Diffusion." *Journal of Nuclear Materials* 58 (1975) 31-38.

[10] Zimmermann, H. "Swelling and Fission Gas Behavior in UO_2." *Journal of Nuclear Materials* 75 (1978) 154-161.

[11] Pahl, R.G. et al. "Experimental Studies of U-Pu-Zr Fast Reactor Fuel Pins in the Experimental Breeder Reactor-II." *Metallurgical Transactions* 21A (1990) 1863-1870.

[12] Turnbull, J.A. and Friskney, C.A. "The Diffusion Coefficients of Gaseous and Volatile Species During the Irradiation of Uranium Dioxide." *Journal of Nuclear Materials* 107(1982) 168-184.

[13] Kirchheim, R. “Reducing Grain Boundary, Dislocation Line and Vacancy Formation Energies by Solute Segregation. I. Theoretical Background.” *Acta Materialia* 55 (2007) 5129-5138.

[14] Matzke, Hj. et al. “Oxide Fuel Transients.” *Journal of Nuclear Materials* 166 (1989) 165-178.

[15] Bagger, C., Mogensen, M., and Walker, C.T. “Temperature Measurements in High Burnup UO_2 nuclear fuel: Implications for Thermal Conductivity, Grain Growth and Gas Release.” *Journal of Nuclear Materials* 211 (1994) 11-29.

[16] Mac Innes, D.A. and Brearley, I.R. “A Model for the Release of Fission Gas from Reactor Fuel Undergoing Transient Heating.” *Journal of Nuclear Materials* 107 (1982) 123-132.

[17] Turnbull, J.A. “The Effect of Grain Size on the Swelling and Gas Release Properties of UO_2 during Irradiation.” *Journal of Nuclear Materials* 50 (1974) 62-68.

[18] Rest, J. and Hofman, G.L. “Dynamics of Irradiation-Induced Grain Subdivision and Swelling in U_3Si_2 and UO_2 Fuels.” *Journal of Nuclear Materials* 210 (1994) 187-202.

[19] Was, G.S. *Fundamentals of Radiation Materials Science*. Springer, New York, 2007.

[20] Kogai, T. “Modelling of Fission Gas Release and Gaseous Swelling of Light Water Reactor Fuels.” *Journal of Nuclear Materials* 244 (1997) 131-140.

[21] Szuta, M. “The Diffusion Coefficient of Fission-Product Rare Gases in Single Crystal Uranium Dioxide During Irradiation.” *Journal of Nuclear Materials* 210 (1994) 178-186.

[22] Griesmeyer, J.M. “A Dynamic Intragranular Fission Gas Behavior Model.” *Nuclear Engineering and Design* 55 (1974) 69-95.

[23] Hayns, M.R. and Wood, M.H. “Models of Fission Gas Behaviour in Fast Reactor Fuels Under Steady State and Transient Conditions.” *Journal of Nuclear Materials* 67 (1977) 155-170.

[24] Turnbull, J.A. and Tucker, M.O. “The Release of Fission Gas from Nuclear Fuels During Temperature Transients.” *Journal of Nuclear Materials* 50 (1974) 53-61.

[25] Iglesias, F.C. et al. “Fission Product Release Mechanisms During Reactor Accident Conditions.” *Journal of Nuclear Materials* 270 (1999) 21-38.

[26] Lee, C.B., Kim, D.H., and Jung, Y.H. “Fission Gas Release and Swelling Model of Metallic Fast Reactor Fuel.” *Journal of Nuclear Materials* 288 (2001) 29-42.

[27] Stan, M. et al. "Models and Simulations of Nuclear Fuel Materials Properties." *Journal of Alloys and Compounds.* 444-445 (2007) 415-423

[28] Freyss, M., Petit, T., and Crocombette, J.P. "Point defects in Uranium Dioxide: Ab Initio Pseudopotential Approach in the Generalized Gradient Approximation." *Journal of Nuclear Materials* 347 (2005) 44-51.

[29] Govers, K. et al. "Comparison of Interatomic Potentials for UO_2. Part I: Static Calculations." *Journal of Nuclear Materials* 366 (2007) 161-177.

[30] Yun, Y. et al. "Defect Energetics and Xe Diffusion in UO_2 and ThO_2." *Acta Materialia* 57 (2009) 1655-1659.

[31] Cromcombette, J.P. "Ab Initio Energetics of Some Fission Products (Kr, I, Cs, Sr and He) in Uranium Dioxide." *Journal of Nuclear Materials* 305 (2002) 29-36.

[32] Ball, R. and Grimes R. "Diffusion of Xe in UO_2." *Journal of Chemical Society Faraday Transactions* 2, 1990 86 (8), 1257-1261.

[33] Shackelford, J.F. *Introduction to Materials Science for Engineers*. Prentice Hall 2005.

[34] Jackson, R.A and Catlow, C.R.A. "Trapping and Solution of Fission Xe in UO_2." *Journal of Nuclear Materials* 127 (1985) 161-166.

[35] Grimes R.W. and Catlow C.R.A. "The Stability of Fission Products in Uranium Dioxide." *Phil. Trans. R. Soc. Lond.* A (1991) 335, 609-634.

[36] Voter, A.F. *Introduction to the Kinetic Monte Carlo Method*. Theoretical Division, Los Alamos National Laboratory, 2005.

[37] Fedorov, G.B. and Smirnov, E.A. *Diffusion in Reactor Materials. Diffusion and Defect Monograph Series No. 8 (1984).* Atomizdat Publishers, Moscow, 1978.

[38] Battaile, C. "The Kinetic Monte Carlo Method: Foundation, Implementation, and Application." *Computational Methods Applied Mechanical Engineering* 197 (2008) 3386-3398.

[39] Flynn, C.P. *Point Defects and Diffusion*. Oxford: Clarendon Press. 1972.

[40] Deo, C.S. et al. "Helium Bubble Nucleation in Bcc Iron Studied by Kinetic Monte Carlo Simulations." *Journal of Nuclear Materials* 361 (2007) 141-148.

[41] Dill, K.A. and Bromberg, S. *Molecular Driving Forces, Statistical Thermodynamics in Chemistry and Biology.* Garland Science, New York, 2003.

[42] Brailsfor, A.D and Bullough, R. “The Rate Theory of Swelling Due to Growth in Irradiated Metals.” *Journal of Nuclear Materials* 44 (1972) 121-135.

[43] Gale, J.D. and Rohl, A.L. “The General Utility Lattice Program (GULP).” *Molecular Simulation* 29, 5 (2003) 291-341.

[44] Morelon, N.D. et al. “A New Empirical Potential For Simulating the Formation of Defects and Their Mobility in Uranium Dioxide.” *Philosophical Magazine*, 2003, Vol. 83, No. 13, 1533-1550.

[45] Willis, B.T.M. “Crystallographic Studies of Anion-Excess Uranium Oxides.” *Journal of Chemical Society, Faraday Transactions 2*, 1987, 83, 1073-1081.

[46] Hofman, G.L., Walters, L.C., and Bauer, T. H. “Metallic Fast Reactor Fuels.” *Progress in Nuclear Energy*, Vol. 31, No. 31, 1997, 83-110.

[47] Hofman, G.L. et al. “Swelling Behavior of U-Pu-Zr Fuel.” *Metallurgical Transactions A*. Vol 21A, March 1990, 517-528.

[48] Leteurtre, J. and Quere, Y. *Irradiation Effects in Fissile Materials*. North-Holland, Amsterdam, 1972.

AUTHOR'S BIOGRAPHY

Benjamin Asher Holtzman was born in Chicago, Illinois, on February 17, 1986. He graduated with honors from the University of Illinois on May 11, 2008, with a Bachelors of Science in Nuclear Engineering. In the spring of 2005, Ben worked as a research assistant to Professor Singer where he produced, "How the Price of Electricity Varies Due to the Cost of Uranium Reprocessing and Direct Disposal Costs." Additionally, during the spring of 2007, he worked as part of a team to compile and clearly present information regarding the impact of the nuclear industry in the state of Illinois using the IMPAN Regional Input Code. In the summer of 2007, Ben worked as an associate intern at Sargent & Lundy LLC. in Chicago, IL, where he worked on Combined Operating License Applications, and tabulated an HVAC ventilation system and valves in a piping system. In the summer of 2008, Ben worked as an intern at GE Hitachi Nuclear Energy in Wilmington, NC, where he made key contributions to the DOE deliverable, "Technology Development Roadmap: Facilities for Closing the Nuclear Fuel Cycle," as well as working toward the completion of a desktop simulator. In the summer of 2009, Ben worked as an intern at Knolls Atomic Power Laboratory in Niskayuna, NY, where he performed fuel assembly criticality analysis and tested temperature feedback through use of a Monte Carlo computer code.